Government of Western Australia

Department of
Mines and Petroleum

REPORT
130

SEDIMENTOLOGY AND STRATIGRAPHY OF THE PALEOPROTEROZOIC FRERE FORMATION, WESTERN AUSTRALIA: IMPLICATIONS FOR THE EVOLUTION OF THE PRECAMBRIAN OCEAN

by SJ Akin

ACADIA UNIVERSITY

Geological Survey of Western Australia

Government of **Western Australia**
Department of **Mines and Petroleum**

REPORT 130

SEDIMENTOLOGY AND STRATIGRAPHY OF THE PALEOPROTEROZOIC FRERE FORMATION, WESTERN AUSTRALIA: IMPLICATIONS FOR THE EVOLUTION OF THE PRECAMBRIAN OCEAN

by
SJ Akin

Perth 2014

Geological Survey of Western Australia

REFERENCE
The recommended reference for this publication is:
Akin, SJ 2014, Sedimentology and stratigraphy of the Paleoproterozoic Frere Formation, Western Australia: implications for the evolution of the Precambrian ocean: Geological Survey of Western Australia, Report 130, 133p.

National Library of Australia Cataloguing-in-Publication entry:

Author:	Akin, Sara Jennifer, author.
Title:	Sedimentology and stratigraphy of the Paleoproterozoic Frere Formation, Western Australia: implications for the evolution of the Precambrian ocean / Sara Jennifer Akin.
ISBN:	9781741685336 (ebook)
Subjects:	Geology, Stratigraphic--Precambrian. Marine sediments--Western Australia. Sedimentology--Western Australia.
Other Authors/Contributors:	Geological Survey of Western Australia
Dewey Decimal Classification:	551.46

ISSN 0508–4741

Grid references in this publication refer to the Geocentric Datum of Australia 1994 (GDA94). Locations mentioned in the text are referenced using Map Grid Australia (MGA) coordinates, Zone 51. All locations are quoted to at least the nearest 100 m.

About this publication
This Report is an MSc thesis researched, written and compiled through an ongoing collaborative project between the Geological Survey of Western Australia (GSWA) and Acadia University, Canada. Although GSWA has provided field and sample support for this project, the scientific content of the Report, and the drafting of figures, has been the responsibility of the author. No editing has been undertaken by GSWA.

Published 2014 by Geological Survey of Western Australia
This product is published in digital format (PDF) and is available online at <www.dmp.wa.gov.au/GSWApublications>.

Further details of geological publications and maps produced by the Geological Survey of Western Australia are available from:
Information Centre
Department of Mines and Petroleum
100 Plain Street
EAST PERTH WESTERN AUSTRALIA 6004
Telephone: +61 8 9222 3459 Facsimile: +61 8 9222 3444
www.dmp.wa.gov.au/GSWApublications

Cover photograph: Outcrop of granular iron-formation (GIF), near Sydney Heads Pass in the Earaheedy Basin. Note the granular, sandstone-like textures and current- or wave-generated structure and coarser banding than typical banded iron-formation; these features suggest a shallow-water, high-energy environment.

SEDIMENTOLOGY AND STRATIGRAPHY OF THE PALEOPROTEROZOIC FRERE FORMATION, WESTERN AUSTRALIA: IMPLICATIONS FOR THE EVOLUTION OF THE PRECAMBRIAN OCEAN

by

Sara Jennifer Akin

Thesis submitted in partial fulfillment of the requirements for
The Degree of Master of Science (Geology)

Acadia University
Spring Convocation 2012

This thesis by Sara Jennnifer Akin was defended successfully in an oral examination on April 16th, 2012.

The examining committee for the thesis was:

Dr. E.W. Bedingfield, Chair

Dr. E.E. Hiatt, External Reader

Dr. I.S. Spooner, Internal Reader

Dr. P.K. Pufahl, Supervisor

Dr. R.P. Raeside, Head

This thesis is accepted in its present form by the Division of Research and Graduate Studies as satisfying the thesis requirements for the degree Master of Science (Geology).

……..

I, Sara Jennifer Akin, hereby grant permission to the University Librarian at Acadia University to reproduce, loan or distribute copies of my thesis in microform, paper or electronic formats on a non-profit basis. I, however, retain the copyright to my thesis.

Author

Supervisor

Date

TABLE OF CONTENTS

TITLE PAGE i

ACKNOWLEDGEMENT OF DEFENSE ii

PERMISSION FOR REPRODUCTION iii

TABLE OF CONTENTS iv

LIST OF TABLES AND FIGURES vi

ABSTRACT vii

ACKNOWLEDGEMENTS viii

CHAPTER 1: INTRODUCTION AND STATEMENT OF PROBLEM 1

1.1 Introduction 1
1.2 Implications 2

CHAPTER 2: BACKGROUND 4
2.1 Paleoproterozoic Iron Formation 4
2.1.1 Continental margin-type iron formation 6
2.1.2 Precipitation mechanisms 9
2.1.3 Deposits in North America 12
2.2 Paleoproterozoic Oceanography 14
2.3 Summary 15

CHAPTER 3: METHODS 17

CHAPTER 4: GEOLOGIC SETTING 19
4.1 Tectonic Setting 19
4.1 Frere Formation 23

CHAPTER 5: LITHOFACIES 26
5.1 F1—Wavy laminated chemical mudstone 26
5.2 F2—Hummocky cross-stratified sandstone 31
5.3 F3—Flaser and lenticular bedded, magnetite-rich sandstone 34
5.4 F4—Planar laminated siltstone 37
5.5 F5—Trough cross-stratified hematitic grainstone 39
5.6 F6—Laminated cherty iron formation (pristine iron formation) 43
5.7 F7—Stromatolitic and microbial laminated siltstone 45
5.8 F8—Quartz arenite 48

CHAPTER 6: SEQUENCE STRATIGRAPHY 51
6.1 Transgressive systems tract 55

6.2 Highstand systems tract 61
6.3 Summary 63

CHAPTER 7: PARAGENESIS 64
7.1 Paragenesis in suboxic paleoenvironments 67
7.1.1 Stage 1- Water column precipitation and pristine iron formation 67
7.1.2 Stage 2- Authigenic cementation (2a) and reworking of pristine iron formation (2b) 69
7.1.3 Stage 3- Authigenic cementation of granular iron formation 73
7.1.4 Stage 4- Late diagenetic processes 77
7.2 Paragenesis in anoxic paleoenvironments 80
7.2.1 Stage 1- Water column precipitation, pristine iron formation, and terrigenous clastic deposition 81
7.2.2 Stage 2- Authigenic cementation of pristine iron formation and terrigenous clastics 82
7.2.3 Stage 3- Late diagenetic processes 85
7.3 Summary 85

CHAPTER 8: DEPOSITIONAL MODEL AND DISCUSSION 87
8.1 Depositional model 88
8.2 Iron formation depositional processes 92
8.2.1 Pristine iron formation 93
8.2.2 Grainstone factory 94
8.2.3 Summary of iron formation depositional processes 95
8.3 Paleoproterozoic ocean chemistry 95
8.3.1 Sulfidic ocean transition 97
8.4 Summary 100

CHAPTER 9: CONCLUSIONS 101

REFERENCES 104

APPENDIX I: STRATIGRAPHIC COLUMNS 115

APPENDIX II: PALEOCURRENT DATA 124

LIST OF TABLES AND FIGURES

LIST OF TABLES

Table 1: Lithofacies attributes and interpretations 29

LIST OF FIGURES

2.1: Abundance of Precambrian iron formation 5
2.2: Depositional model of continental margin type iron formation 8
2.3: Biological and abiological oxidation mechanisms 11

4.1: Western Australia and Capricorn Basins 20
4.2: Geometry of Earaheedy Basin and cross section 22
4.3: Stratigraphic nomenclature of the Earaheedy Group 25

5.1: F1 Wavy laminated mudstone 28
5.2: F2 Hummocky cross-stratified sandstone 33
5.3: F3 Flaser and lenticular bedded sandstone 36
5.4: F4 Planar laminated siltstone 38
5.5: F5 Trough cross stratified hematitic grainstone 41
5.6: F5 Trough cross stratified hematitic grainstone outcrop expression 42
5.7: F6 Laminated cherty iron formation (pristine iron formation) 44
5.8: F7 Stromatolitic and microbial laminated siltstone 46
5.9: F7 Mudcracks 47
5.10: F8 Pitted quartz grains 49
5.11: F8 Quartz arenite 50

6.1: Hierarchy of orders 53
6.2: Sea level curves and systems tracts 54
6.3: Regional stratigraphic correlation and legend 56
6.4: Section location and paleocurrent rose diagrams 58
6.5: Parasequences and mineral assemblages in TDH-26 60
6.6: Distribution of clastic-dominated facies in TDH-26 and Yappi Creek sections 62

7.1: Paragenetic pathways in suboxic and anoxic environments 65
7.2: Precipitation of redox-sensitive minerals with a chemocline 66
7.3: Textural relationships in laminated cherty iron formation 68
7.4: Backscattered electron image of laminated cherty iron formation 71
7.5: Textural relationships in hematitic grainstones 72
7.6: Pore-filling and replacement cements in grainstones 75
7.7: Backscattered electron image and elemental map of grainstones 79
7.8: Hummocky cross stratified sandstone from anoxic paleoenvironments 84

8.1: Depositional model for the Frere Formation 90

ABSTRACT

The Paleoproterozoic Frere Formation (ca. 1.80 Ga) of Western Australia is a 600 m thick sedimentary succession of iron formation and siltstone that accumulated in shallow water environments on an unrimmed continental margin. Lithofacies suggest that deposition occurred during a marine transgression punctuated by higher frequency relative sea level fluctuations that produced five parasequences. Parasequences are decameter-scale and defined by a basal flooding surface overlain by interbedded magnetite-bearing, hummocky cross-stratified sandstone that grade into microbially laminated, hematite-rich mudstone and trough cross-stratified grainstone. Each cycle is interpreted to record progradation of intertidal and tidal channel sediments over middle shelf deposits. The presence of eolian dunes, beach facies, mud cracks, absence of coarse clastics, and preponderance of siltstone and very fine-grained sandstone indicate deposition along an arid coastline marked by input of wind-blown sediment.

Iron formation of the Frere Formation is restricted to peritidal and middle-shelf paleoenvironments, contrasting with older Paleoproterozoic iron formations in North America, which accumulated in the full spectrum of shelf environments. Lithofacies associations and paragenetic pathways identified within the Frere Formation also suggest deposition in seawater with a prominent oxygen chemocline. Dilution by clastic input to middle-shelf environments is interpreted to have prevented iron formation from developing in deeper settings. The absence of pyrite in middle shelf lithofacies implies upwelled bottom water was not euxinic, supporting recent studies that demonstrate the Paleoproterozoic transition to a sulfidic ocean was not as widespread as previously surmised.

ACKNOWLEDGEMENTS

I would first and foremost like to thank my supervisor Dr. Peir Pufahl for giving me the opportunity to work with him on an amazing project at Acadia University and in Western Australia. Peir has given me the necessary tools to become a well-rounded scientist, and his expertise in sedimentology, teaching and writing is something for which I will forever be grateful. I would also like to thank him and his family for many dinners, laughs and for being my "Canadian family".

I would also like to thank Dr. Eric Hiatt for his guidance throughout my entire academic career in geology. He helped to bridge the transition between undergraduate and graduate studies, and his knowledge, discussions and friendship are invaluable.

Other people who made this project possible and enjoyable include Franco Pirajno and his field assistant Tony Zama. Franco arranged and led the field work for this thesis and shared his wealth of knowledge of the area. I would also like to thank Don Osburn for help making thin sections and Haixin Xu for assistance with the scanning electron microscope. The Earth and Environmental Science faculty at Acadia also deserve much thanks, as their doors were always open for many questions.

My personal acknowledgements go out to my friends and family, who supported my move to Canada and have listened to countless rants about rocks. My biggest acknowledgement goes out to my mother, Kari Chapple. She was the original motivator in my life to pursue something I am passionate about. If she were here today, she would have proof-read this iron-filled thesis with a smile and told me I am the Queen of Commas. Without her influence and support, I would not be where I am today.

CHAPTER 1: INTRODUCTION AND STATEMENT OF PROBLEM

1.1 Introduction

The Paleoproterozoic was a time of profound environmental change (Papineau, 2010; Pufahl and Hiatt, 2012). Supercontinent growth, the evolving biosphere, and the first of the snowball glaciations contributed to modifying atmosphere-ocean composition (Anbar and Knoll, 2002; Canfield, 2005; Nelson et al., 2010, Pufahl, 2010). Most important, however, was the Great Oxidation Event (GOE; Papineau, 2010; Bekker et al., 2010; Pufahl and Hiatt, 2012)—the rise in atmospheric oxygen that occurred between ~2.3 and 2.4 Ga (Catling and Claire, 2005; Bekker et al., 2010). For the first time in Earth history the products of oxic chemical weathering were delivered to the ocean, forever changing the chemical composition of seawater. Bacterial sulfate reduction of ever-increasing amounts of sulfate is thought to have produced a concomitant rise in sulfide (Canfield, 1998; Poulton et al., 2004), causing widespread euxinia and a nearly one billion year hiatus in the evolution of eukaryotes (Anbar and Knoll, 2002). Such conditions are also attributed to the demise of iron formation (Canfield, 1998) and phosphorite deposition (Nelson et al., 2010).

In spite of a tremendous amount of research (Anbar and Knoll, 2002; Canfield, 2005; Konhauser et al., 2005; Poulton et al., 2004, 2010), the exact nature of the GOE and resultant changes in ocean chemistry remain unclear (Pufahl et al., 2010). This is partly due to a focus on the large, continental margin iron formations in the Lake Superior region of North American that ostensibly bracket the transition to a sulfidic ocean (Poulton et al., 2004; Poulton et al. 2010). The focus of this thesis is to further refine what is known about ocean chemistry during this transition by examining iron

formation and associated lithofacies forming the Paleoproterozoic Frere Formation of Western Australia. The Frere Formation is ~1.8 Ga, which is slightly younger than continental margin iron formations in North America, and accumulated on a margin of a different proto-continent of a Paleoproterozoic supercontinent (Pirajno et al., 2009). Thus, it adds to our understanding of oceanic change in the Paleoproterozoic.

Insight into the nature of the sulfidic ocean transition was investigated by documenting the sedimentology and stratigraphy of the Frere Formation to reconstruct paleoenvironments of deposition and stratigraphic stacking patterns. Mineral paragenetic pathways forming lithofacies were assessed to determine the timing of the precipitation of redox-sensitive phases. Such information assisted in understanding seawater and pore-water chemistry to construct a depositional model for the Frere Formation. On a more applied level, these aspects of the Frere Formation can also be used to further refine iron formation exploration and resource models.

1.2 Implications

Because the Frere Formation is the only continental margin iron formation outside of North America (Lake Superior Region, USA; Labrador Trough, Canada; Gole and Klein, 1981; Klein, 2005; Pirajno et al., 2009) that ostensibly bridges the sulfidic ocean transition, it provides an important perspective to changing ocean-atmosphere chemistry during the Paleoproterozoic. Recent studies suggest that the development of euxinic conditions was not as widespread as previously surmised (e.g. Lyons et al., 2009; Pufahl, et al., 2010). Furthermore, the majority of what is known about this transition comes from a single basin in North America, the Animikie Basin, which has been interpreted as

having restricted circulation (Slack et al., 2007; Pufahl, 2010). Such conditions make it a poor choice for understanding the global open ocean during the change to sulfidic conditions. In contrast, the Frere Formation is interpreted to have accumulated on an unrimmed shelf with open circulation (Pirajno et al., 2009; this study). Thus, investigation of the Frere Formation will assist in obtaining a more complete understanding of the sulfidic ocean transition under conditions that are likely more reflective of the global ocean.

The Frere Formation also permits further assessment of iron formation depositional processes, which is directly linked to the cycling of the bioessential elements Fe and P on the early Earth (Pufahl, 2010). The origin of iron formation remains controversial as there are no modern analogs. Debate centers on whether the precipitation of Fe-rich facies was biotic, abiotic, or a combination (Cloud, 1973; LaBerge, 1973; Klein, 2005; Konhauser et al., 2005; Pufahl, 2010). The establishment of a sequence stratigraphic framework to interpret the deposition and paleoceanography of the Frere Formation is anticipated to provide novel insight into formation depositional processes and the biogeochemical cycling of Fe and P in the Paleoproterozoic ocean.

CHAPTER 2: BACKGROUND

2.1 Paleoproterozoic Iron Formation

Iron formation is generally regarded as a Precambrian phenomenon and is defined as a "chemical sediment, typically thin bedded or laminated, whose principal chemical characteristic is an anomalously high content of iron, commonly but not necessarily containing layers of chert" (Klein, 2005). Iron formation is the most significant source of iron ore, and an understanding of its genesis is required to adequately assess this important resource (James and Sims, 1973). As well as being economically significant, iron formation may also contain information that can be used to interpret the Precambrian biosphere, atmosphere and oceans (Pufahl, 2010).

Iron formation deposition is generally associated with the Precambrian, and there is variation among styles of deposition that closely relate to the time period in which they formed. Iron formation is classified based on the tectonic setting in which it was deposited, and new nomenclature divides iron formation into exhalative iron formation (formerly Algoma-type) and continental margin iron formation (formerly Lake Superior-type; Pufahl, 2010; Pufahl and Hiatt, 2012). Continental margin-type iron formation is more common in the Paleoproterozoic than the Archean, and coincides with the generation of tectonically stable shelves and rise of atmospheric oxygen (Pufahl, 2010). The Frere Formation is a continental margin-type iron formation and is interpreted to have been deposited during the decline of iron formation accumulation at the end of the Paleoproterozoic (Fig. 2.1; Klein, 2005).

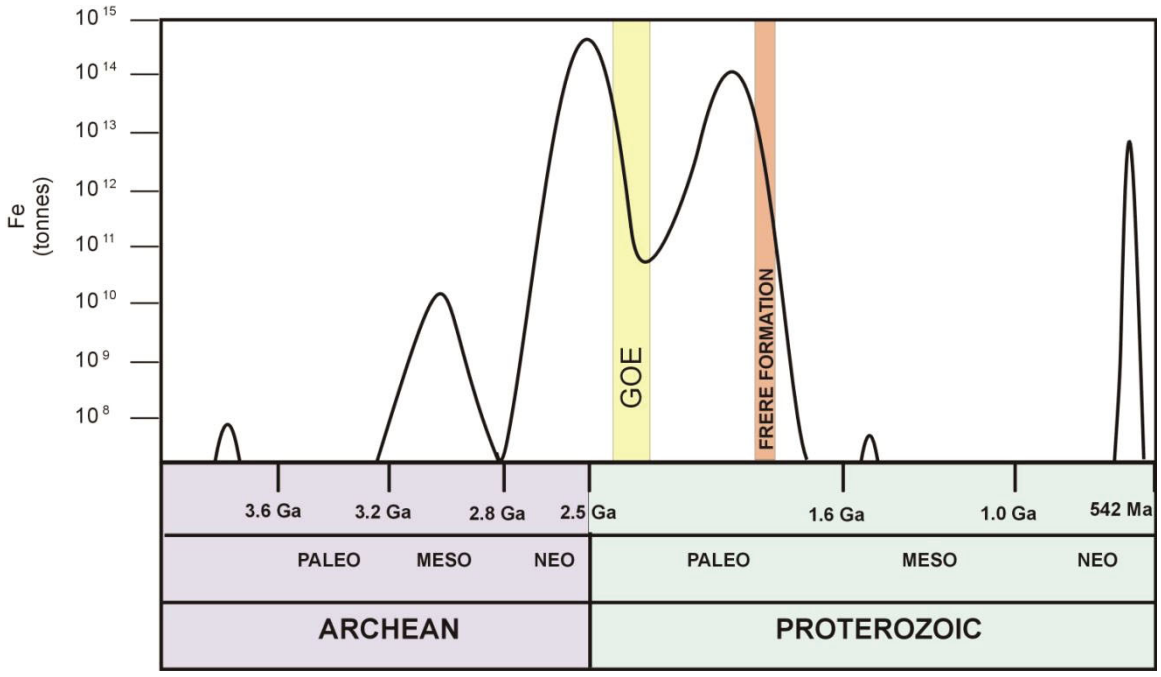

Figure 2.1. Relative abundance of iron formation through geologic time. The Isua deposit in Greenland at ~3.8 Ga marks the first appearance of iron formation. Deposition peaks at ~2.5 Ga and ceases at ~1.6. The few occurrences in the Neoproterozoic are attributed to process different than those responsible for deposition of older deposits. Modified after Pufahl and Hiatt, 2012.

2.1.1 Continental margin-type iron formation

The Frere Formation is a continental margin-type iron formation (CMTIF), which differs from exhalative iron formation in lithological, spatial and temporal abundance. Exhalative iron formation is more common in the Archean, associated with spreading centers, and produced thin deposits (Trendall, 2002; Pufahl, 2010). While exhalative iron formation is generally associated with Archean deposits and continental margin iron formation with Paleoproterozoic deposits, they are not exclusive to these specified eons (Pufahl, 2010).

CMTIF are larger deposits, common to the Paleoproterozoic eon, and contain lithofacies that represent shallow-water deposition (Fig. 2.2; Pufahl, 2010). Despite variation in classification and nomenclature throughout the literature, sedimentological aspects of continental margin-type iron formation have been documented as containing prominent similarities among deposits of this type. Granular iron formation (GIF) is a distinctive lithofacies that is characteristic of CMTIF, consists of cross-stratified chert- and hematite-rich coated grains and intraclasts, and is suggested to be a result of current- or wave-generated processes (Simonson and Hassler, 1996). Other sedimentary features indicative of CMTIF include ripple lamination, stromatolites, and fine-grained lithofacies that contain beds of granule to pebble-sized intraclasts, all of which indicate deposition in shallow water paleoenvironments (Simonson, 1985; Pufahl, 2010).

Peritidal environments consist primarily of chert and hematite, whereas middle and outer shelf deposits are characterized by containing abundant fine grained siliciclastic sediment, chert, Fe-silicate minerals and magnetite (Klein, 2005; Pufahl, 2010). The spatial distribution of Fe-bearing minerals of discordant redox conditions suggests there

was an oxygen chemocline present during deposition; this would have separated suboxic peritidal environments from anoxic middle-outer shelf environments (Pufahl, 2010).

The differences in iron formation deposition between the Archean and Paleoproterozoic reflects not only the tectonic regime in which each was deposited, but also the evolution of atmospheric and oceanic chemistry. The Great Oxidation Event (GOE) at ~2.4-2.3 Ga is proposed as the first major rise of atmospheric oxygen, resulting from the accumulation of photosynthetically-produced O_2, and the shift of volcanic outgassing from reducing gases to oxidizing gases (Holland, 2002; Bekker et al., 2010). The appearance of CMTIF temporally relates to the GOE (Pufahl, 2010), as accumulation of shallow-water lithofacies could precipitate in a water column that contained O_2 that could readily oxidize Fe^{2+} (Cloud, 1973; Klein, 2005; Poulton et al., 2010; Pufahl, 2010; Pufahl and Hiatt, 2012).

The mechanism responsible for the termination of iron formation deposition in the Paleoproterozoic, however, remains unclear. At ~1.8 Ga, iron formation deposition ceased for almost a billion years into the Mesoproterozoic as a result of deep waters becoming oxygenated or euxinic (Cloud, 1973; Anbar and Knoll, 2002). Iron formation deposited at this proposed transition may provide insight into the oceanic chemistry at this major transition.

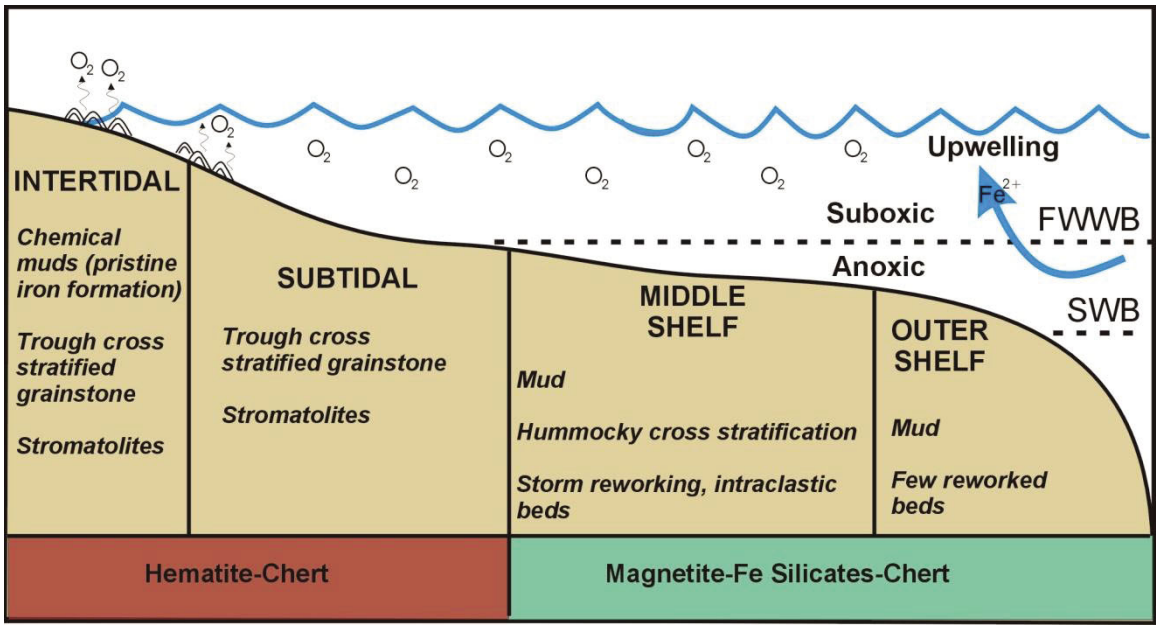

Figure 2.2. Depositional environments associated with continental iron formation. Intertidal and subtidal environments are dominated by trough cross-stratified grainstone and commonly contain sedimentary structures similar to those found in peritidal carbonate environments. Lithofacies fine basinward to mudstone and are often interrupted by coarse-grained, intraclastic beds. Lithofacies above a chemocline contain chert and Fe^{3+} -bearing mineral assemblages. Below the chemocline, minerals containing Fe^{2+} are more common. FWWB = fair-weather wave base; SWB = storm wave base. Modified after Pufahl, 2010.

2.1.2 Precipitation Mechanisms

Precambrian iron formation is composed of mineral assemblages that indicate deposition under suboxic and anoxic conditions (Klein, 2005). This is consistent with the assumption that the Precambrian ocean and atmosphere did not contain abundant free oxygen, as evident by the presence of detrital uraninite and pyrite before the GOE (Cloud, 1973; Pufahl and Hiatt, 2012). Minerals such as magnetite, siderite, greenalite and minnesotaite require anoxic conditions to provide the ferrous iron present in their compositions (Klein, 2005). REE data from CMTIF provides evidence of a deep ocean, hydrothermal source for Fe^{2+}. Positive Eu anomalies are found in many CMTIFs, which suggests alteration of oceanic basalts by high-temperature hydrothermal fluids (Beukes and Gutzmer, 2008). The mechanism responsible for oxidizing Fe^{2+} to Fe^{3+} has been one of the major controversies associated with iron formation (Klein, 2005; Clout and Simonson, 2005; Bekker et al., 2010; Pufahl, 2010; Pufahl and Hiatt, 2012).

Biological and abiological models regarding the oxidation of ferrous iron have been proposed and are summarized in Figure 2.3. The two biological models are 1) direct oxidation by ferrophototrophic bacteria (Fig. 2.3b; LaBerge, 1973; Konhauser et al., 2002; Kappler and Newman, 2004; Bekker et al., 2010) and 2) indirect oxidation through O_2 produced by cyanobacteria (Fig. 2.3c; Cloud 1973). The source of oxygen needed to precipitate Fe^{3+}-bearing minerals was suggested by Cloud (1973) as being of a biologic origin. This was based on microstructures documented in the work of LaBerge (1968), which provided evidence for a relationship between iron formation and oxygenic photosynthesizers or iron-precipitating organisms (Cloud, 1973). Multiple studies have been conducted that examined the amount of Fe^{2+} that can be produced via

chemolithoautotrophic and photoautotrophic bacteria (Widdel et al., 1993; Ehrenreich and Widdel, 1994; Konhauser et al., 2002; Kappler and Newman, 2004; Konhauser et al., 2005) and have found that these organisms can oxidize the amount of ferric iron needed to produce the largest documented iron formations (Figure 2.3b). A caveat to the biologic hypotheses is the lack of organic matter and microfossil evidence associated with all Fe-rich lithofacies within iron formations; however, stromatolites have been found in Paleoproterozoic iron formation, including this study, which suggest an indirect biological relationship.

Abiological models proposed employ photo-oxidation by ultraviolet light (Fig. 2.3a; Bekker et al., 2010) or ultraviolet photolysis of water vapor as the mechanism to oxidize ferrous iron (Kasting et al., 1979). These mechanisms have been experimentally shown to produce an insufficient amount of Fe^{2+} (Braterman and Cairns-Smith, 1986; Konhauser et al., 2005).

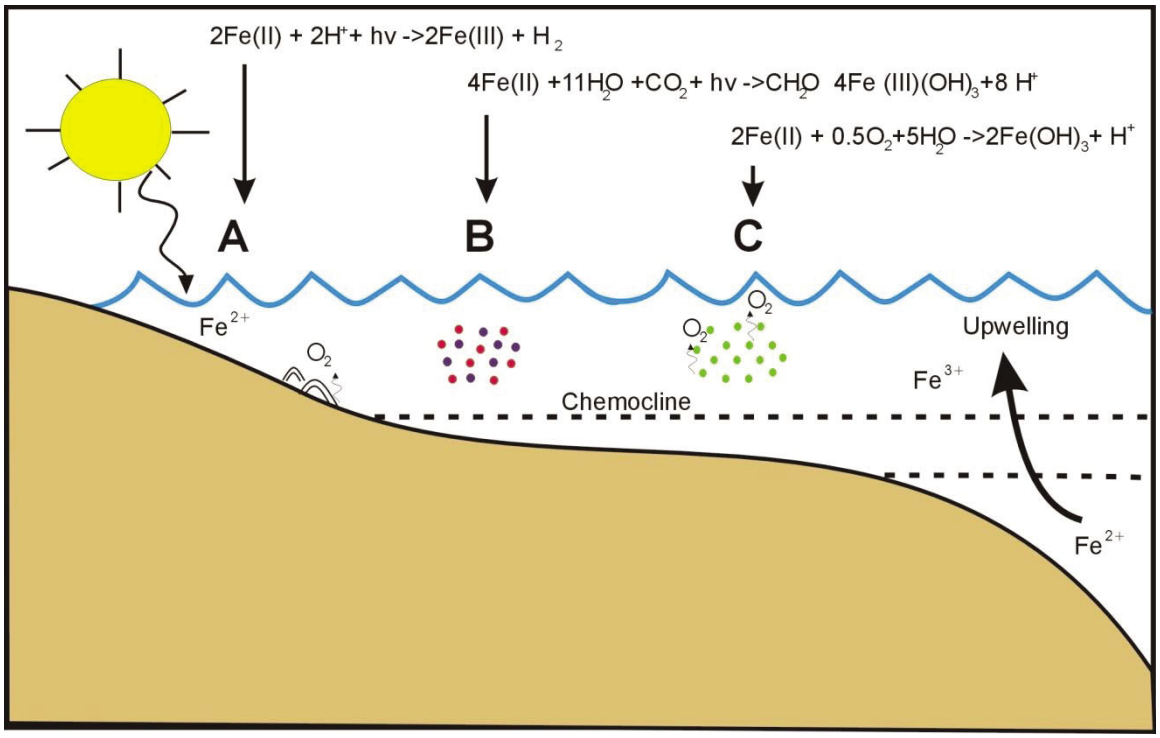

Figure 2.3. Mechanisms proposed for the oxidation of ferrous iron. All models assume Fe^{2+} is derived from a hydrothermal source. A) Abiological processes through uv-induced photo-oxidation. B) Direct oxidation of Fe^{2+} through anoxygenic photosynthesis. C) Indirect oxidation of Fe^{2+} through O_2 produced by cyanobacteria. Modified after Pufahl, 2010 and Bekker et al., 2010.

2.1.3 Deposits in North America

CMTIF from the Lake Superior region, USA and Canada, and Labrador Trough, Canada contain sedimentological aspects similar to those found in the Earaheedy Basin, Australia. Economic iron formation is exposed in "iron ranges" around Lake Superior, most noteworthy are the Mesabi, Gunflint, Gogebic, and Marquette Ranges (Simonson, 1985). These iron ranges are CMTIF and are ~2.1-1.85 Ga (Simonson, 1985). The Animikie Group is present in both the Mesabi and Gunflint Ranges and contains a basal quartzite, overlain by iron formation, and capped with flysch-type sandstone and shale (Ojakangas et al., 2001; Simonson, 1985). Lake Superior deposits are associated with volcanic activity, are stratigraphically located between a basal sand-rich deposit, an upper shale-rich deposit (Trendall, 1968), and contain thick, organic-rich mudstone and shale intervals (Simonson, 1985). Iron formation is found in a thick deposit at one stratigraphic location, rather than dispersed in thin intervals (Trendall, 1968). These iron formations are interpreted to have been deposited in environments ranging from upper subtidal to outer shelf, basinal environments (Simonson, 1985; Pufahl, 1996; Nelson et al., 2010). The Sokoman Formation in the Labrador Trough region is ~1.9 Ga, and also contains lithofacies indicative of deposition in the full spectrum of shelf environments (Knoll and Simonson, 1981; Anderson, 2009; Edwards, 2010; Edwards et al., in press).

CMTIF has been well studied in North America, and it has become clear that its origin was strongly influenced by the increase of accommodation space with the generation of continental shelves at 2.5 Ga, as well as the GOE ca. 2.4-2.3 Ga (Pufahl, 2010). North American deposits share many similar characteristics to the Frere Formation, however, important differences identified show: 1) volcaniclastic beds are

absent in the Frere Formation and 2) the Frere Formation contains iron-rich lithofacies indicative of supratidal and intertidal environments, but deeper water, "banded iron formation" is absent.

Iron formation deposits of North America and the Frere Formation were deposited near the end of the Paleoproterozoic and contain similar lithofacies. However, sulfide mineral occurrences and organic- and iron-rich lithofacies are not present in the Frere Formation. An explanation for differences between CMTIF of the same age may be paleogeographic in nature. North American basins have been interpreted as intracratonic basins within proto-Laurentia, whereas the Northern and Western Australian continents were possibly one landmass during deposition of CMTIF (Betts et al., 2008). Iron formation of the Lake Superior region, among other Paleoproterozoic deposits may have been deposited along a different margin of a larger supercontinent (Columbia) in intracratonic basins, and may not reflect global ocean conditions.

The supercontinent *Columbia* is hypothesized to have existed ~750 Ma before the assembly of Rodinia, based on emplacement of large igneous provinces (LIPs; Ernst et al., 2008) and correlative accretionary terranes and basin development in Australia and Laurentia (Betts et al., 2008). Reconstructive configurations based on paleomagnetic studies place the Earaheedy Basin 5-10^{o} N of the paleoequator at 1.78 Ga and on a proto-continent consisting of only the North Australian and West Australian cratons (Betts et al., 2008). Proto-Laurentia is placed in a landmass separated from proto-Australia at 1.78 Ga, which may provide an explanation as to why this transitional phase of Earth history has given rise to many interpretations with respect to evolving ocean chemistry.

2.2 Paleoproterozoic Oceanography

The temporal distribution and mineralogical assemblages of Precambrian iron formation have often been used to reconstruct the atmospheric and oceanic chemistry of early Earth (Canfield, 1998; Ohmoto et al., 2006). These studies have used geochemical proxies such as REE concentrations, and sulfur fractionation as a proxy to understand oxygenation of the atmosphere. It is generally accepted, based on these proxies, that the Great Oxidation Event (GOE) occurred between 2.3-2.4 Ga (Holland, 2002; Catling and Claire, 2005; Holland, 2009; Pufahl and Hiatt, 2012). Despite controversy over the mechanism(s) that oxidized ferrous iron in the Precambrian, most studies agree that the atmosphere was essentially anoxic until the GOE (Catling and Claire, 2005; Konhauser et al., 2005; Bekker et al., 2010). Studies that disagree and claim the atmosphere and ocean have maintained constant O_2 levels since 3.8 Ga (Ohmoto et al., 2006) base this interpretation on the presence of hematite in the Archean.

The end of continental margin iron formation is interpreted to coincide with the onset of sulfidic ocean conditions at ~ 1.84 Ga (Anbar and Knoll, 2002; Poulton et al., 2004; Poulton et al., 2010) when ferrous iron combined with sulfide to produce pyrite instead of Fe-oxides. The change from anoxic to euxinic conditions allegedly occurred when atmospheric oxygen levels facilitated oxic weathering pyrite, thus increasing the delivery of SO_4 transported to the oceans (e.g. Canfield, 1998; Poulton et al., 2004). It is postulated that sulfate was reduced to H_2S through bacterial sulfate reduction, thus increasing the concentration of available sulfide to combine with Fe^{2+}. This is thought to have removed Fe^{2+} from the oceans by once again producing pyrite, thus removing the Fe^{2+} needed to precipitate Fe-bearing minerals needed to form iron formation (Pufahl et

al., 2010). This hypothesis is based on iron speciation and sulfur isotope data from pyrite samples collected from the Animikie Group from the Lake Superior region (ca. 1.87-1.84 Ga), and provides evidence for a shift from anoxic to euxinic conditions (Poulton et al., 2004; Pufahl et al., 2010). This transition to a sulfidic ocean is hypothesized to have caused the Mesoproterozoic "Boring Billion" until the second major rise of atmospheric oxygen, and has often been cited as the cause for the cessation of iron formation deposition (Anbar and Knoll, 2002; Shen et al., 2002).

The use of the Animikie Group as a proxy for determining oceanic chemistry to deduce the mechanism responsible for the abrupt termination of iron formation deposition has recently been questioned by Pufahl et al. (2010). Comparison of $\delta^{34}S$ values from the Rove Formation, Animikie Group, and the correlative Michigamme Formation, Baraga Group, show a discrepancy. Proponents of a sulfidic ocean transition use the increase of $\delta^{34}S$ values to suggest pyrite precipitation under sulfidic conditions (Pufahl et al., 2010). Data presented by Pufahl et al. (2010) suggests that the Rove Formation was deposited in a basin with restricted circulation, and is therefore not a reliable basin to infer global oceanic conditions. The same $\delta^{34}S$ trend was not observed in the Michigamme Formation to the south, which may be a result of regional differences, or the consequence of diagenetic or metamorphic over-printing of samples analyzed by Poulton et al. (2004).

2.3 Summary

There is a clear distinction between iron formations that typify Archean and Paleoproterozoic deposits which imply a change in the dynamics between tectonics and

atmospheric and oceanic chemistry. The shift from extensive exhalative iron formation to CMTIF closely coincides with the development of continental shelves that served as a repository for shallow water deposits. Although the mechanism for the oxidation of Fe^{2+} continuous to remain enigmatic, it is clear that Fe^{2+} was oxidized in shelf environments in the Paleoproterozoic.

Paleoproterozoic iron formations of North America share similar attributes that include close associations with volcanics, and lithofacies representing paleoenvironments from the outer shelf to peritidal settings. CMTIF disappeared at ~1.8 Ga, when oceans were titrated of dissolved iron by either oxygenation of sulfidification of the deep ocean, removing the iron source. Due to the uncertainty associated with using the Animikie Basin as a benchmark for the sulfidic ocean transition, the Frere Formation may provide an important perspective into the evolving Paleoproterozoic Ocean. Because the Frere Formation was deposited between anoxic Archean and oxic Phanerozoic conditions at ~1.8 Ga, paleoenvironmental parameters identified in this study will help to redefine what is known about this transitional period.

CHAPTER 3: METHODS

The Frere Formation is accessible by vehicular transportation to outcrops and is generally well exposed due to a lack of vegetation. Strata are generally flat-lying except near the Stanley Fold Belt where folding and faulting become more prominent. Outcrop and drill core provided vertical and lateral stratigraphic context of sedimentological units. Lateral facies changes were traced by walking out units within gullies, where possible. Emphasis was placed on understanding paleoenvironments, regional stratigraphic trends, and collection of samples for petrographic analysis. Interpretations were based on bed-by-bed descriptions and samples taken from all lithofacies present in two drill cores that penetrate the Frere Formation. Nine stratigraphic sections were measured that range between 15-444 m, two of which are drill cores TDH-26 and TDH-28.

The field season for this project was conducted in Western Australia with the assistance of the Geologic Survey of Western Australia (GSWA). Four areas were identified as having relatively complete stratigraphic successions through the Frere Formation. Seven outcrop stratigraphic sections were measured (Figure 6.4; Appendix I): Nabberu Creek (51J 0266285, 7158216; 94 meters), Yappi Creek (51J 0347194, 7177557; 306 meters), West Yappi Creek (51J 0343258, 7177318; 444 meters), Von Treuer Section 1 (51J 0480324, 7054877; 54 meters), Von Treuer Section 2 (51J 0501681, 7054913; 22 meters), Kingston Sections 1 (51J 0383703, 7084880) and Kingston Section 2 (51J 0387275, 7083589; composite sections, ~15 meters each). Samples were collected from each lithofacies that compose stratigraphic sections and used for petrographic analysis. Stratigraphic sections in outcrop and drill core were used to determine paleoenvironments of deposition and vertical and lateral trends.

Drill core was logged at the core repository located at the GSWA in Perth, Western Australia. TDH-26 is a 253 m thick core drilled at 51 J 256600E, 7166400 N, and TDH-28 is 209 m thick, drilled at 51 J264400 E, 7161250 N. Both drill cores contain the contact between the underlying Yelma Formation and overlying Frere Formation of the Tooloo Subgroup. Contacts and lithologic relationships were identified and described, and pictures were taken of the drill core using a Panasonic DMC-TZ3. Drill core descriptions were used to calibrate observations in outcrop and samples taken were used to assess diagenesis and metamorphism.

Percentages of chemical and clastic grains were estimated from 54 polished thin sections. Modal compositions were determined for minerals present within each thin section and occurrences of pyrite and magnetite in drill core were given an abundance index of rare (1-10%) and abundant (>10%). Thin sections were examined using a Nikon transmitted and reflected light microscope. Textures and grain relationships were further investigated using a JEOL JSM-5900 LV scanning electron microscope with a Princeton Gamma-Tech IMIX-PC EDS detector in the Acadia Centre for Microstructural Analysis. Such data assisted in interpreting mineral paragenesis.

CHAPTER 4: GEOLOGIC SETTING

4.1 Tectonic Setting

The Frere Formation is a ~1.8 Ga succession of chemical and clastic sedimentary rocks that forms the upper unit of the Tooloo Subgroup (Fig. 4.3; Pirajno et al., 2009). The Tooloo Subgroup in turn defines the basal portion of the Earaheedy Group (Pirajno et al., 2009). The Earaheedy Group was deposited in the Earaheedy Basin, which is one of four Paleoproterozoic basins that developed between the Yilgarn and Pilbara cratons 2.2-1.8 Ga (Halilovic et al., 2004). These basins were deformed in the last stage of the Capricorn Orogeny, producing a 700 km belt located near the northern margin of the Yilgarn Craton in Western Australia (Pirajno et al., 2004). The Earaheedy Basin (Fig. 4.1, 4.2) resides on the southeastern end of the Capricorn Orogen, and is the final basin to develop and deform (Halilovic et al., 2004).

Prior to the development of the Earaheedy Basin, three other basins formed: the Yerrida, Bryah, and Padbury basins (Fig. 4.1). The intracratonic Yerrida Basin was established at ~2.17 Ga on the northern margin of the Yilgarn craton as a result of mantle upwelling and related thermal relaxation (Pirajno et al., 2004). Seafloor spreading at ~2.0 Ga occurred between the northwest Yilgarn craton and an Andean-type margin containing the Glenburgh and Gascoyne terranes (Cawood and Tyler, 2004).

Eventual accretion of oceanic crust and island arcs produced the Errabiddy shear zone. At ~1.9 Ga, uplift and thrusting across the Errabiddy shear zone generated the Padbury Foreland Basin, within which the Bryah Group accumulated.

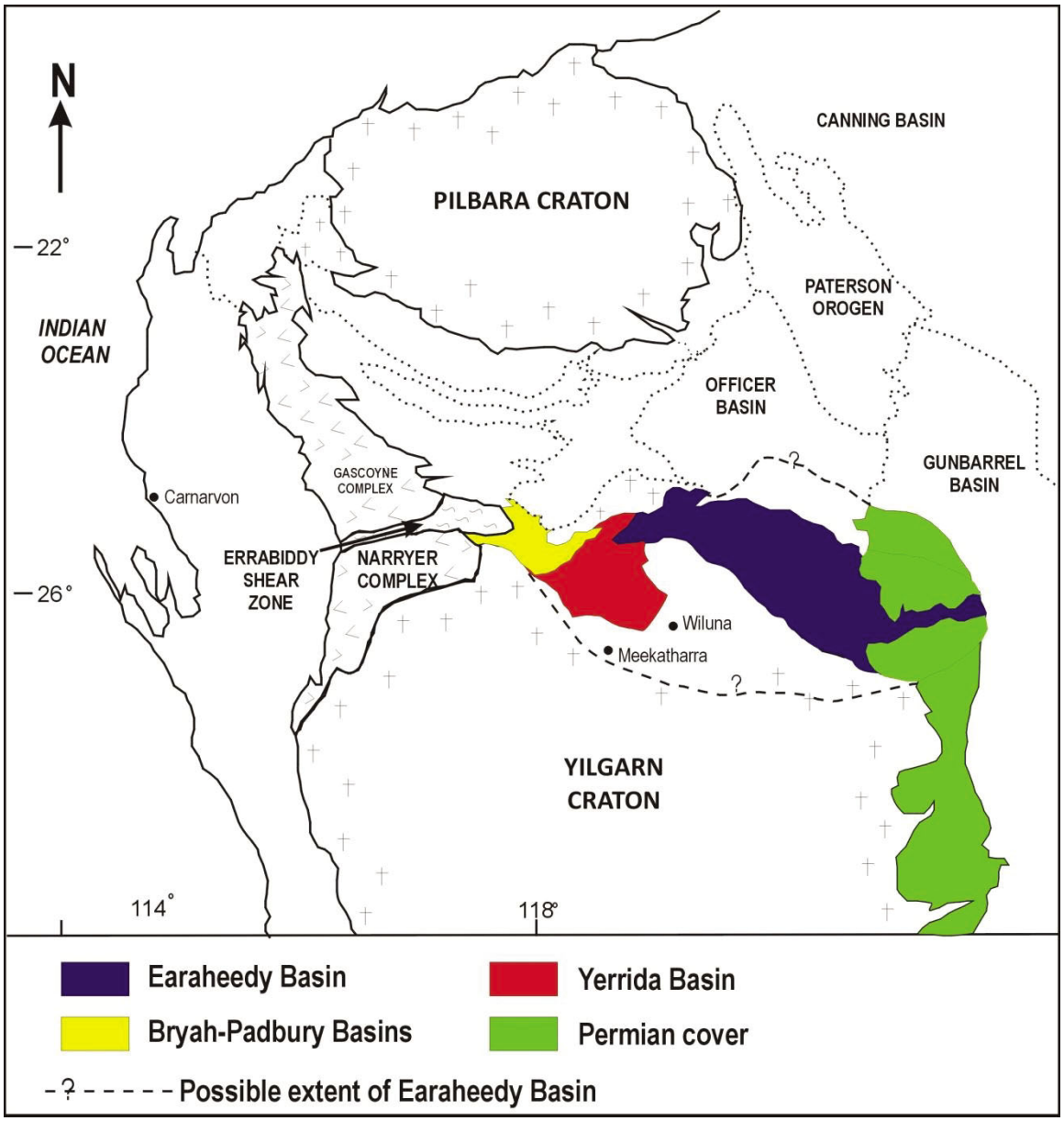

Figure 4.1. Map of Western Australia and location of Paleoproterozoic basins associated with the Capricorn Orogeny (Modified after Pirajno et al., 2004).

The Capricorn Orogeny occurred between 1.83-1.78, when the Pilbara and Yilgarn cratons obliquely collided in the western part of the orogen. Seafloor spreading and continental breakup occurred after this and produced a passive margin on the north and east margin of the Yilgarn (Pirajno et al., 2009).

The Earaheedy Group was deposited on the established passive margin, with an inferred spreading center located to the east-northeast, based on the presence of flood basalts of the Mooloogool Group (Pirajno et al., 2009). It was deformed from either the Yapungku Orogeny from south-directed compression as the North Australian and West Australian craton converged 1.79-1.76, or from the Mangaroon Orogeny between 1.68 and 1.62 Ga. This deformation is restricted to the northern edge of the basin (Pirajno et al., 2004) and resulted in the development of the Stanley Fold Belt (SFB; Pirajno et al., 2004), and folded the Frere Formation into an asymmetric, east-plunging syncline (Fig. 2; Pirajno et al., 2009). Deformation was focused to the northeast area of the Stanley Fold Belt (Pirajno et al., 2004) and produced reverse faults, shearing, and tight folding (Pirajno et al., 2009).

In the southeast part of the Earaheedy Basin deformation is centered around the Shoemaker impact structure. This crater is approximately 30 km in diameter and is defined by a margin of folded and faulted iron formation from the Frere Formation (Pirajno et al., 2003). The age of this impact structure is poorly constrained, however two ages have constrained the impact between 550 Ma and 1070 Ma. However, these ages may reflect the isotopic signatures being reset from tectonics or hydrothermal activity (Pirajno et al., 2003).

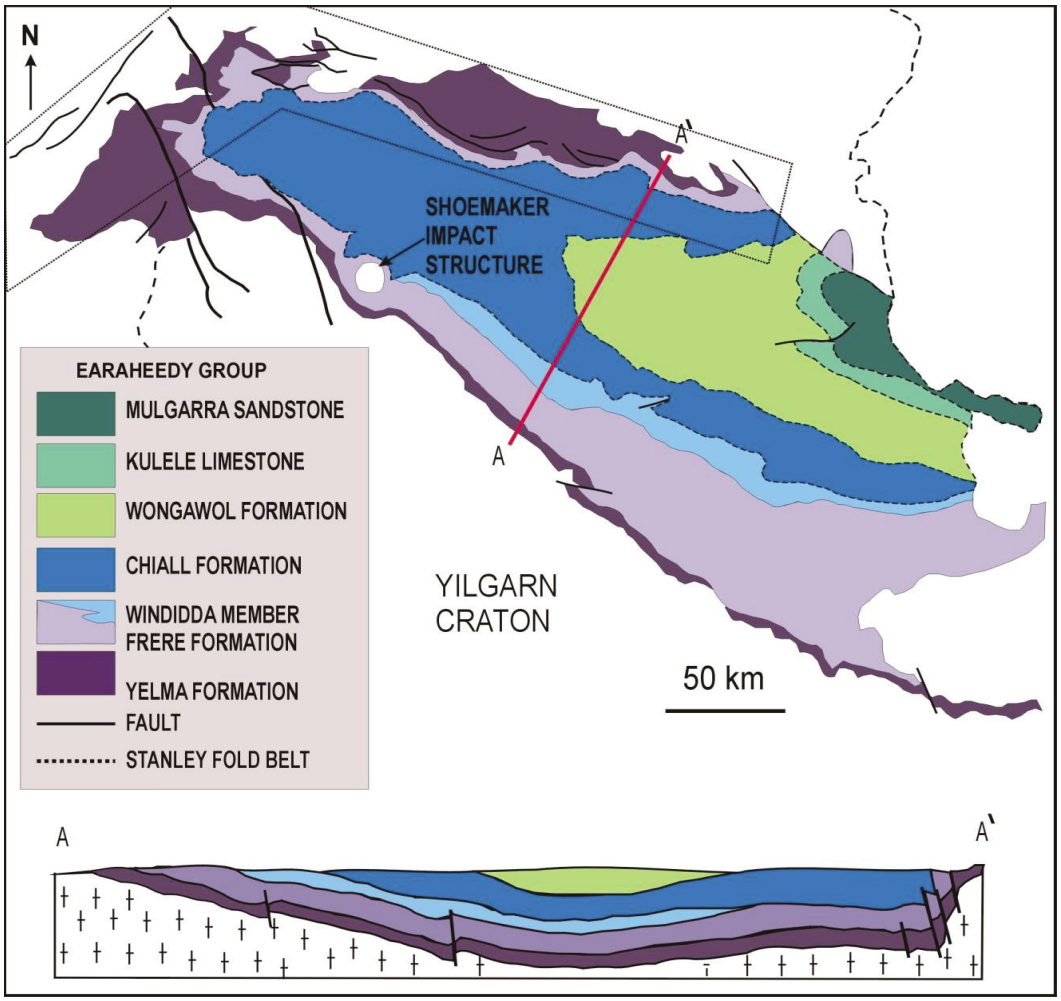

Figure 4.2. Geometry of the Earaheedy Basin. The Frere Formation is shown in light purple and outcrops at a NW strike in the SW and NE parts of the basin. The cross-section shows the syncline produced from north to south, with the Stanley Fold Belt located in the north (modified after Pirajno et al., 2009).

4.2 Frere Formation

Until recently the thickness of the Frere Formation was not well constrained, as there are no continuous sections available that contain contacts with both the underlying Yelma Formation and the Chiall Formation (Bunting, 1986). Bunting (1986) originally estimated the thickness to be 1200-1300 m, but re-mapping of the Earaheedy Basin by the Geological Survey of Western Australia (Bunting, 1986; Pirajno et al., 2009) and observations from this study has decreased the estimated thickness to ~600 m from the original estimation of 1200 m.

The Frere Formation is a succession of iron formation, stromatolites, and clastic sedimentary rocks that form the upper unit of the Tooloo Subgroup within the Earaheedy Group (Pirajno et al., 2004; Figure 3). Its basal contact is a well developed unconformity on the Yelma Formation (this study). The upper Frere Formation is not well preserved, but sparse outcrops of stromatolites from the Windidda Member (Fig. 4.3) suggest its upper contact with overlying sandstone of the Chiall Formation, the lowermost unit in the Minningarra Subgroup, is also an unconformity (this study). The Minningarra Subgroup is a ~2900 m thick, clastic-dominated succession containing coarsening-upward packages of shale, siltstone, mudstone, sandstone and intraclastic breccias (Pirajno et al., 2009).

The age of the Frere Formation is based on a Pb-Pb age of ca. 1.81 Ga from a hydrothermal monazite within the underlying Yelma Formation (Table 1; Muhling et al., 2011). Because evidence for hydrothermal alteration and associated MVT mineralization does not extend into the Frere Formation, the deposition of iron formation is inferred to have occurred after this event. Such an interpretation is supported by U-Pb Sensitive High Resolution Ion Micro Probe (SHRIMP) ages from detrital zircon at the top of the

Earaheedy Group. The youngest of these ages is 1808±36 Ma from the Mulgarra Sandstone, ca. 1,300 m stratigraphically above the Frere Formation, which provides a maximum depositional age for the uppermost Earaheedy Group. Although it is uncertain whether the basal contact of the Mulgarra Sandstone is tectonic or stratigraphic, these data taken together suggest an age of less than ca. 1.80 Ga for iron formation in the Frere Formation.

Previous work on the sedimentology of Frere Formation has focused on two drill cores (TDH-26 and TDH-28) that penetrate nearly the entire formation (Price, 2003; Pirajno, 2009). Based on these cores the stratigraphy has been divided into four intervals of Fe-rich, granular iron formation that alternate with four intervals of siltstone (Pirajno, 2009) and are interpreted to have been deposited in a shallow marine environment (Jones et al., 2000). It has been suggested that the alternation of Fe-rich intervals with clastic intervals was a response to fluctuations in relative sea level resulting from tectonism and eustatic sea level changes, as well as the influx of Fe and Si into the system (Pirajno, 2009). This study will help further constrain iron formation depositional processes as well as provide new information regarding the nature of the Paleoproterozoic Ocean immediately after the sulfidic ocean transition.

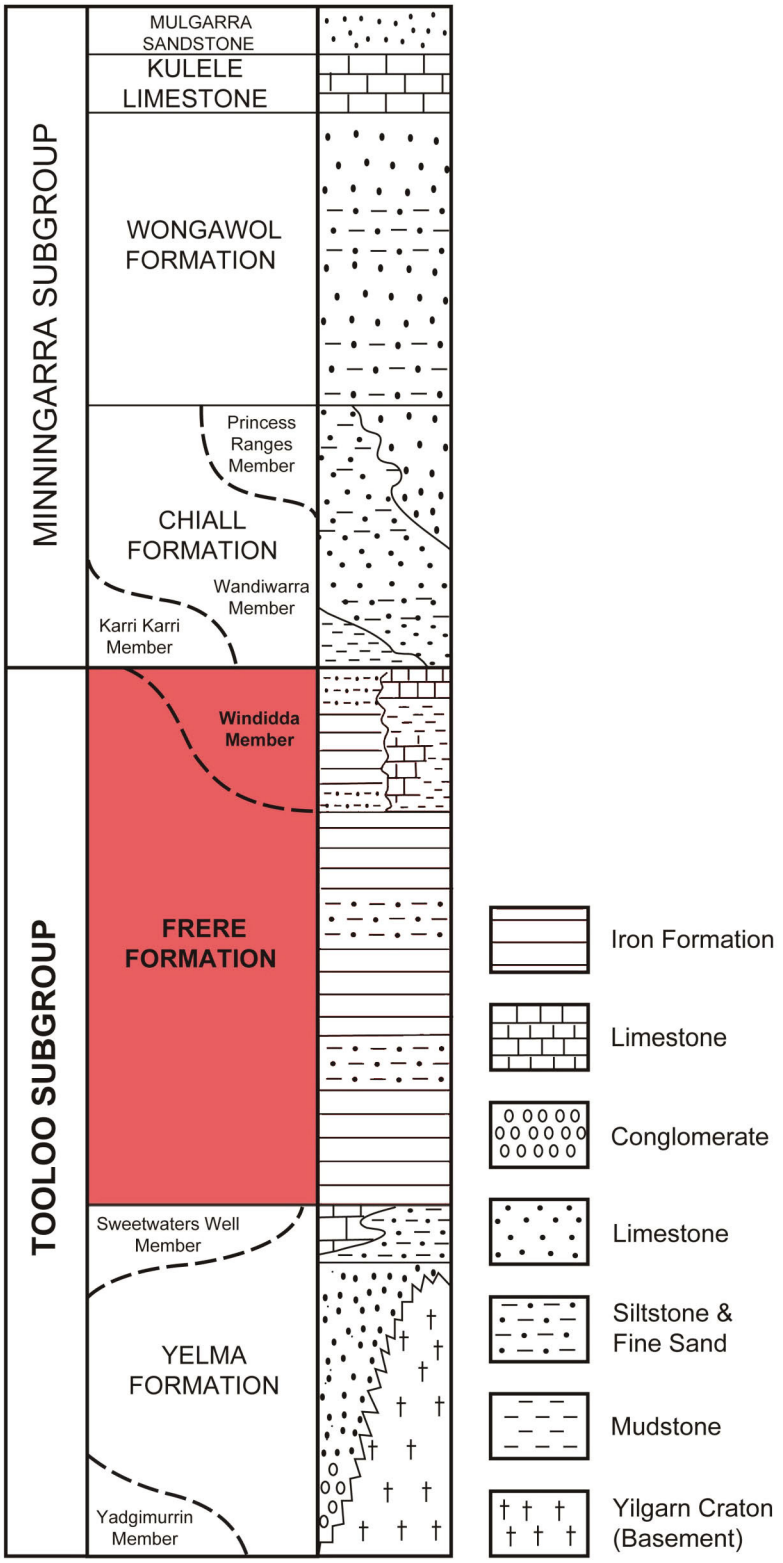

Figure 4.3. Stratigraphic nomenclature of the Earaheedy Group (modified after Pirajno et al., 2009).

CHAPTER 5: LITHOFACIES

Eight lithofacies have been identified in the Frere Formation that accumulated in peritidal to middle shelf environments (Table 1). Lithofacies were defined based on differences in lithological classification, primary sedimentary structures, clastic sediment content, and chemical variations, specifically within iron oxide minerals compared to vertically and laterally adjacent units. Observations from both outcrop and drill core provided information on lithological and sedimentological characteristics, which were used to interpret paleoenvironments of deposition.

5.1 F1 – Wavy laminated chemical mudstone

Facies 1 (F1) is a black to dark grey, magnetite and silt-rich, wavy laminated chemical mudstone (Fig. 5.1). Mud and silt laminae are 1-10 mm thick and interbedded with 1-2 cm thick grainstone beds. Grainstone beds 1-4 cm thick are interbedded with 0.5-5 mm thick, discontinuous mudstone laminae. Grainstone beds are composed of normally graded, fine to medium sand-sized, round, chert intraclasts.

Interpretation: The interbedding of wavy laminated mudstone with thin, normally graded, grainy beds is characteristic of deposition on a storm-dominated middle shelf (Reineck and Singh, 1980). Clastic and chemical mudstones layers are interpreted to have accumulated from suspension during fair-weather conditions when grainy sediment was restricted to shallower environments (Plint, 2010). The lack of a coarse clastic fraction in F1 and evidence for an eolian source in F8, suggests wind was the primary transport mechanism of siliciclastic sediment to the shelf. Magnetite-rich laminae are interpreted to have accumulated as chemical muds from magnetite precipitated directly in seawater or

from iron (hydroxy)oxides that were later diagenetically converted to magnetite just beneath the seafloor (Chapter 7; Johnson et al., 2008; Pufahl, 2010; Pufahl and Hiatt, 2012). Grainy beds are interpreted to be tempestites, their normal grading reflecting deposition during waning storm conditions (Plint, 2010).

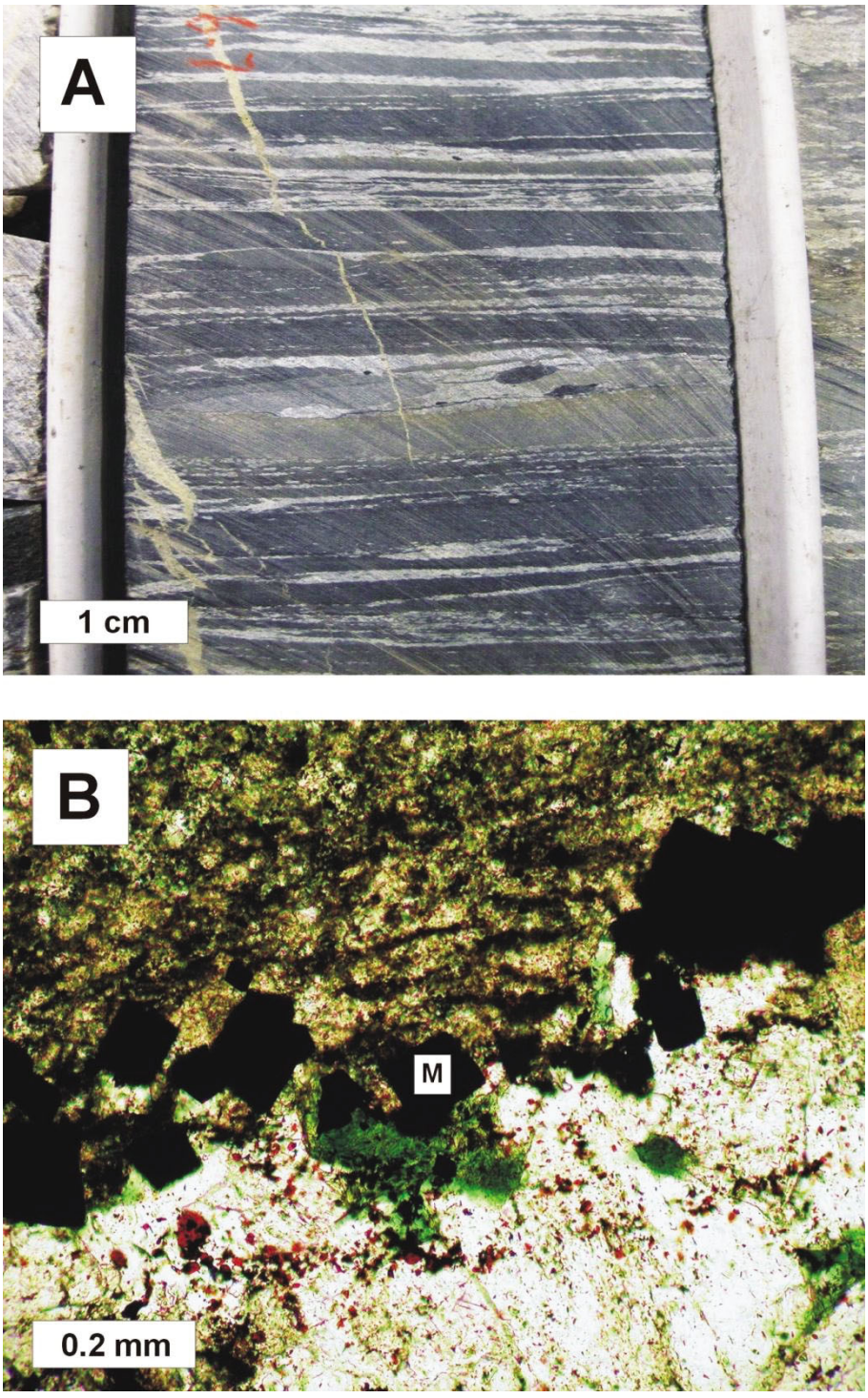

Figure 5.1. Wavy laminated mudstone. A) TDH-26, 365 m in drill core. B) Photomicrograph of TDH-26 in PPL, 384.9 m; euhedral magnetite (M) crystals between laminae.

Table 1. Summary of lithofacies attributes and environmental interpretation.

	Facies	Lithology/Sedimentary Structures	Interpretation
F1	Wavy laminated chemical mudstone	Black to dark grey, magnetite and silt-rich, wavy laminated chemical mudstone. Mud and silt laminae are 1 to 10 mm thick and are interbedded with 1 to 2 cm thick grainstone beds. Grainstone beds, 1-4 cm thick, are interbedded with 0.5-5 mm thick, discontinuous mudstone laminae. Grainstone beds are composed of normally graded, fine to medium sand-sized, rounded chert intraclasts.	Middle shelf mudstone deposited on a storm dominated shelf (Dalrymple, 1992).
F2	Hummocky cross stratified sandstone	Hummocky cross-stratified (HCS) silty, very fine-grained quartz-rich sandstone. It is green-black in drill core and tan-pink in outcrop. In three-dimensional exposures bedsets containing abundant low angle truncation surfaces ($<15^{o}$) are 10–30-cm-thick and pinch laterally over 1–5 m. Individual laminae forming hummocks grade from a base of recrystallized magnetite siltstone to a sand-rich top composed of subangular quartz grains. Thin, planar bedded, sand-rich grainstones demarcate hummocky cross-stratified bedsets, and have a sharp contact with underlying and overlying sand.	Middle shelf deposits below FWWB and above SWB from oscillatory flow (Quin, 2011). Disturbances with coarser grained material and intraclasts a result of storm transport.
F3	Flaser and lenticular bedded magnetite-rich sandstone	Flaser and lenticular bedded sandstone that is green-black in drill core and tan-pink in outcrop. Ripples are composed of very-fine to fine, sub-angular quartz sand with pitted surfaces, and 5-10% subhedral-euhedral magnetite grains in a silt matrix with silica and dolomite-ankerite cements. Laminae are 1-2 mm thick within 3-4 cm thick foresets and are lined with Fe-oxides. F3 contains asymmetrical ripples with mud drapes (flaser bedding) and lenticular bedding. Wavy laminated chemical mudstone drapes are formed of 0.25–2.0-mm-thick layers of interlocking crystals of magnetite. Few occurrences of poorly sorted, distorted bedding contain angular to sub-angular siltstone intraclasts 0.5-2 mm in size, and are 1-5 cm thick. Where F3 is closely associated with stromatolites of F7, hematite is the only iron-oxide present.	Deposition of chemical and clastic sediments in an intertidal to subtidal environment. Varying hydraulic conditions associated with tides produced flaser and lenticular bedding (Boggs, 2006; Dalrymple, 1992; Reinick and Singh, 1980).
F4	Planar laminated hematitic siltstone	Tan to pink siltstone and contains less than 5% sub-angular to sub-rounded very-fine to fine-grained quartz. Quartz grains are well sorted within the silt component and have pitted surfaces, similar to those found in F2 and F3. F4 also contains 10-15% anhedral hematite, and ~10% subhedral muscovite. F4 contains planar, thick laminae to thin beds that exhibit a slight normal grading, and is associated with F2 and F3.	Middle shelf deposit; suspension settling of silt during waning storms (Plint, 2010)
F5	Trough-cross stratified intraclastic grainstone	Trough cross-stratified hematitic grainstone. Sub-angular to rounded grains that are 0.25-2.0 mm in diameter make up 85% of the total composition of F5. Of the grain component of this facies, ~75% are intraclasts. Intraclasts are dominantly chert, with some anhedral and platy Fe-chlorite in the interstices of chert; stilpnomelane is rare. Micro-platy hematite is often found in intraparticle cracks with chert, and at grain boundaries. Minor occurrences of secondary hematite, magnetite and siderite were found within intraclasts. Coated grains in F5 are similar to those found in carbonate systems. Most contain a quartz nucleus, surrounded by discontinuous, wavy laminae. Approximately 5-10% of grains are coated with cortices containing up to ~20 layers, but most commonly 2-5 layers. Composite grains, 1 to 4 mm in diameter, make up less than 5% of the coated grains within F5 and contain 2-	Intertidal channel deposits; intraclasts that originated as an amorphous Fe- and Si-rich gels from F6 were reworked by currents and waves (Pufahl, 2010).

		4 coated grains and/or intraclasts. These grains are rimmed with 1-4 hematitic laminae and are cemented with chert and quartz cements. Discontinuous beds are 10-40 cm thick with erosive bases that reach a lateral extent of 1-3 meters. This contact is concave, and grainstone beds are thicker at the top of F5 compared to the base.	
F6	Laminated cherty iron formation	Pink, green and grey laminated chemical mudstone composed of chert, magnetite, dolomite-ankerite and Fe-chlorite. Planar to slightly undulatory laminae (1 mm to 1.5 cm) of white-red chert alternate with green to black Fe-rich mudstone. Laminae are composed of magnetite, dolomite-ankerite and Fe-chlorite. Grains of the same type described in F5 occur in 1 to 2 cm thick beds and have a sharp, wavy contact with other laminae.	Low energy, anoxic, intertidal environment. Si- and Fe-rich laminae and beds were precipitated with little to no reworking (Pufahl, 2010).
F7	Stromatolitic and microbial siltstone	Stromatolitic and microbial laminated siltstone; stromatolites of the taxa *Pilbaria deverella* and *Windidda granulose.* F7 is a tan, pink and red siltstone containing less than 5% sub-angular to sub-rounded quartz, and 10-20% hematite. Both quartz and dolomite-ankerite cements were found in F7. Wavy laminae, 1-5 mm thick is interbedded with minor amounts of fenestral fabric, occurrences of mudcracks and is closely associated with hematite-rich F3, and F8.	Upper intertidal-supratidal environment. Periods of submergence followed by sediment exposure and subsequence drying to form mudcracks (Boggs, 2006).
F8	Quartz Arenite	White-tan quartz arenite, composed of 90-95% sub-angular to sub-rounded, well sorted very fine to fine grained quartz with pitted surfaces; up to 10% subhedral muscovite and <1% anhedral glauconite, and <1% matrix. Low-angle cross beds, 2-3 cm thick, within 20 to 50 cm-thick bedsets.	Eolian, beach deposit evident by consistent grain size, pitted quartz grains, sorting and low angle stratification (Ekdale and Picard, 1985). Source of detrital quartz in F2, F3 and F4.

5.2 F2 – Hummocky-cross stratified sandstone

Facies 2 (F2) is a hummocky cross-stratified (HCS) silty, very fine-grained quartz-rich sandstone. It is green-black in drill core and tan-pink in outcrop (Fig. 5.2). In three-dimensional exposures bedsets containing abundant low-angle truncation surfaces (<15^{o}) are 10–30 cm-thick and pinch laterally over 1–5 m. Individual laminae forming hummocks grade from a base of recrystallized magnetite siltstone to a sand-rich top composed of subangular, pitted quartz grains. Thin, planar bedded, sand and intraclast-rich beds demarcate hummocky cross-stratified bedsets, and have a sharp contact with underlying and overlying sand.

Interpretation: Facies 2 is interpreted to have accumulated below fair-weather wave base (FWWB) and above storm wave base (SWB) in a middle shelf environment in slightly more shallow water than F1. HCS is a diagnostic feature of storm-dominated shelves and forms under conditions of combined flow (Boggs, 2006). Such flow suspends fine-grained sediment in the water column so that reworking by oscillatory storm waves produces large-scale ripples that coalesce to form hummocks (Dott and Bourgeois, 1982; Quin, 2011). In F2 much of this suspended material was windblown quartz silt and sand from F8 that bypassed deposition in coastal environments; as in F1, evidence for this lies in the consistent very fine to fine sand size of subangular detrital quartz within F2. It is also possible that very-fine to fine grained quartz grains were washed out of nearshore environments and transported to middle-shelf environments, as indicated by the depressed coarse fraction in peritidal lithofacies. The coarser beds separating HCS bedsets are also interpreted as tempestites, but formed of coarser material derived from

shallow-water environments that was transported to the middle shelf during the height of the most severe storms.

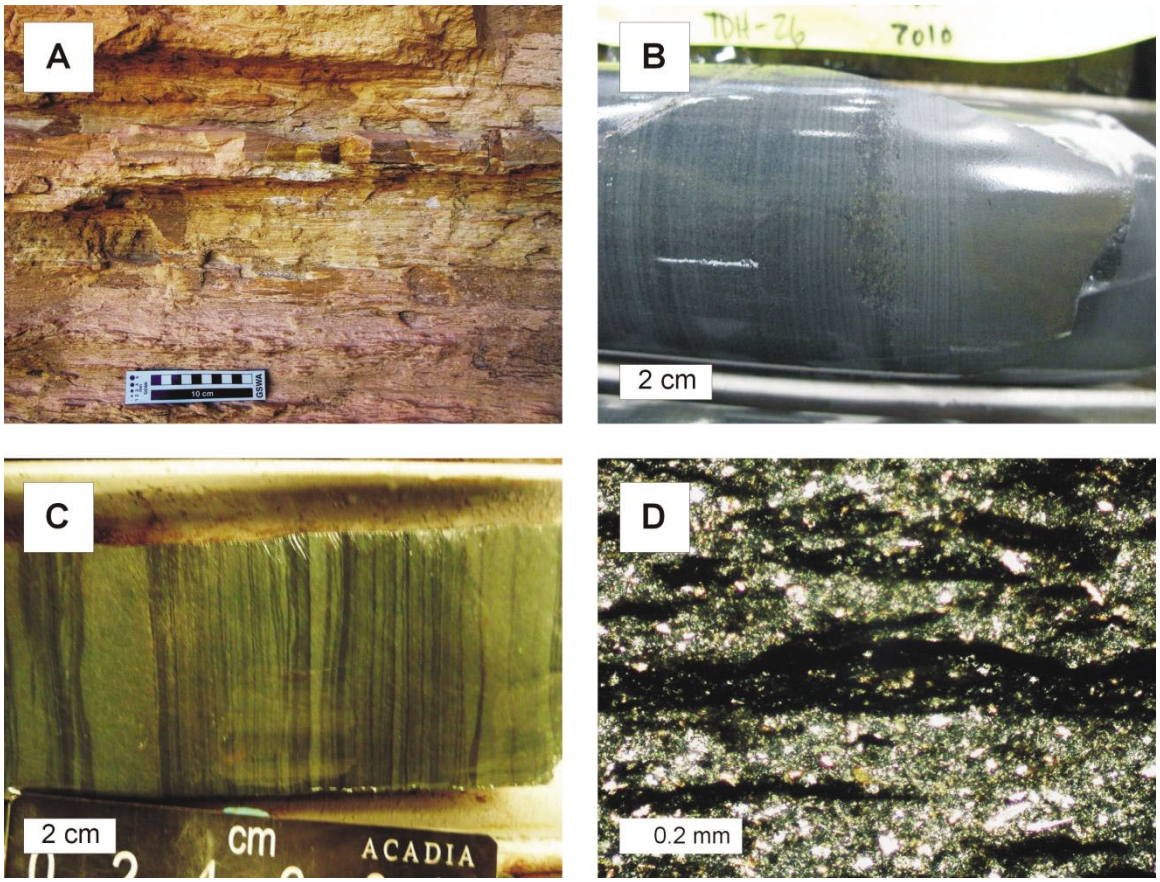

Figure 5.2. Hummocky cross-stratified sandstone. A) Nabberu Creek Section ~46 m; outcrop expression of HCS siltstone. B) TDH-26, ~309 m; coarse interval interpreted as storm deposit between very fine sand and magnetite rich laminae. C) TDH-26, ~214 m; laminae dip at a low angle and appear planar laminated in drill core. D) Photomicrograph of TDH-26 in XPL, 307 m; magnetite-rich laminae alternate with quartz-rich laminae.

5.3 F3 – Flaser and lenticular bedded, magnetite-rich sandstone

Facies 3 is a flaser and lenticular bedded sandstone that is green-black in drill core and tan-pink in outcrop (Fig. 5.3). Ripples are composed of very-fine to fine, sub-angular quartz sand with pitted surfaces, and 5-10% subhedral-euhedral magnetite grains in a silt matrix with chert, quartz, and dolomite-ankerite cement. Laminae are 1-2 mm thick within 3-4 cm thick foresets and are lined with Fe-oxides. F3 contains asymmetrical ripples with mud drapes (flaser bedding) and intervals that are more muddy (lenticular bedding). Wavy laminated chemical mudstone drapes are formed of 0.25–2.0-mm-thick layers of interlocking crystals of magnetite (Fig. 5.2D). Few occurrences of poorly sorted, convoluted bedding contains angular to sub-angular siltstone intraclasts 0.5-2 mm in size, and are 1-5 cm thick. Where F3 is closely associated with stromatolites of F7, hematite is the only iron-oxide present.

Interpretation: F3 is interpreted to reflect deposition of chemical and clastic sediment in an intertidal to shallow subtidal environment. Flaser bedding forms under varying hydraulic conditions associated with tides, where sand accumulates as traction deposits during the higher-energy flood stage of the tidal cycle, and mud is deposited from suspension rain during the ebb flow (Reinick and Singh, 1980; Dalrymmple, 1992; Boggs, 2006). The prevalence of sand in F3 suggests deposition of detrital sand was more prevalent than Fe-rich mudstone precipitation, which explains the lack of thick Fe-rich mudstone in this facies. Chemical mudstone laminae may have formed originally as an Fe-(oxyhydr)oxide from the combination of upwelled Fe^{2+} and oxygen in the water column or close to the sediment-water interface (Pufahl, 2010). The formation of

hematite in close association with stromatolites of F7 suggests precipitation and deposition under suboxic conditions, where nearshore oxygen oases impinged on the shelf.

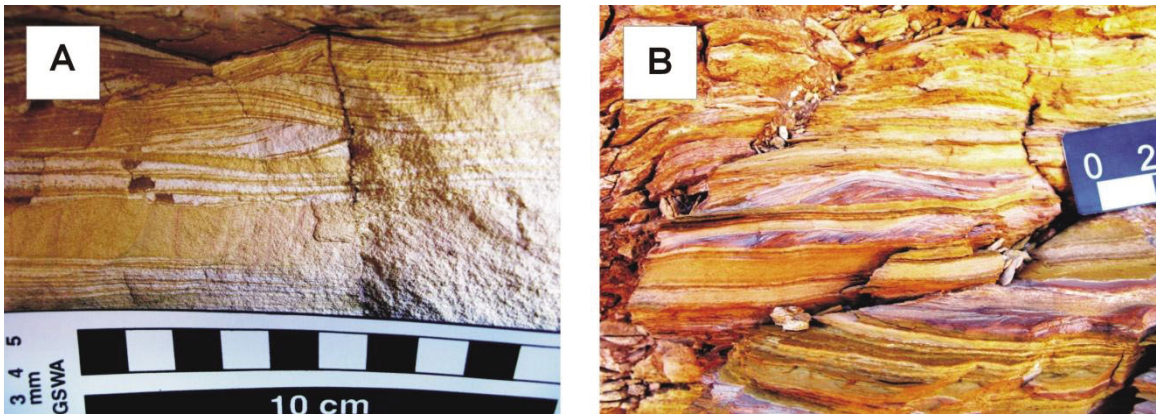

Figure 5.3. Flaser and lenticular bedded sandstone. A) Nabberu Creek Section, ~55 m. Sand-rich laminae outlined with hematite. B) Kingston Section 2, 4.5 m; hematite (pink) located in troughs between ripples.

5.4 F4 – Planar laminated siltstone

Facies 4 (F4) is a tan to pink siltstone and contains less than 5% sub-angular to sub-rounded very-fine to fine-grained quartz sand (Fig. 5.4). Quartz grains are well sorted within the silt fraction and have pitted surfaces, similar to those found in F2 and F3. F4 also contains 10-15% anhedral hematite, and ~10% muscovite. F4 contains planar, thick laminae to thin beds that exhibit a slight normal grading, and is associated with F2 and F3.

Interpretation: Planar laminated siltstone is interpreted to have accumulated in a middle shelf environment based on the fine-grain size and lack of internal cross-stratification (Boggs, 2006). F4 is associated with HCS sandstone of F2 but is not cross-stratified. The normal grading in parallel laminae indicates deposition by waning storms, when fine sand and silt settled out of suspension (Plint, 2010).

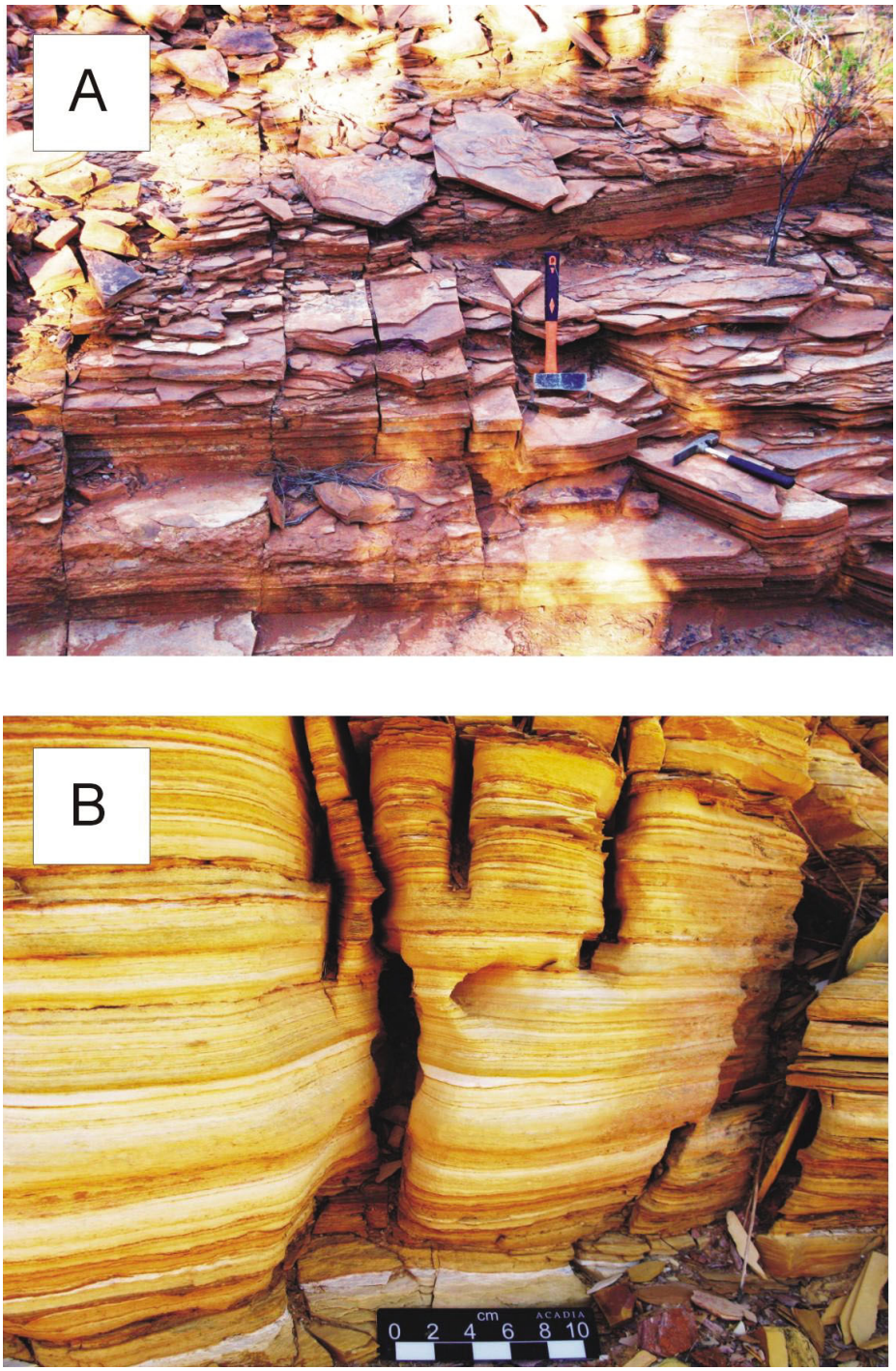

Figure 5.4. Planar laminated siltstone in outcrop. A) Von Treuer Section 1, 51 m; hematite-rich siltstone; B) Kingston Section 2, 5 m; planar laminated siltstone, iron-oxides leached out. Silt and sand content is consistent between the two locations.

5.5 F5 – Trough cross-stratified hematitic grainstone

Facies 5 is a trough cross-stratified hematitic grainstone. Individual troughs are 10-40 cm thick, have erosive bases, and extend laterally 1-3 m (Fig. 5.6). Where F5 is associated with chemical and clastic mudstone of F3 and F6 the contact is marked by pebble-sized intraclasts derived from the underlying deposits.

Sub-angular to rounded grains comprise 85% of the total composition of F5. Grains range between 0.25-2.0 mm in diameter and ~75% are intraclasts. These intraclasts are usually composed of 50-60% chert, but can have a composition of up to 90% chert (Fig. 5.5A). Micro-platy hematite is found in intraparticle cracks, dispersed throughout chert, and at grain boundaries (Fig. 5.5C). Minor occurrences of secondary hematite, magnetite and siderite cross-cut primary original minerals and occur within intraclasts.

Coated grains represent ~25% of the coarse fraction and are of similar appearance to those found in carbonate systems, although they do not necessarily have the same genetic connotations. Most contain a quartz nucleus and cortex composed of discontinuous, wavy layers that alternate between micro-platy to globular hematite and quartz. Cortices generally contain 2 to 5 layers, but 5 to 10% of grains possess cortices containing up to ~20 layers. Composite grains, 1 to 4 mm in diameter make up less than 5% of the coated grains within F5, and contain 2 to 4 coated grains and/or intraclasts (Fig. 5.5E, F). Composite grains are rimmed with 1 to 4 hematitic laminae.

Pore spaces are completely occluded with 1 to 4 generations of isopachous chalcedony and quartz cements. Where drusy quartz fills pores it is characterized by a decrease in crystal size from the pore walls inward. Anhedral and platy Fe-chlorite

commonly occurs between grains, enveloped by quartz cements, and replacing grain centers. Stilpnomelane is also present within interparticle pores, but is a rare constituent (Fig. 5.5D).

Interpretation: Trough cross stratified intraclastic grainstones of F5 are interpreted as tidal channel deposits that erosively scoured intertidal-subtidal deposits as channels migrated laterally across the tidal flat (Dalrymple, 2010). Intraclasts composing granular beds were formed when tidal currents and storms reworked chemical muds into grains (Pufahl, 2010;). This is indicated by the similarity in mineralogy between intraclasts from F5 and associated lithofacies (F3, F6). Intraclasts are interpreted as originating from a suboxic environment where precursors to chert, hematite and Fe-Mg-Al silicates precipitated in the water column or seafloor (Pufahl, 2010). Coated grains are interpreted to originate from the same intertidal environments, but in an area where intraclasts could roll through chemical muds to produce multiple generations of laminae (Pufahl, 2010). The lateral and vertical extent of trough cross-stratified beds within channels indicates intraclasts and coated grains were deposited through the migration of large-scale, subaqueous dunes (Boggs, 2006). Multiple generations of isopachous silica cement, along with the preservation of an open, grain-to-grain fabric suggests cementation occurred early in its diagenetic history (Dimroth and Chauvel, 1973).

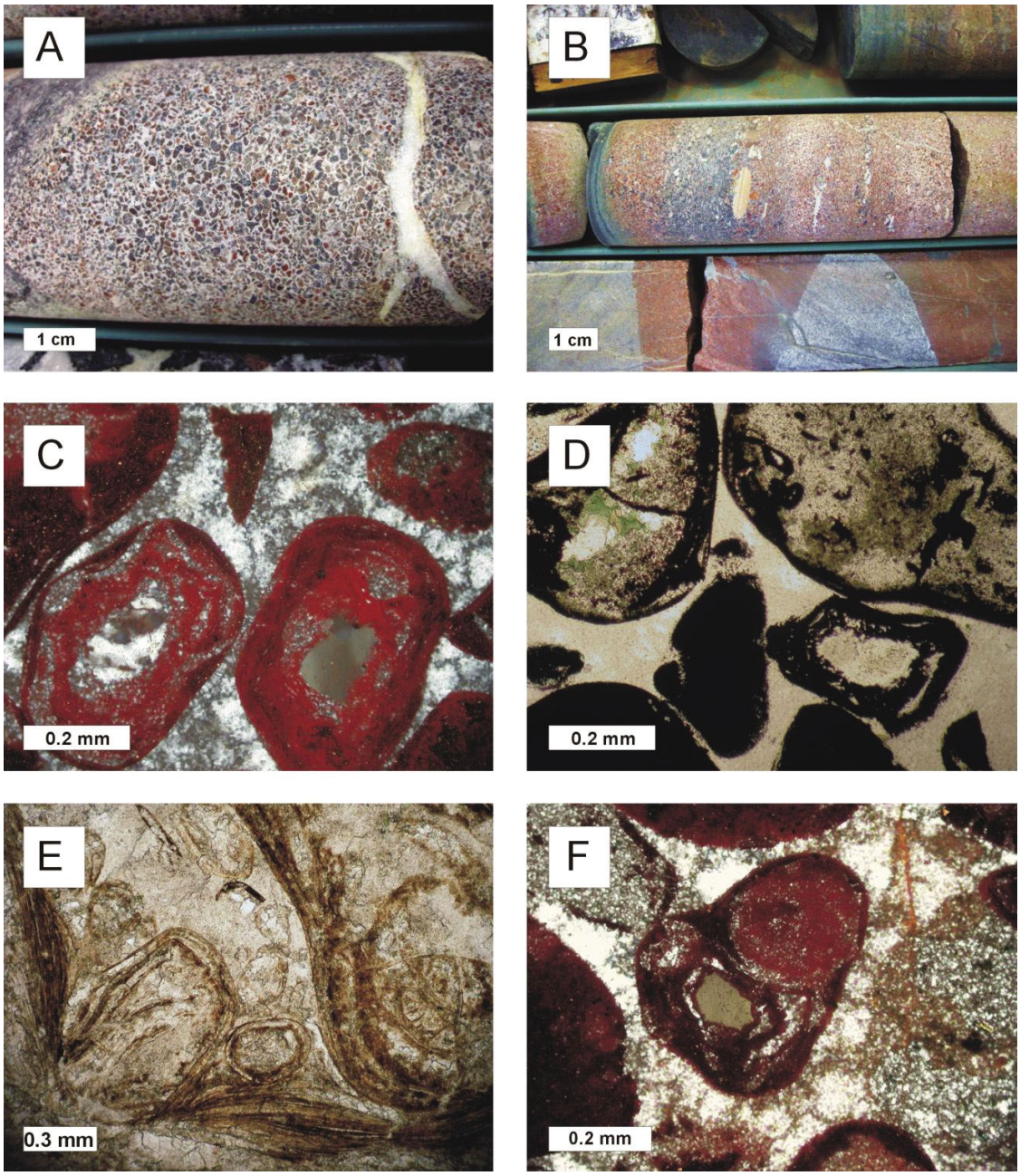

Figure 5.5. Trough cross-stratified hematitic grainstone. A) TDH-26, 384 m in drill core. B) TDH-26, 245 m (up direction to the right); intraclasts near base of contact with F3. C) Photomicrograph of TDH-26 in CPL and reflected light (RL), 155 m; sub-rounded coated grains with non-concentric lamina and angular intraclasts, surrounded by chalcedony cement. D) Photomicrograph of TDH-26 in PPL, 155 m; intraclasts showing internal Fe-chlorite (green), minor stilpnomelane (fine-grained brown), and chert component. Black grain-rimming material is hematite. E) Photomicrograph of TDH-26 in PPL, 389.1 m; composite grain containing multiple coated grains outlined with hematite. F) Photomicrograph of TDH-26 in CPL and RL, 155 m. Composite grain containing a rounded peloid, and a coated grain with a quartz nucleus, within a hematite-rich intraclast.

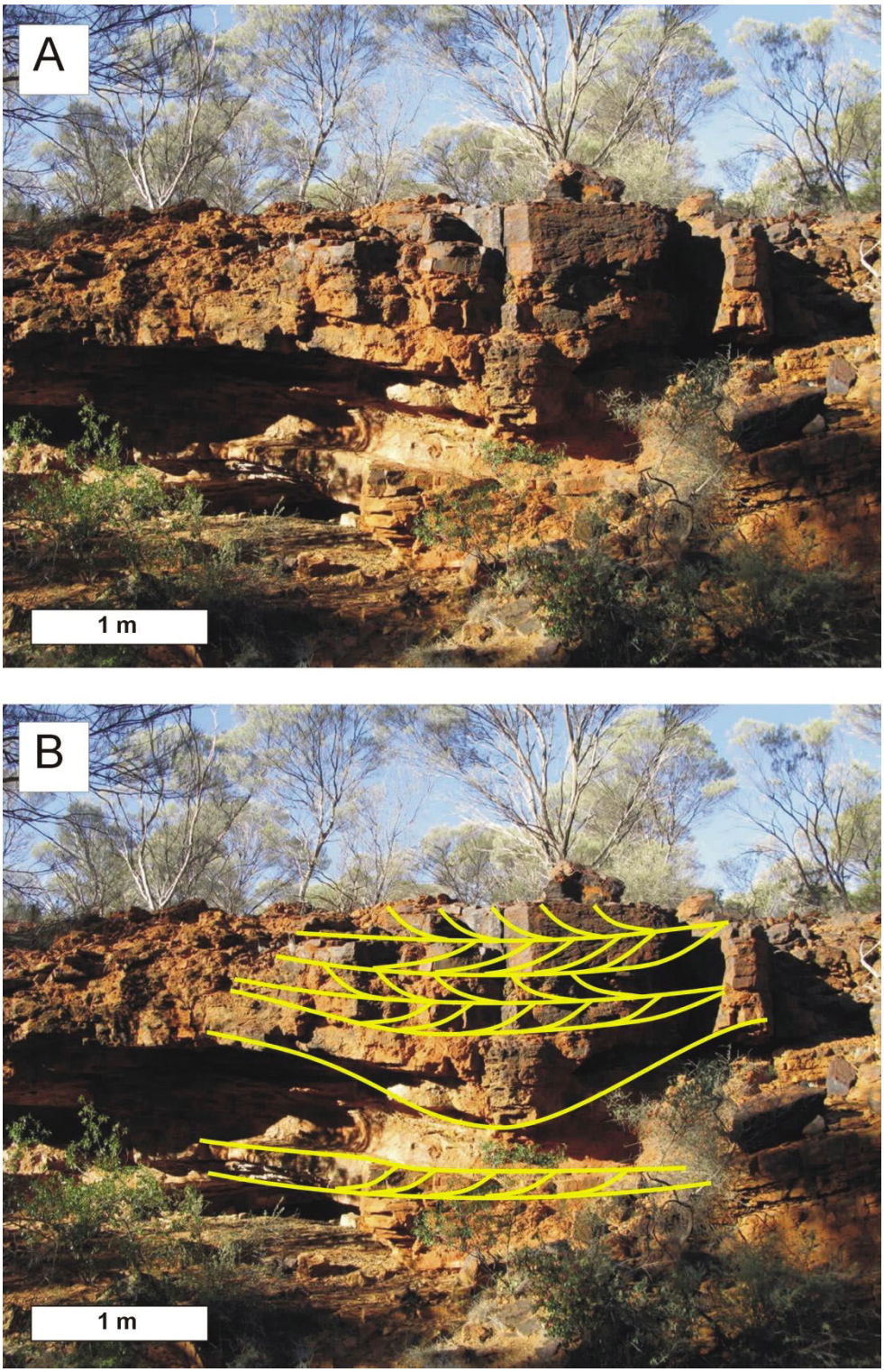

Figure 5.6. Von Treuer Section 1 trough cross stratified hematitic grainstone; outcrop expression of relationship between F3 and F5. Grainstone beds with a concave base scour into F3 and often contain rip up clasts of the underlying unit.

5.6 F6 – Laminated cherty iron formation (pristine iron formation)

Facies 6 is pink, green and grey wavy laminated to thinly bedded chemical mudstone composed of chert, magnetite, dolomite-ankerite and Fe-chlorite (Fig. 5.7). Pink chert layers are 1-15 mm thick and are interlaminated with 1-5 mm thick, green to grey layers of magnetite, dolomite-ankerite and Fe-chlorite. Hematitic, intraclastic grainstone beds punctuate these chemical mudstones. Beds are 1-2 cm thick, very slightly normally graded, and have sharp basal contacts (Fig. 5.7C). Grain textures and compositions are identical to those in F5.

Interpretation: The depositional environment for F6 is interpreted as the low-energy intertidal flat between active tidal channels. The presence of magnetite, Fe-chlorite, and dolomite within some laminae suggest that shallow pools where Fe-(oxyhydr)oxides were precipitating were anoxic (Klein, 2005; Pufahl, 2010). Laminated chert within F6 is interpreted to have formed in intertidal ponds from the evaporative concentration of silica (Maliva et al., 2005; Pufahl, 2010). This is analogous to the precipitation of evaporite minerals observed in supratidal-upper intertidal environments in arid settings (Boggs, 2006). Grainstone beds likely reflect storm reworking and transport of *in situ* anoxic sediments as well as hematitic deposits from suboxic peritidal environments.

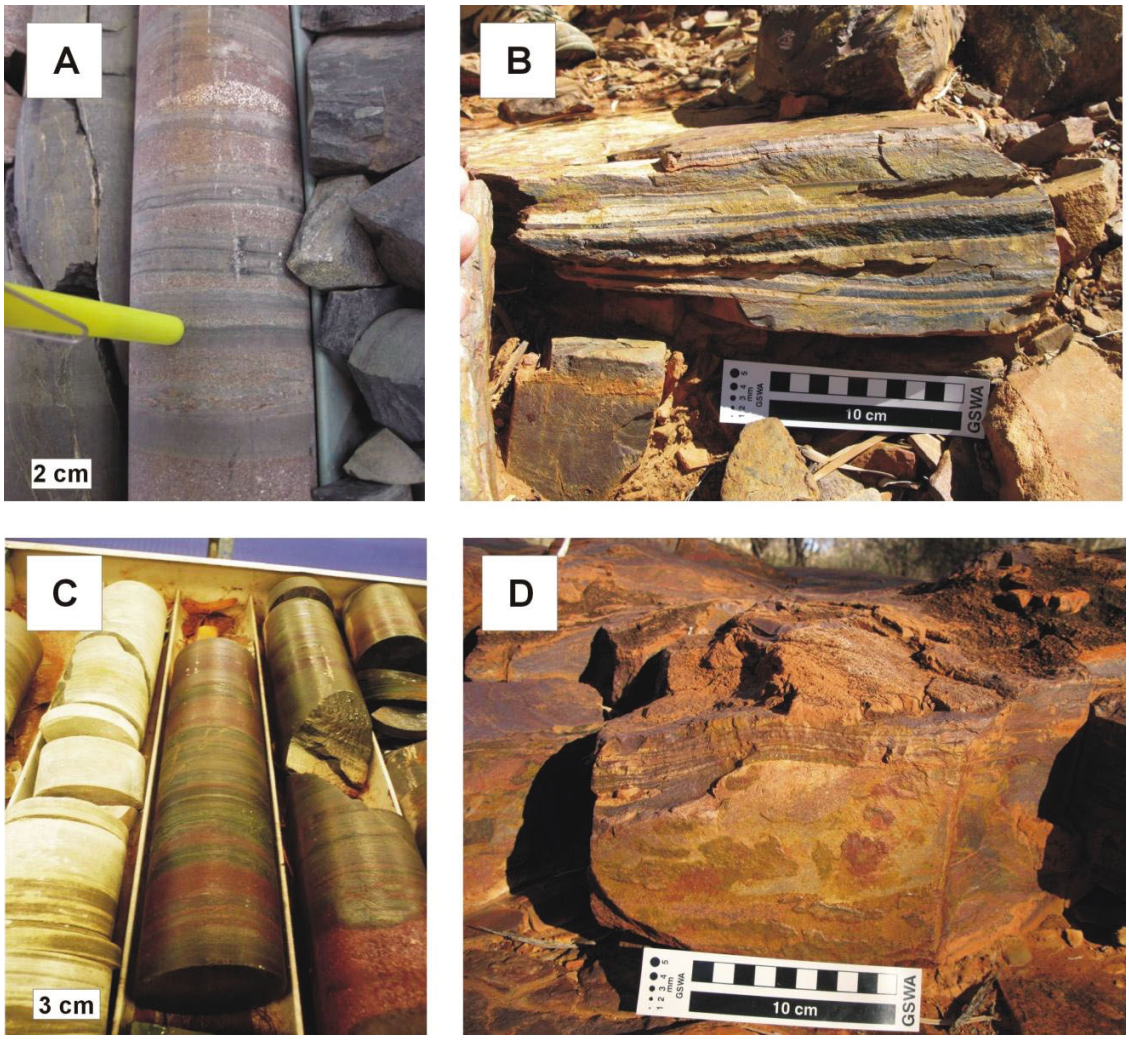

Figure 5.7. Laminated cherty iron formation in outcrop and drill core. A) TDH-26, ~258 m; alternating thick lamina-thin beds of hematite-rich grainstone and magnetite-rich mudstone. B) Nabberu Creek Section, ~85 m; alternating thick lamina-thin beds of jasper, chert and grainstone. C) TDH-26, ~175m. D) Von Treuer Section 1, ~41 m; F6 overlying domal stromatolite.

5.7 F7 – Stromatolitic and microbial laminated siltstone

Facies 7 is characterized by domal stromatolites of the taxa *Pilbaria deverella* and *Windidda granulosa* (Price, 2003; Fig. 5.8B). Interbedded microbial laminated siltstone (Fig. 5.8A,C) is either tan, pink or red and contains less than 5% sub-angular to sub-rounded quartz, and 10-20% hematite. Microcrystalline chert and dolomite-ankerite are the dominant cement types. F7 is also mudcracked (Fig. 5.9) and contains a well developed fenestral porosity, especially when associated with F3.

Interpretation: F8 is interpreted as having accumulated in a lower supratidal to upper intertidal environment, adjacent to intertidal ponds. The stromatolites, microbial, layering, abundance of mudcracks and the development of fenestral pores are all attributes of deposition in shallow peritidal settings that experienced periods of subaerial exposure (Pratt, 2010; Boggs, 2006).

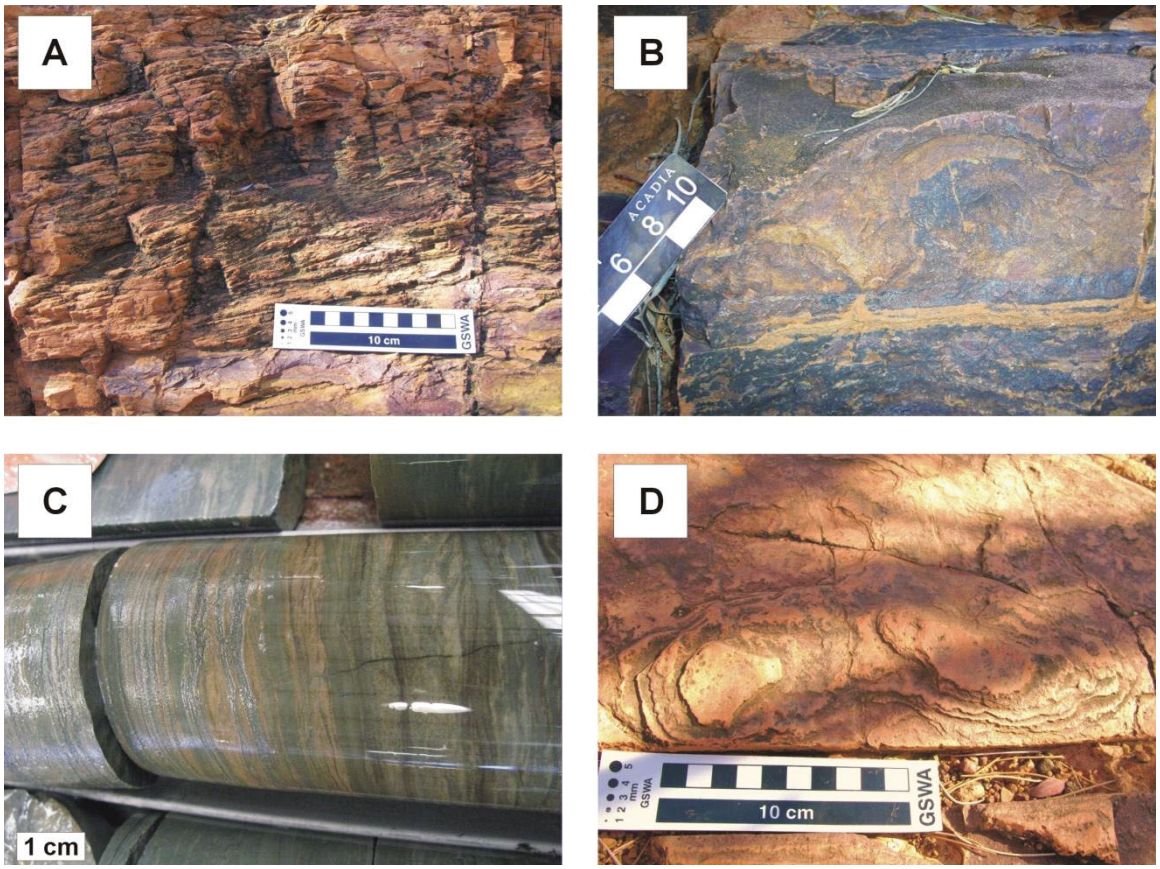

Figure 5.8. Stromatolitic and microbial laminated siltstone in outcrop and drill core. A) Nabberu Creek Section, ~3 m; microbial laminated siltstone. B) Nabberu Creek Section, ~10 m; cross section of stromatolite. C) TDH-26, 194 m; drill core expression of microbial laminated siltstone. D) Von Treuer Section 1, ~43 m, plan view of stromatolitic siltstone showing eroded tops of domal stromatolites.

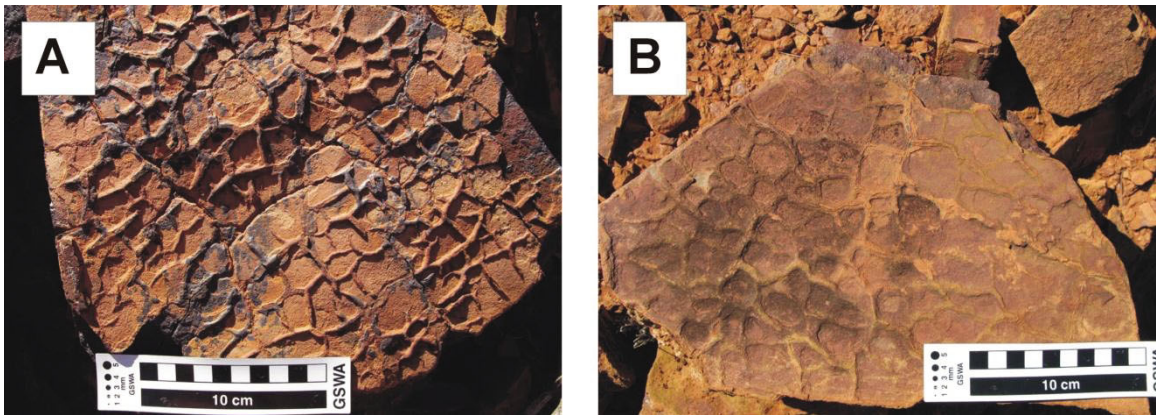

Figure 5.9. Mudcracks of Facies 7. A) Von Treuer Section 1, 43 m; B) Von Treuer Section 2, 17 m. Both photos show three-dimensional surfaces containing mudcracks in outcrop, associated with a supratidal-upper subtidal environment in an arid setting.

5.8 F8 – Quartz arenite

Facies 8 (F8) is a white-tan quartz arenite, composed of 90-95% sub-angular to sub-rounded, well sorted, very fine to fine-grained quartz sand with pitted surfaces. There is up to 10% subhedral muscovite and <1% rounded glauconite and <1% matrix. F8 contains low-angle cross beds, 2-3 cm thick, found in 20 to 50 cm-thick bedsets. It is closely associated with F3 and F7. Similar pitted detrital quartz grains are abundant in F2, F3 and F4.

Interpretation: Cross-bedded quartz arenite is interpreted to record the progradation of eolian dunes across supratidal and intertidal environments. Evidence for eolian transport includes: the consistent grain size and sub-rounded to sub-angular nature, distribution throughout the siltstone, lack of matrix, low-angle cross-stratification, and pitted grain surfaces (Fig. 5.10; Ekdale and Picard, 1985). In terrestrial and upper supratidal environments, mud and silt-sized grains are easily winnowed by wind, leaving sand-sized grains to be organized into dunes. Pitted surfaces are diagnostic of windblown sediment and reflect the bombardment from other grains during transport. Such a process can only occur when water is not available to act as a barrier between grains in a subaqueous environment (Reineck and Singh, 1980). The fine-grained nature and the abundance of pitted, detrital quartz grains in F2, F3 and F4 further suggests that much of the clastic sediment on the Frere shelf bypassed the nearshore and was carried to deeper water environments by the wind.

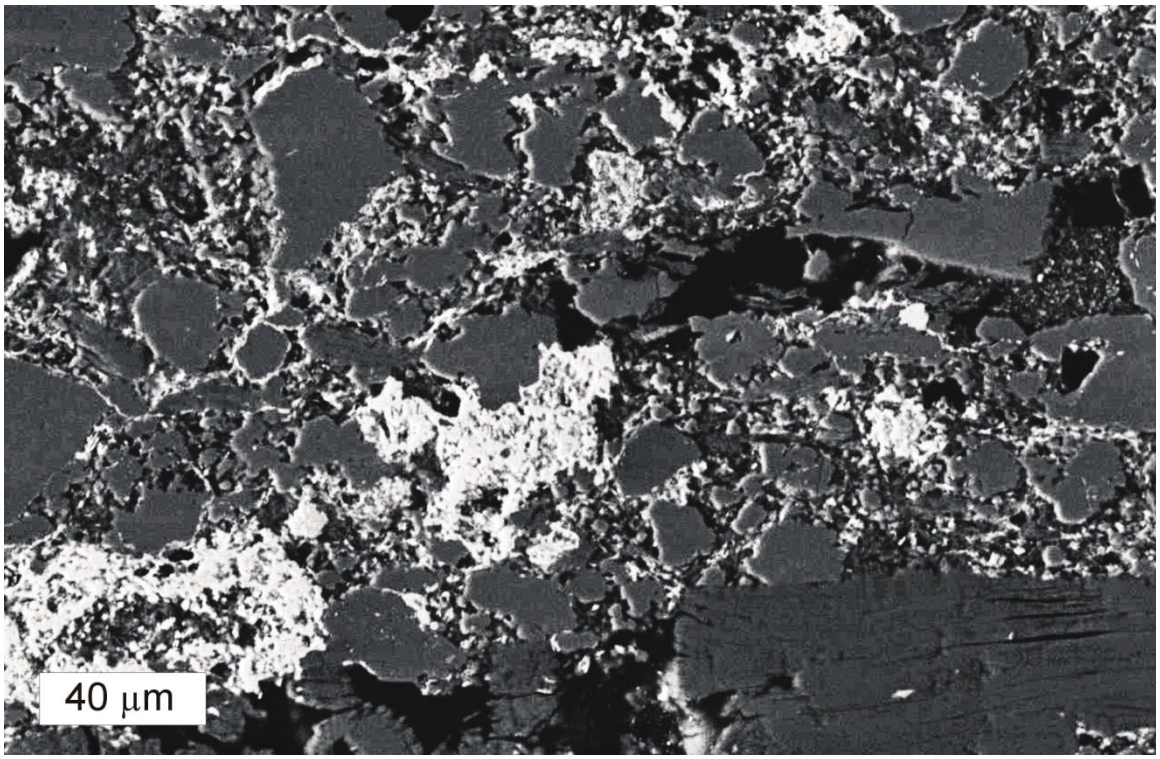

Figure 5.10. Backscatter electron image of Von Treuer Section 1 quartz arenite. Silt to very fine sand shows pitted surfaces indicating eolian transport. Porosity shows up black (Carbon-coated slides).

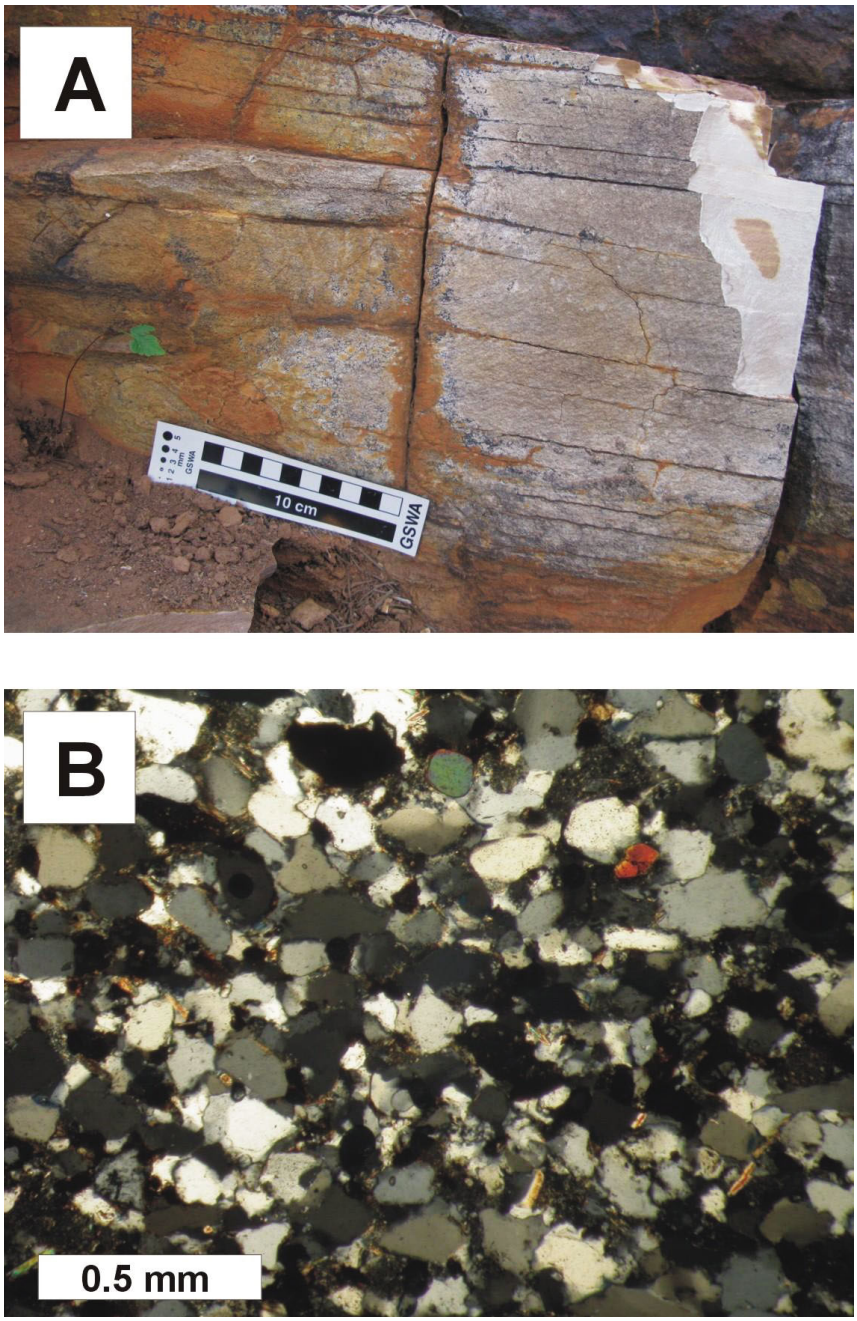

Figure 5.11. Quartz arenite (F8). A) Von Treuer Section 1, ~1m; quartz arenite with low-angle cross-stratification; B) Photomicrograph from Von Treuer Section 1, ~11m in CPL; sub-rounded to sub-angular quartz grains, minor matrix constituent. Evidence of moderate burial shown with sutured grain contacts.

CHAPTER 6: SEQUENCE STRATIGRAPHY

Sequence stratigraphy defines lithofacies within a chronostratigraphic framework in order to establish the relationship between relative sea level and depositional environments through time (Johnson and Murphy, 1984; Posamentier and Vail, 1988; Galloway, 1989; Coe et al., 2003; Catuneanu et al., 2009). Vertical and lateral lithofacies stacking patterns within the Frere Formation are interpreted to record an overall marine transgression punctuated by higher-order fluctuations in relative sea level (Fig. 6.1). Transgressive sediments rest directly on a prominent disconformity between the underlying Yelma and overlying Frere formations (Pirajno et al., 2009; this study). Reworked pebbles from the underlying Yelma Formation characterize this sequence boundary, which is interpreted to represent a significant period of subaerial exposure. Because hydrothermal Mississippi Valley Type (MVT) mineralization cross-cuts the underlying Yelma Formation, but does not extend into the overlying Frere Formation, this unconformity is interpreted to represent a substantial amount of missing time.

During marine inundation higher-order fluctuations in relative sea level produced at least five parasequences (Fig. 6.2). Each parasequence is a decameter-scale aggradational succession of iron formation and clastic sediments reflecting a gradual change from subtidal to peritidal deposition. The contact between parasequences is the sharp transition between underlying shallow and deeper water lithofacies. Defining a parasequence in this way permits interpretation of the range of allocyclic and autocyclic depositional processes producing cycles without the need to identify "classic" marine flooding surfaces (Catuneanu et al., 2009), which is difficult in shallow-water paleoenvironments. *Sensu stricto* flooding surfaces form in middle and distal shelf

environments and are characterized by submarine erosional surfaces, hardgrounds, or basinal muds, which are often not present within peritidal environments (Van Wagoner et al., 1988). This definition is also too restrictive because it is derived from terrigenous clastic depositional systems and thus does not consider the effects of changing seawater chemistry or rates of clastic and chemical sedimentation on parasequence development (Catuneanu et al., 2009).

Parasequences within the Frere Formation are considered second-order cycles, and are the building blocks of the transgressive systems tract (TST) and high stand systems tract (HST). These systems tracts represent a first-order, depositional sequence (Figs. 6.1, 6.2). Because the length of time to produce cyclicity in the Frere Formation is unknown, the hierarchical nature of cycles is used only as an aid in stratigraphic correlation and for understanding depositional processes.

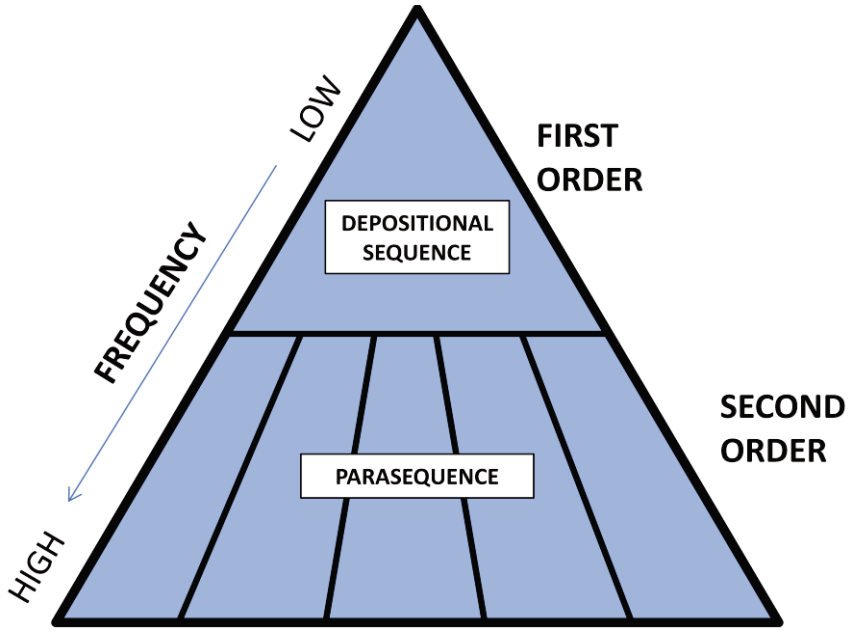

Figure 6.1. Hierarchy of stratigraphic orders used to relate stratigraphic relationships observed in the Frere Formation. Five parasequences (second-order) are the building blocks of the TST and HST, and are nested in the overall depositional sequence (first-order; modified after Catuneanu et al., 2009).

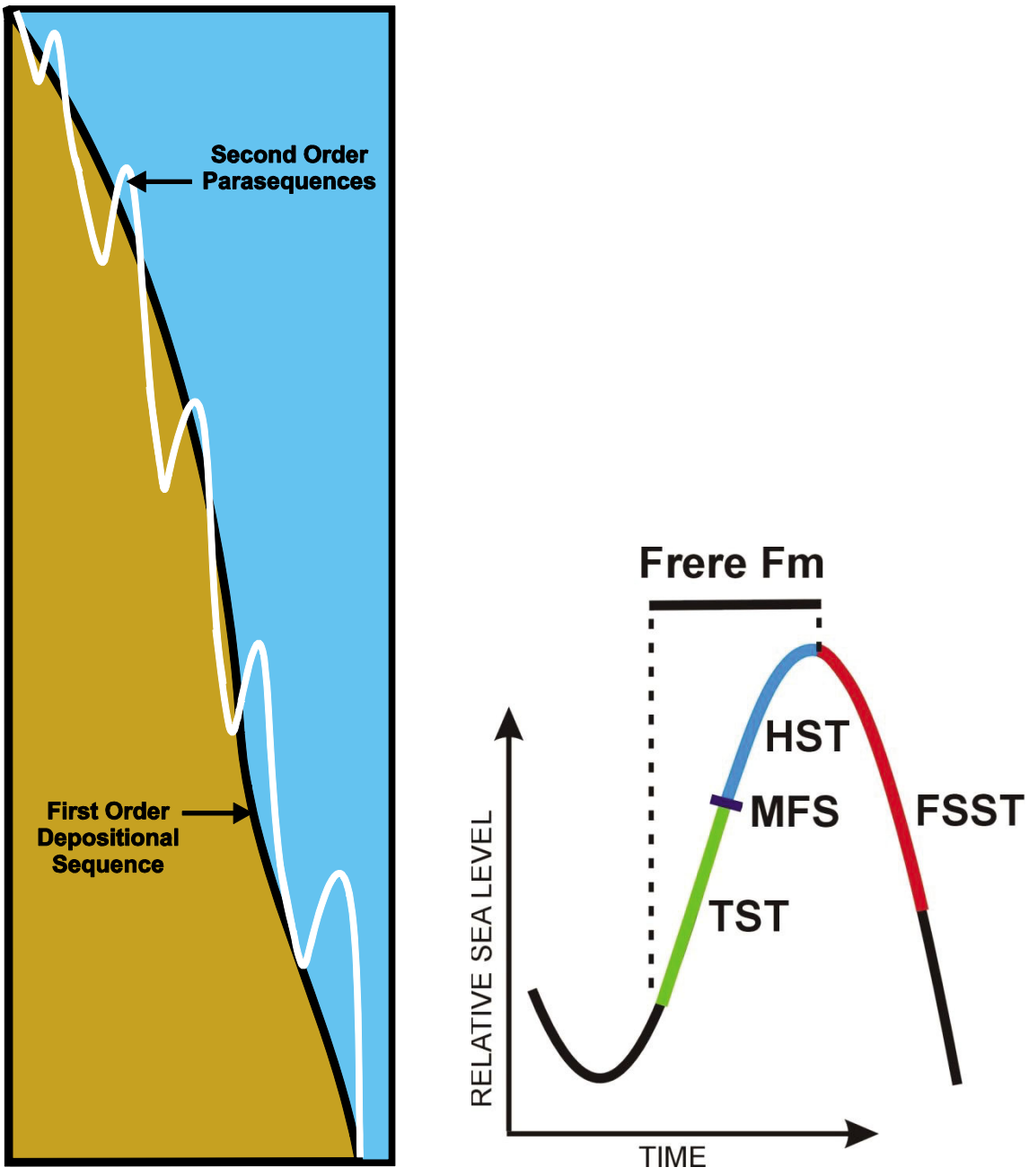

Figure 6.2. (*Left)* Orders of sea-level change within the Frere Formation. First order sea-level change shows an overall transgression. Second-order, higher frequency curves are superimposed on the first-order curve. *(Right)* Deposition of the Frere Formation occurred during a TST and HST separated by a max-flooding surface (MFS); the falling stage systems tract (FSST) is not preserved in continuous stratigraphic sections of the Frere Formation.

6.1 Transgressive systems tract (TST)

The TST consists of interbedded peritidal and shallow subtidal lithofacies that blanket the basal bounding unconformity with the Yelma Formation. It is 150–170 m thick and formed of three parasequences. At the base of the TST, Parasequence 1 (Figs. 6.3, 6.5, 6.6; TDH-26, TDH-28) is generally 30 to 55-m-thick and initiates with eolian dunes (F8) that prograded into supratidal and intertidal environments. These flaser and lenticular bedded sandstone (F3) and hematitic siltstone (F4) are transitional into either tidal channel (F5) or granular shoreface deposits (F6). Where tidal channels overlie these peritidal lithofacies the contact is a scoured surface that is interpreted to have been created when subaqueous grainstone dunes (F5) incised tidal flats as accommodation space filled. Paleocurrent data measurements from trough-cross stratified grainstone (F5) in Von Treuer section indicate a N-NE directed flow, which is consistent with the interpretation of a paleoshoreline that strikes NNW-SSE (Fig. 6.4).

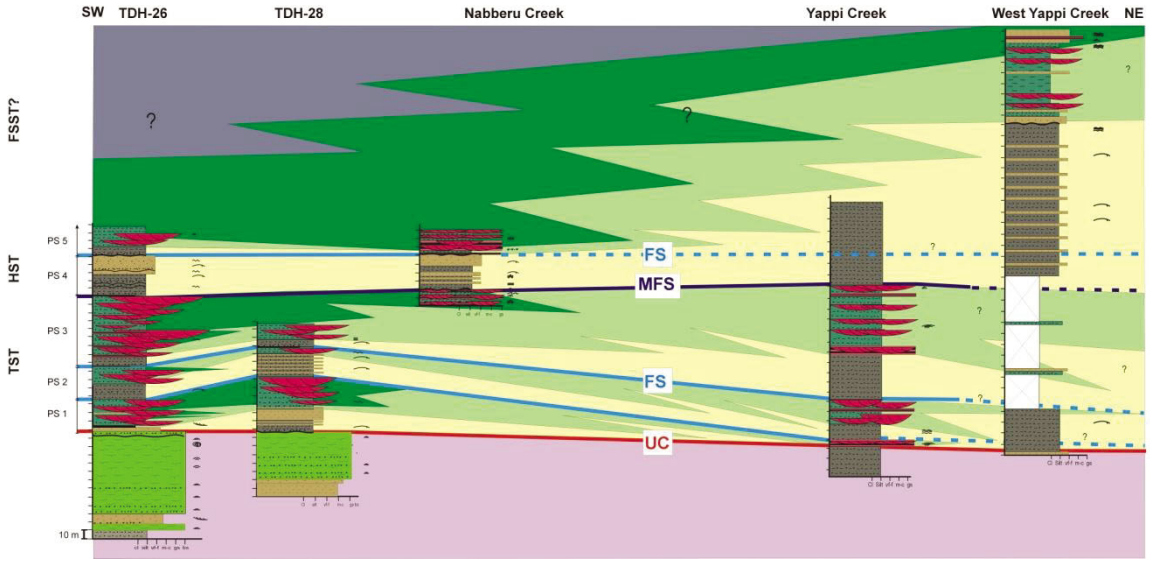
SW
TDH-26
TDH-28
Nabberu Creek
Yappi Creek
West Yappi Creek
NE
FSST?
HST
TST
PS 5
PS 4
PS 3
PS 2
PS 1
FS
MFS
FS
UC
10 m

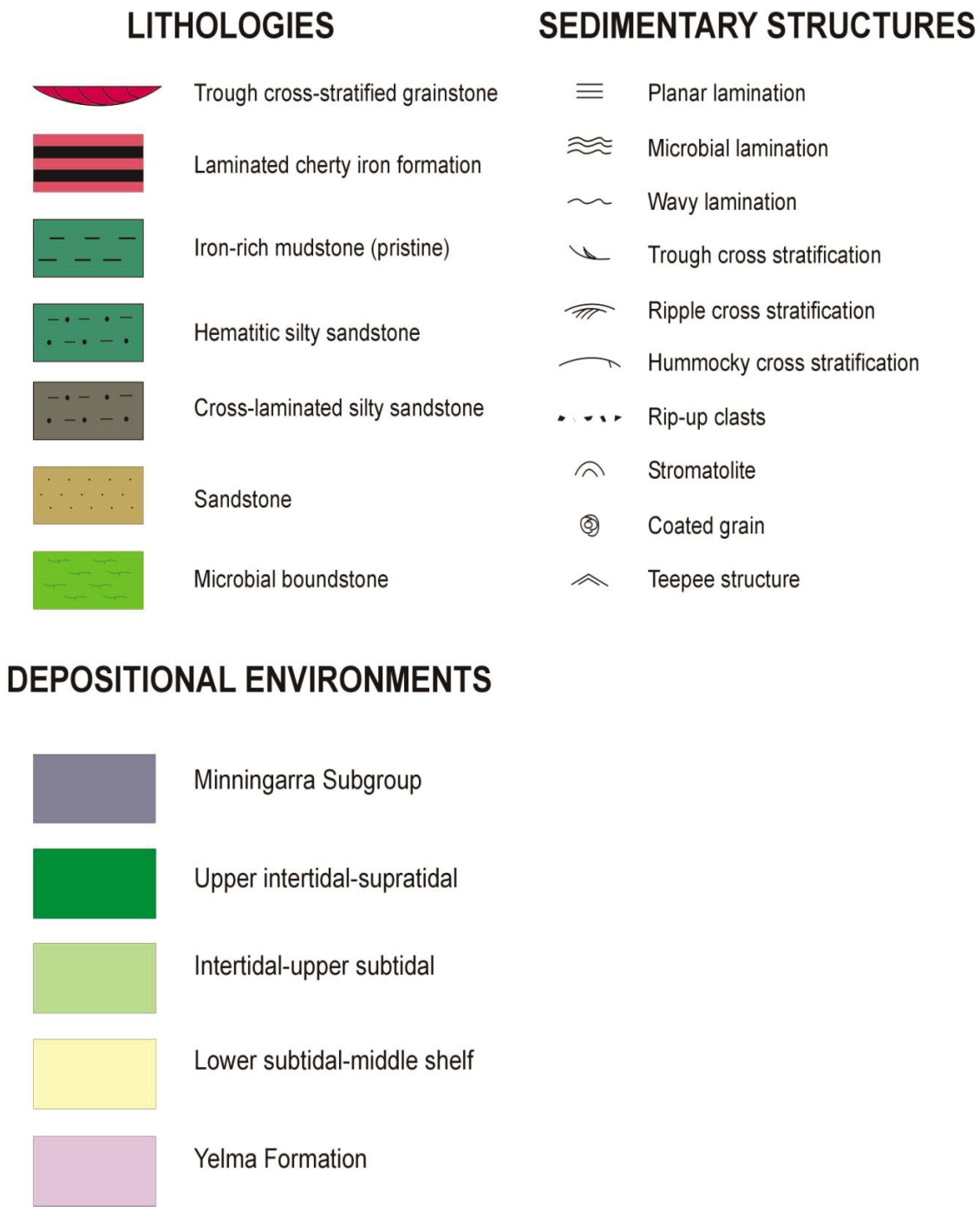

Figure 6.3. Stratigraphic correlation of lithofacies within the Frere Formation. Datum used for correlation is the contact between the Yelma and Frere formations. Legend includes the key for lithologies, sedimentary structures and interpreted paleoenvironments used in the regional stratigraphic correlation and all stratigraphic columns within this study. FS=flooding surface; MFS=maximum flooding surface; UC=unconformity; TST=transgressive systems tract; HST=high stand systems tract; PS=parasequence.

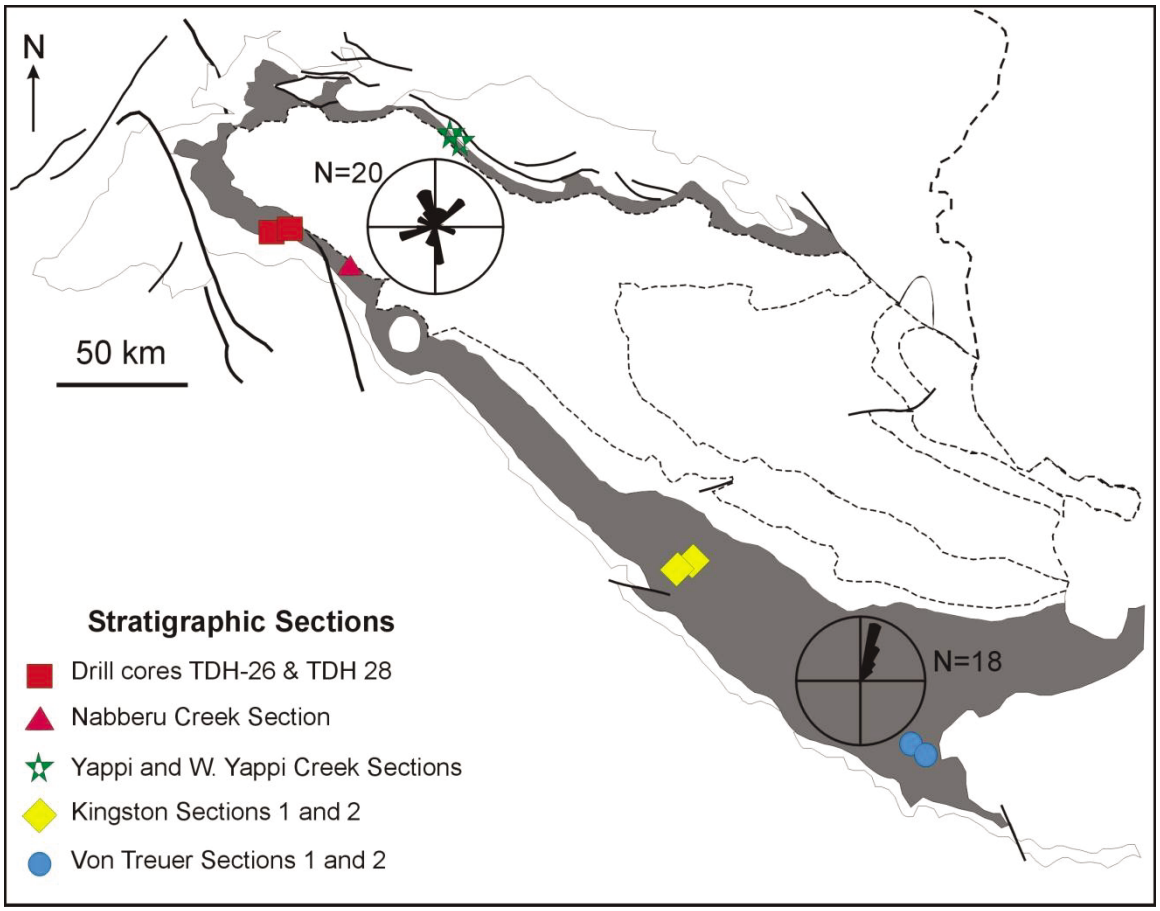

Figure 6.4. Location of stratigraphic sections measured through the Frere Formation. Paleocurrent rose diagrams show data collected from Nabberu Creek and Von Treuer 1 sections.

Parasequence 2 is 35 to 40-m-thick and consists predominantly of silt and magnetite-rich, HCS and ripple-laminated sandstone (F2, F3) that is overlain by hematitic, supratidal and intertidal deposits (F5, F6, F7; Figs. 6.3 and 6.5) similar to those in Parasequence 1. Petrographic characteristics (pitted surfaces, angular shape) of the abundant quartz grains composing HCS sandstone suggest an eolian source for this storm-reworked sediment. Such an interpretation is consistent with the chemical-dominated nature of shallow-water lithofacies and the conspicuous absence of appreciable terrigenous clastic sediment in peritidal paleoenvironments.

Parasequence 3 is 85 to 110 m thick and records the change from pure aggradation to progradational stacking of lithofacies (Fig. 6.3). Such a change is interpreted to reflect the decrease in accommodation volume associated with the onset of highstand conditions (Fig. 6.5). Thus, the top of Parasequence 3 is interpreted as the maximum flooding surface. In outcrop the MFS scours F5 and F6, is heavily silicified, and is overlain by F2 and F3. In drill core the MFS is organic- and magnetite-rich, and is underlain and overlain by the same facies identified in outcrop. Also demarcating the MFS is a hardground surface composed of angular, reworked intraclasts from underlying lithofacies (F8, F7). This scoured surface is interpreted to record a period of arrested or net negative sedimentation when windblown clastic sediment could not be transported to distal shelf environments during highstand conditions.

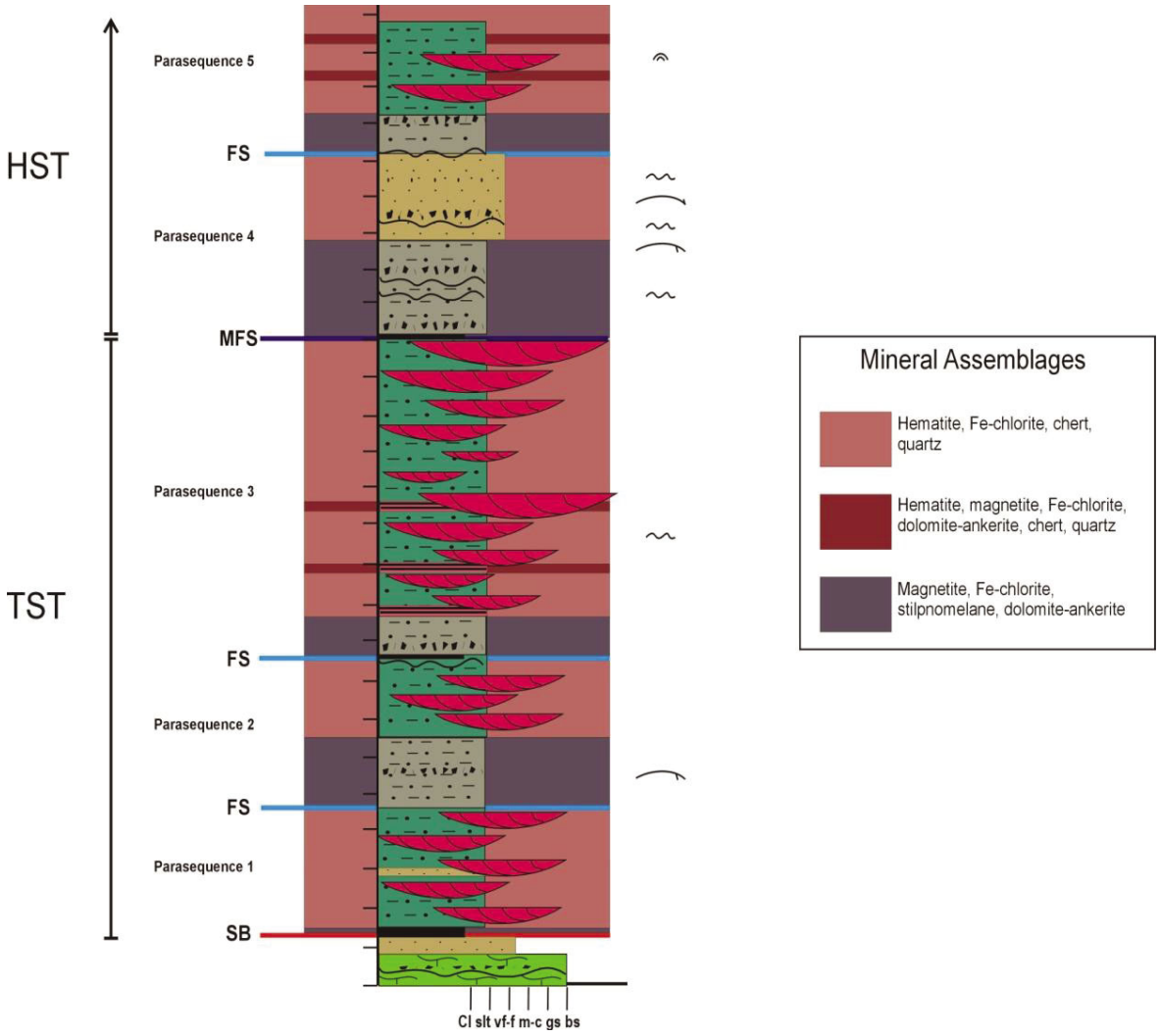

Figure 6.5. TDH-26 stratigraphic column displaying the five parasequences within the most complete section through the Frere Formation. Parasequence 1, 2 and 3 are within the TST, and Parasequences 4 and 5 are in the HST. (SB= sequence boundary; FS= flooding surface; MFS= maximum flooding surface). Mineral assemblages associated with each lithofacies are shown in key and closely relate to their interpreted paleoenvironment. Note: Dark red is associated with F6 and contains both hematite and magnetite.

6.2 Highstand systems tract (HST)

The HST is formed of two stacked progradational parasequences (Figs 6.3, 6.5, 6.6; TDH-26, Nabberu Creek). Parasequence 4 is 40-m-thick in proximal settings and up to 140-m-thick in middle shelf settings (Figs. 6.3, 6.6). It generally reflects shallowing and basinward migration of storm deposits (F2, F4) on the middle shelf. In more proximal areas the HCS and wavy bedded, fine-grained sandstone is transitional into intertidal mudstone and grainstone (F3) as well as eolian dunes (F8). Paleocurrent data from trough cross-stratified dunes in tidal channels indicate a N-NW directed flow (Fig. 6.4).

Parasequence 5 is the uppermost parasequence preserved within the Frere Formation (Fig. 6.3, 6.5; TDH 26, Nabberu Creek, West Yappi Creek). This parasequence is ~40 m thick in proximal sections, ~80 m in distal sections, and is interpreted to record further shallowing through loss of accommodation during late highstand conditions. Storm deposits containing clastic material are found at the base of the parasequence, but are thinner than overlying peritidal deposits. These hematite-rich, stromatolitic supratidal and tidal flat sediments (F5, F6) are 35 to 45 m thick and indicate the development of a suboxic seafloor beneath long-lived, nearshore oxygen oases.

The remainder of the HST and the entire FSST is missing due to post-depositional erosion prior to, or after, deposition of the Chiall Formation of the Minningarra Subgroup. Whilst not preserved in continuous stratigraphic context, the spatial relationship of stromatolites in the overlying Windidda Member suggests dramatic shallowing and development of a poorly preserved falling stage systems tract (FSST).

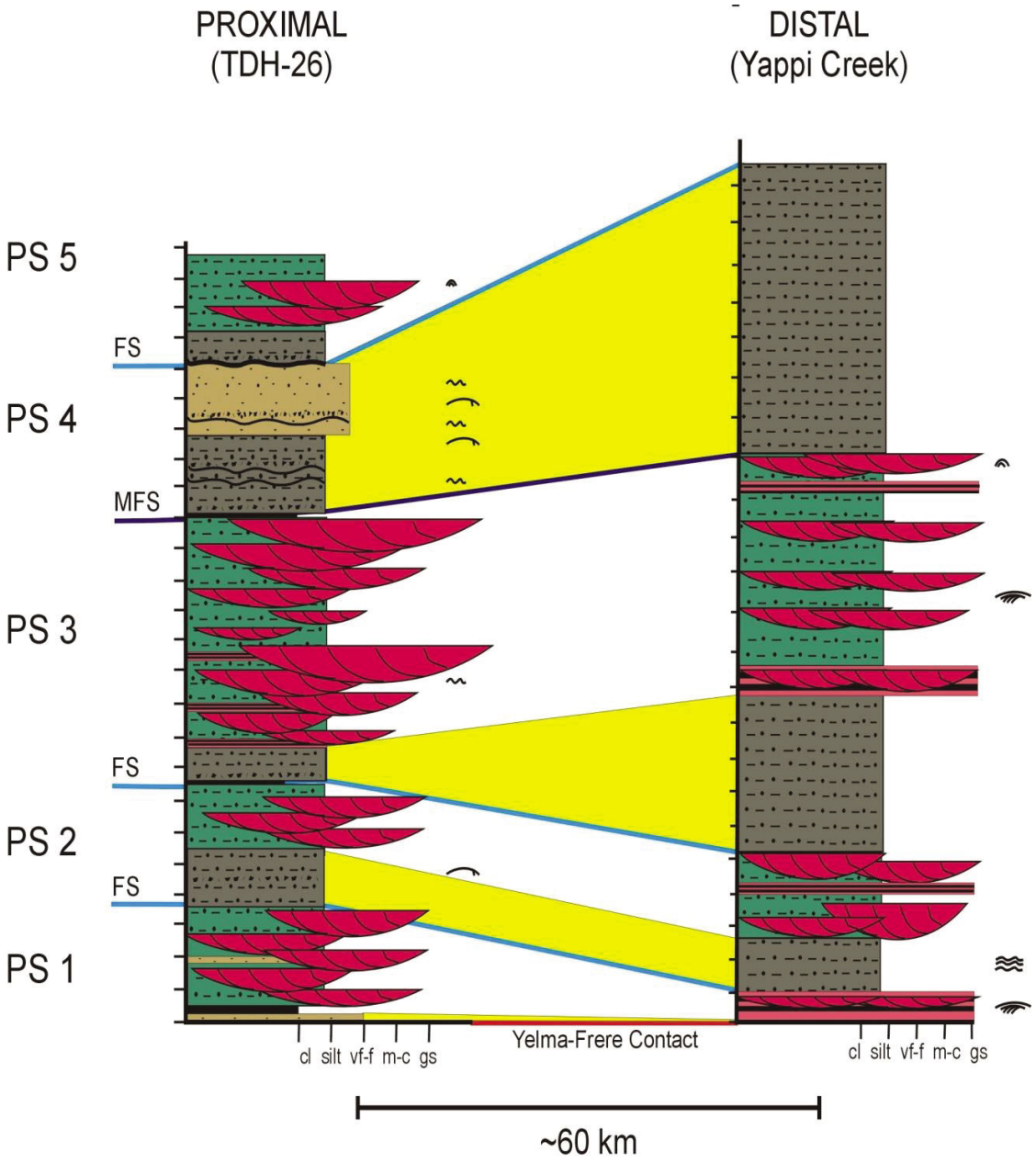

Figure 6.6. Distribution of clastics using TDH-26 as a proximal section and Yappi Creek as a distal section. Clastic-dominated facies (F2, F3 and F4, highlighted in yellow) thicken distal to the interpreted paleoshoreline. The thickest interval of clastic-dominated facies occurs in Parasequence (PS) 4, after the maximum flooding surface (MFS).

6.3 Summary

Continuous stratigraphic sections through the Frere Formation show five parasequences indicative of both the transgressive and high stand systems tracts during an overall marine transgression. The TST is characterized by three parasequences (Parasequence 1, 2, 3) that contain lithofacies representative of storm-dominated middle shelf deposits that shallow upward into intertidal and supratidal deposits. The top of the TST is a MFS, demarcated by a heavily silicified magnetite and organic-rich mudstone and hardground surface. The HST contains two progradational parasequences (Parasequence 4 and 5) that change from storm-dominated, clastic, middle shelf environments to peritidal settings where iron formation accumulated.

CHAPTER 7: PARAGENESIS

Petrographic analysis of lithofacies within the Frere Formation show that two paragenetic pathways exist depending on the redox potential of paleo-pore water (Fig. 7.1). Mineral assemblages indicate that a suboxic paragenetic sequence typifies shallow-water lithofacies associated with stromatolites that accumulated in the presence of photosynthetic oxygen. An anoxic paragenetic sequence characterizes deeper subtidal and middle shelf environments that apparently accumulated away from nearshore oxygen oases or in deeper water environments below a prominent oxygen chemocline (Fig. 7.2). Similarities in the composition of primary chemical mud and authigenic cement suggest that pore-water redox conditions can be extrapolated to the water column, providing information on seawater chemistry at the time of deposition.

SUBOXIC PARAGENETIC PATHWAY

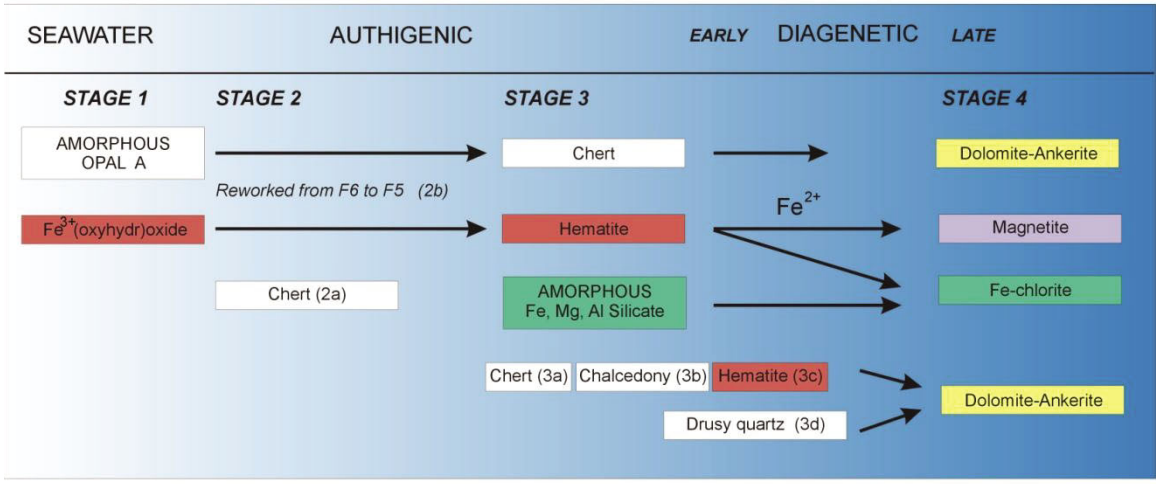

ANOXIC PARAGENETIC PATHWAY

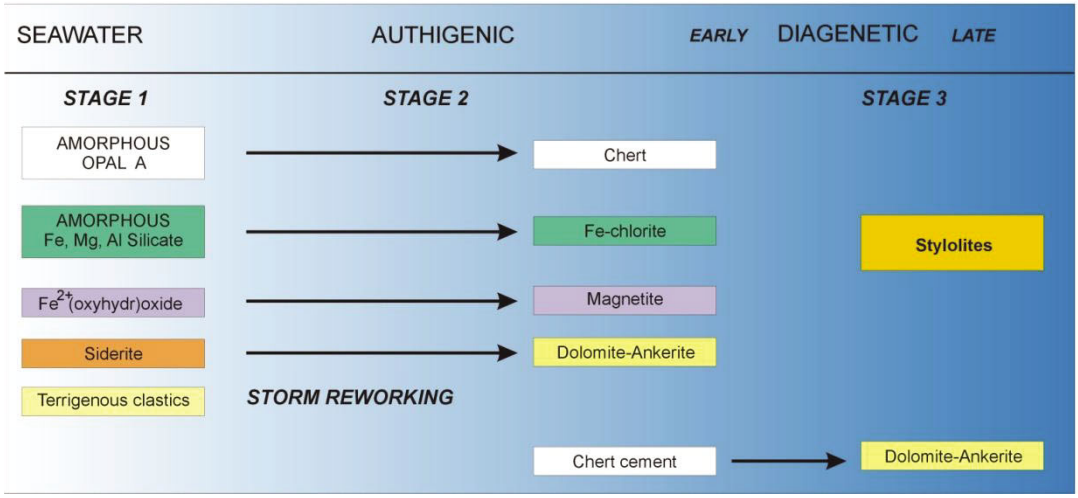

Figure 7.1. Paragenetic pathways of the Frere Formation. A) The suboxic pathway contains four stages ranging from seawater precipitation to late diagenetic alteration. B) The anoxic pathway consists of three stages ranging from seawater precipitation to late diagenetic alteration. *Note terrigenous clastics of Stage 1 is listed under the "Seawater" column, as seawater precipitates in nearshore anoxic environments are interpreted to have occurred concurrent with clastic deposition.

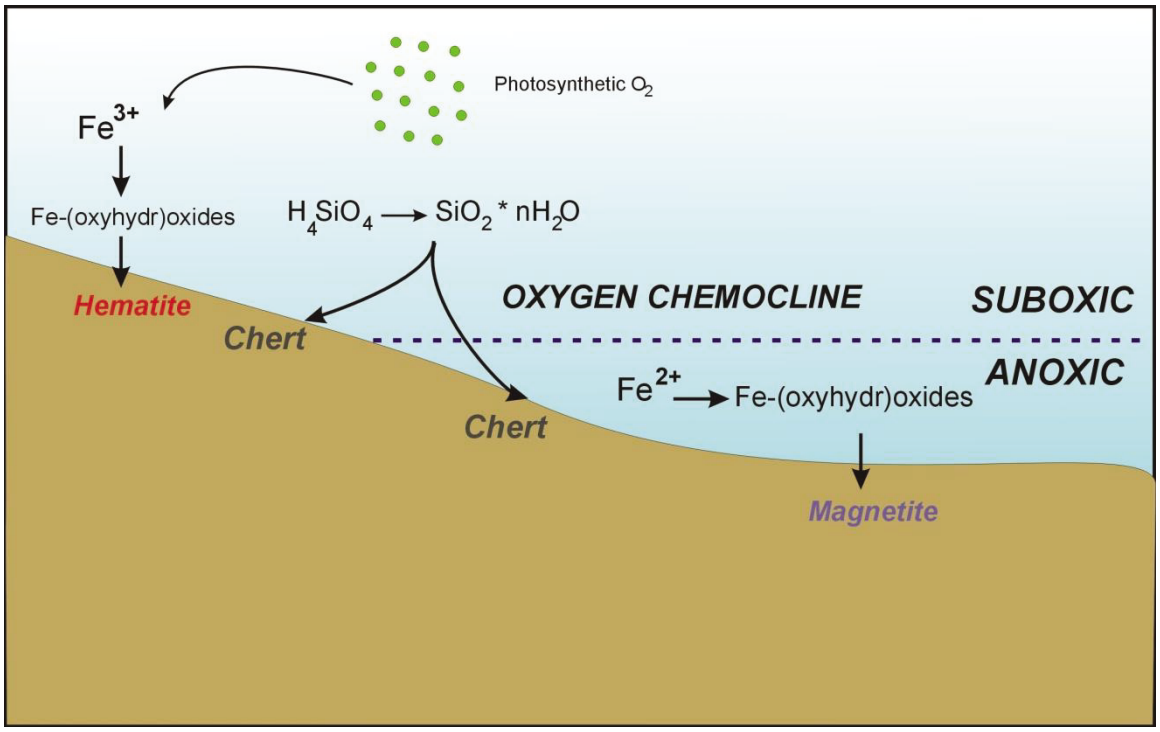

Figure 7.2. Schematic diagram showing the precipitation of Fe-oxides above and below a chemocline. Fe^{2+} and H_4SiO_4 is supplied through upwelling onto shelf environments. Chert can precipitate in the full spectrum of redox conditions.

7.1 Paragenesis in suboxic paleoenvironments

Suboxic lithofacies (F3, F5, F6, F7, F8) accumulated in peritidal environments along segments of the coastline bathed in photosynthetic oxygen (Fig. 7.2). In such nearshore settings laminated iron formation is formed primarily of hematite and chert. These *in situ* precipitates, or *pristine iron formation* (cf. Pufahl, 2010; Pufahl and Hiatt, 2012), indicate precipitation from suboxic seawater and later cementation in pore water of similar Eh. Grainstones were produced when tide and storm currents reworked pristine iron formation into hematite- and chert-rich granular deposits. Cements within this *grainstone factory* also indicate pore waters were suboxic. The paragenesis of suboxic pristine and granular iron formation is discussed below and is summarized in Figure 7.1.

7.1.1 Stage 1–Water column precipitation and pristine iron formation

Laminae within F7 are composed of hematite and chert with other laminae-forming minerals such as magnetite, Fe-chlorite and siderite. Textural relationships indicate these Fe^{2+}-bearing minerals are later precipitates. Intraclastic grainstone from F5 was observed in F6 and in rare occurrences, stretched grains with the long axis parallel to bedding were found inside magnetite-rich laminae (Fig. 7.3 D). These intraclasts are dominantly composed of chert and are not enclosed in isopachous cements that are common in F5.

Stage 1 Interpretation: Laminae in F6 are interpreted to represent precipitation in a suboxic water column (Pufahl, 2010). Elongated patches of chert may have been

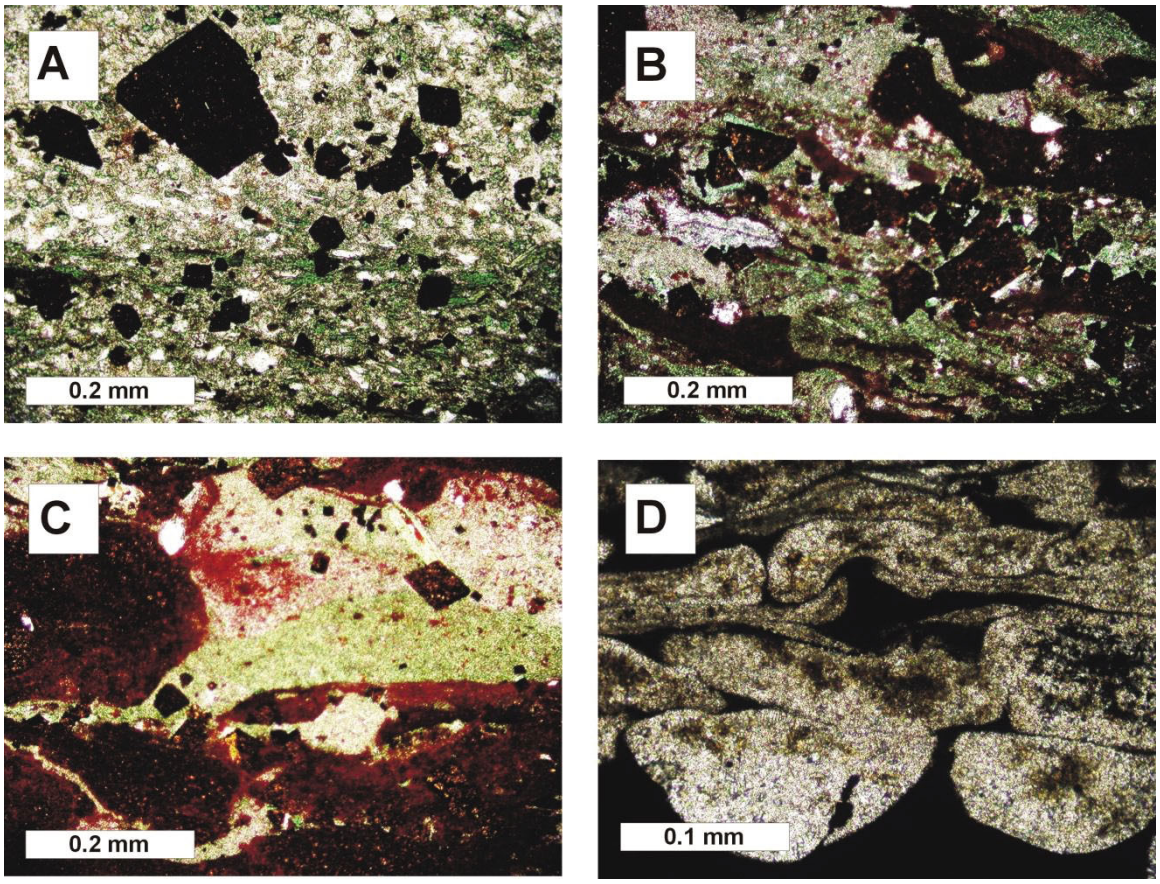

Figure 7.3: Textural relationships within laminated cherty iron formation (*pristine iron formation*). A) TDH-26, PPL, 174.5; chert and Fe-chlorite laminae shown with euhedral magnetite. B) TDH-26, PPL,174.5; seawater precipitates hematite-rich chert and Fe-chlorite with authigenic, euhedral magnetite. C) TDH-26, PPL, 174.5; rounded hematite intraclasts in chert and Fe-chlorite laminae. Euhedral magnetite cross cuts all textures. D) TDH-26, PPL, 346.2; rounded chert intraclasts in magnetite laminae. Grains are elongated parallel to bedding and appear to have had a viscous, amorphous origin before dehydration and cementation.

a chemical precipitate that were semi-lithified and gently reworked on the seafloor, before lithification. Precipitation of chert may have occurred by the concentration of upwelled, orthosilicic acid (H_4SiO_4) through evaporation in the peritidal environment. This could have formed from amorphous Opal A ($SiO_2 * nH_2O$), which upon dehydration crystallized to chert (Klein, 2005; Pufahl, 2010).

Grainstone beds are interpreted to have been transported into these suboxic inter-channel environments during storm events. Sub-rounded, elongate intraclasts that are plastically deformed contain less hematite than those that are rounded and equant. This may be a result of shorter residence times of grains in tidal channels, which are interpreted as being a more agitated and oxygenated environment.

7.1.2 Stage 2–Authigenic cementation (2a) and reworking of pristine iron formation (2b)

Stage 2 is comprised of two processes that occurred contemporaneously—the emplacement of authigenic cements and Fe^{2+}bearing minerals in F6 (Stage 2a), and the reworking and generation of intraclasts in F5 (Stage 2b).

Microcrystalline chert is the primary cement in pristine iron formation which encapsulates the Fe^{2+}-bearing minerals magnetite and Fe-chlorite. Chert and Fe-chlorite are most commonly found together within a single lamina (Fig. 7.3 A), whereas laminae with magnetite and dolomite-ankerite are more homogeneous, and are associated with diagenetic magnetite and organic laminae. Fe-chlorite is interpreted as diagenetic alteration of hematite from Stage 1.

Stage 2b is interpreted to have occurred concurrently with Stage 2a, and represents the mechanical reworking of pristine iron formation to form the intraclasts in

F5. Intraclasts are composed of Fe-rich chlorite and chert (Fig. 7.5 A, B) and are generally enclosed within larger intraclasts (0.25-2 mm in diameter). Fe-rich chlorite is expressed as 10-50 μm, fibrous masses surrounded by chert. Acicular hematite crystals surround the smaller intraclasts and grow normal to the boundary (Fig. 7.5 B). Larger intraclasts are composed of one to several sub-rounded to rounded masses of Fe-chlorite and chert intraclasts. Within large intraclasts, shrinkage cracks are ubiquitous throughout the grain, and cross-cut Fe-chlorite and chert. Shrinkage cracks are lined with fibrous hematite and identical to the hematite that surrounds smaller intraclasts (Fig. 7.5 B). In samples where shrinkage cracks exceed a width of ~50 microns, chert appears to fill the void space between hematite-lined walls.

Coated grains within F5 contain fewer Fe-chlorite and chert intraclasts within the boundary of larger grains. These grains often contain a quartz nucleus surrounded by multiple concentric and non-concentric laminae of alternating microplaty or globular hematite and chert. There are a few occurrences where coated grains are composed of blocky quartz, and laminae are outlined with hematite dust.

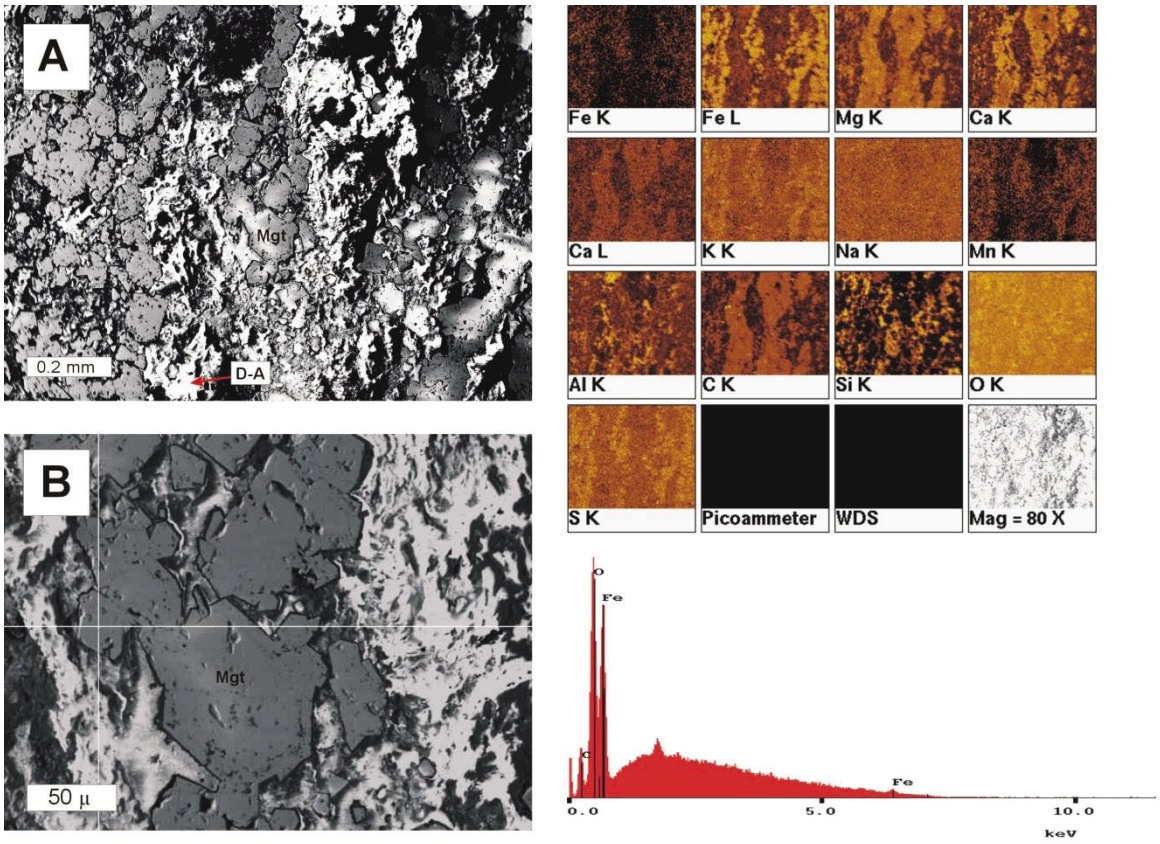

Figure 7.4. Backscatter electron images of laminated cherty iron formation from TDH-26, 384.9 m. A) Laminae are ~0.2 mm thick. Fe-rich laminae are composed of euhedral to subhedral magnetite (Mgt), which alternate with anhedral dolomite-ankerite (D-A) (up direction to the left). B) Close up of magnetite crystals surrounded by carbonate, spectrum for magnetite is shown on the right. Elemental mapping shows Ca and Mg-rich laminae are found in the white areas of the backscatter electron image and magnetite in grey. Magnetite associated with organic-rich laminae of pristine iron formation.

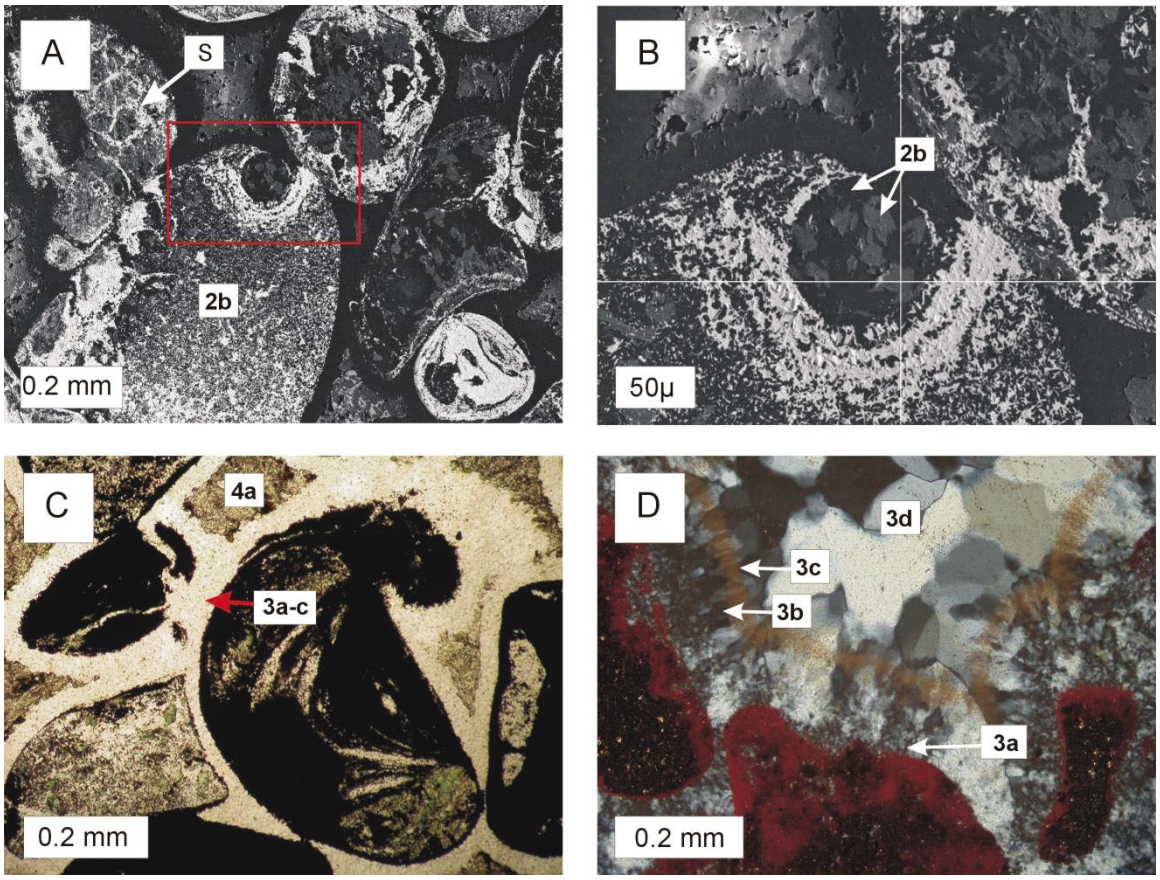

Figure 7.5: Example of Stage 2 and 3 intraclasts and cements in suboxic lithofacies. A) TDH-26, 155a; SEM backscatter electron image of intraclastic grainstone. Red box shows spatial relationship of smaller intraclasts within larger grain. S= shrinkage cracks; shrinkage cracks are lined with fibrous hematite and shows up white in BES imaging. B) Magnified image of A; cross bar located on Fe-chlorite within smaller intraclast. The smaller intraclast is rimmed with alternating laminae of microplaty hematite and chert. C) TDH-26, 155a in plane-polar light; shows relationship of intraclasts with isopachous, chert cement and interparticle quartz cement replaced with dolomite-ankerite. D) TDH-26, 155b in cross-polar and reflected light; shows multiple generations of chert-quartz cements in grainstone lithofacies.

Stage 2 Interpretation: The close association of magnetite with organic matter suggests these laminae precipitated in pore water that was more reducing than the water column (Klein, 2005; Pufahl, 2010) that precipitated chert and hematite in Stage 1. Magnetite could form through the addition of Fe^{2+} to Fe-(oxyhydr)oxides through bacterial dissimilatory iron reduction (Johnson et al., 2008). Authigenic cementation of Stage 1 precipitates is interpreted to have occurred after initial precipitation, in pore waters saturated with respect to silica.

Stage 2b is interpreted as the reworking of pristine iron formation from Stage 1. Intraclasts are interpreted to have been derived from low-energy intertidal flats and pools where pristine iron formation precipitated. These precipitates are considered to have an amorphous origin, and do not appear to have crystallized before being transported to tidal channels. Coated grains are interpreted to have originated from the rolling of grains through hematite-rich gel or mud on the seafloor (Pufahl, 2010). Composite grains record multiple episodes of reworking, deposition and cementation at the seafloor, indicating they formed in an agitated environment.

7.1.3 Stage 3-Authigenic cementation of granular iron formation

Stage 3 incorporates the dehydration and crystallization of precursor gels and authigenic cementation of granular iron formation (F5). Cementation of grainstones includes both grain-rimming (Stage 3a, 3b, 3c) and pore-filling cements (Stage 3d).

Grains in F5 contain an array of septarian-style shrinkage cracks that are lined with microplaty or globular hematite and microcrystalline chert. Up to three generations of grain-rimming cements are present in F5 (Stage 3a, 3b, 3c; Figure 7.5 D). Stage 3a is

a microcrystalline chert that precipitated contemporaneously with the dehydration of precursor gels as infiltration of chert into shrinkage cracks is of the same fine-grained anhedral habit. Chert that fills shrinkage cracks is connected to a 20-50 μm thick, isopachous chert cement that rims intraclasts (Fig. 7.5 D; Stage 3a). A second generation of grain-rimming isopachous chalcedony cement (Stage 3b) surrounds chert from Stage 3a, and is up to 50 μm thick (Fig. 7.5 D; Stage 3b). A third generation of isopachous cement envelopes Stage 3b, and is a ~25-40 μm thick rim that shows a relict, fibrous texture outlined with hematite dust (Figure 7.5 D; Stage 3c). Both Stage 3b and 3c cements are oriented perpendicular to the grain boundaries. The majority of grains are not in contact with each other, and grains that do touch are in point or tangential contact with one another. Few concavo-convex contacts were observed.

Stage 3d is the final authigenic, pore-filling cement in F5. Interparticle pore space between pore-rimming cements is occupied by drusy quartz, up to 0.2 mm in size (Fig. 7.5 A; Stage 3d). Quartz crystals impinge on isopachous cements, and the size of crystals increase from the pore walls to the center of pore space (Fig. 7.5 D; Fig. 7.6 A).

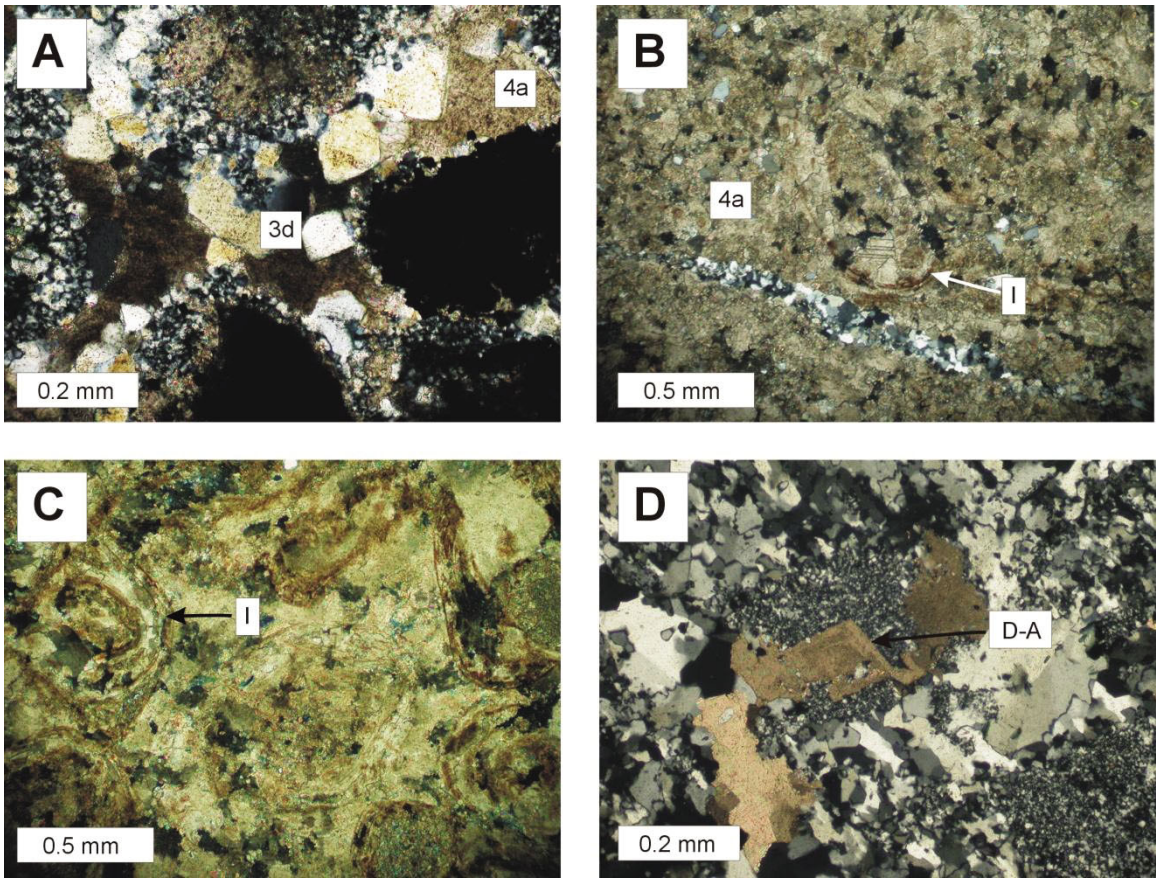

Figure 7.6: Diagenetic and authigenic and replacement cements in grainstone. A) TDH-26, 384.9; drusy quartz fills interparticle pore space in Stage 3d. Brown crystals are dolomite-ankerite replacement cements. B) TDH-26, 389.1; replacement of quartz cement with dolomite-ankerite, Stage 4a. Relict intraclast (I) is outlined with hematite dust, and internal texture is replaced with blocky dolomite-ankerite crystals. Fine-grained dolomite-ankerite replaces quartz cement from Stage 3a, 3b and 3c. C) TDH-26; 385.7; hematite lined relict coated grain replaced with blocky quartz and subsequently replaced with dolomite-ankerite. D) TDH-26, 389.1; euhedral dolomite-ankerite (D-A) crystal cross cuts chert cement.

Stage 3 Interpretation: Intraclasts, coated grains and shrinkage cracks are all lined with microplaty or globular hematite. Hematite can form throughout the full range of a paragenetic sequence in a suboxic environment (Pufahl, 2010), and Eh-pH stability fields demonstrate $Fe(OH)_3$ as a precursor to hematite lead to common mineral assemblages in iron formation (Klein, 2005). When hydrous Fe-silicate phases are removed from the system, $Fe(OH)_3$ can form in a larger range of PO_2 values compared to hydrous Fe-silicate (Klein, 2005). The nature of hematite lining void space could have resulted from dehydration and restructuring of $Fe(OH)_3$.

Chert and chalcedony isopachous cements from Stage 3 a-c are interpreted as precipitating just after the generation intraclasts from Stage 2. Evidence for this is the presence of chert that is incorporated within intraclasts, which implies it was precipitated before intraclasts reached burial depths or subaerial exposure that would compact or erode intraclasts before lithification (Simonson, 1987). Isopachous, chert cements indicate these grains were cemented in a phreatic environment, saturated with respect to silica. The un-compacted, open grain-to-grain fabric further suggests that these cements were added before the sediment was buried to significant depths (100's of meters). This is in agreement with the hypothesis that the Precambrian ocean was saturated with silica (Simonson, 1987; Pufahl, 2010) before the evolution of silica-secreting organisms (Pufahl, 2010).

Stage 3d pore-filling cements are interpreted to have originally precipitated as blocky quartz. Evidence for this is the prevalence of blocky quartz occluding pore space, and the lack of carbonate replacement in the majority of samples from F5.

7.1.4 Stage 4-Late diagenetic processes

Stage 4 includes all characteristics of suboxic lithofacies that are interpreted to have occurred during meteoric and shallow burial diagenesis, after sea-floor processes had taken place. These attributes include: replacement of grains and cements with dolomite-ankerite and the alteration of hematite to Fe-chlorite (Stage 4a); recrystallization of hematite and magnetite into euhedral crystals (Stage 4b); and mechanical fracturing of grains and cements (Stage 4c).

Stage 4a is characterized by the non-fabric selective replacement of grains and cements with dolomite-ankerite. In ~75% of samples, both isopachous and pore-filling cements maintain a primary mineralogy; the remaining 25% of samples show replacement of grains and all cement types with dolomite-ankerite. Where intraclasts have been replaced with dolomite-ankerite, isopachous cements were obliterated (Fig. 7.6 B, C), and ~ 75% of interparticle pore space is replaced with fine-grained dolomite-ankerite. A few occurrences of euhedral-subhedral baroque dolomite were observed in Stage 4a.

The final stages in the paragenetic sequence for suboxic lithofacies consists of recrystallization of Fe-oxides forming euhedral crystals of hematite and magnetite (Stage 4b), and mechanical fracturing of magnetite (Stage 4c). Euhedral magnetite crystals identified through backscattered electron imaging and elemental mapping are located at grain contacts and cross-cut all cements (Fig. 7.7; Stage 4b). In rare occurrences, euhedral magnetite crystals were found inside intraclasts, and were altered to Fe-chlorite. Magnetite crystals are 5 to 100 μm in diameter and are commonly fractured (Stage 4c).

Few occurrences of fractured grains and cements are infilled with quartz or dolomite-ankerite.

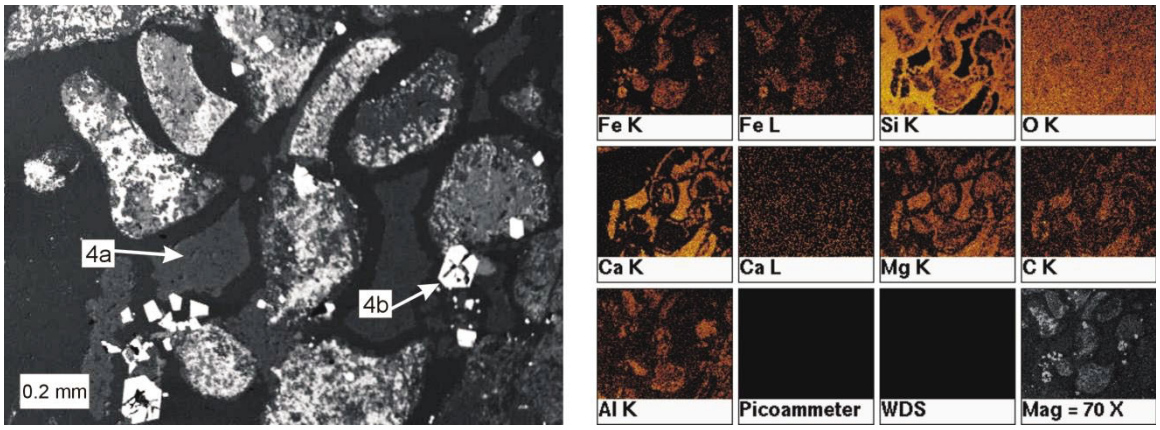

Figure 7.7. Backscatter electron image of TDH-258.4 showing an overall view of intraclasts, grain-rimming cements, interparticle cements, and magnetite overgrowths. Elemental mapping was used to extrapolate mineralogical compositions. Replacement of Stage 3 cements by dolomite-ankerite cement is labeled (Stage) 4a. A euhedral magnetite crystal is shown to cross cut grains and cements from all previous stages, and is labeled (Stage) 4b.

Stage 4 Interpretation: Quartz crystals are enclosed by dolomite-ankerite cement, where all original quartz was not replaced. In samples with abundant carbonate replacement, dolomite-ankerite rhombs range from euhedral to anhedral and are often of similar crystal size compared to quartz grains that were not replaced. Replacement of interparticle quartz cements by dolomite-ankerite may be a result of a change in pH at shallow burial depths. Chert or quartz is soluble at higher pH values than carbonate (of values between 5 and 9), and a decrease in pH favors precipitation of silica and dissolution of carbonate (Walker, 1960). This variation most likely occurred later in the diagenetic history during meteoric or shallow-burial processes. Because early cements are preserved, it is unlikely F5 and F6 experienced deep burial. Cross-cutting relationships show some compaction occurred after Stage 3 cements were in place; however, there is no evidence of deep burial as evident by minimal fracturing or stylolites (Moore and Druckman, 1981).

7.2 Paragenesis in anoxic paleoenvironments

Anoxic lithofacies (F2, F3, F4, ± F6) accumulated in shallow environments away from nearshore oxygen oases and in deeper subtidal settings below a prominent oxygen chemocline (Fig. 2). Thus, shallow water lithofacies are texturally similar to those formed in suboxic environments, but contain magnetite instead of hematite because they reflect precipitation under lower Eh conditions (Pufahl, 2010; Pufahl and Hiatt, 2012). Deeper subtidal deposits are characterized by storm-worked windblown clastic sediment and are cemented with microcrystalline chert. Paragenetic stages within anoxic nearshore and deep subtidal environments are described below and summarized in Figure 7.1.

7.2.1 Stage 1–Water column precipitation, pristine iron formation and terrigenous clastic deposition

Stage 1 incorporates minerals that precipitated in nearshore, anoxic environments away from oxygen oases. Minerals that indicate anoxic conditions during deposition include magnetite, Fe-chlorite and chert. The following description includes the Fe^{2+}-rich minerals within pristine iron formation (F6), which is included in the same lithofacies as described in Section 7.1.1 (suboxic precipitates).

Stage 1 contains anhedral to subhedral magnetite grains that are 10-100 μm in size. It is often closely associated with organic-rich discontinuous laminae up to 0.5 mm wide, and dolomite-ankerite (Fig. 7.4). In few occurrences, subhedral to euhedral siderite crystals, 5-75 μm in size, were found to be closely associated with magnetite-rich laminae.

Stage 1 also incorporates the deposition and storm-reworking of terrigenous clastic deposits in deeper-water environments. Very fine- to fine-grained quartz is the most common mineral, however, there is up to 10% muscovite. A detailed description of sedimentological features associated with these lithofacies can be found in Chapter 5.

Stage 1 Interpretation: The close spatial relationship between authigenic magnetite, Fe-rich carbonate (siderite and dolomite-ankerite) and organic-rich laminae indicates precipitation occurred in anoxic conditions. Magnetite could form through the addition of Fe^{2+} to Fe-(oxyhydr)oxide through the overlying water column or dissimilatory iron reduction (Pufahl, 2010; Johnson et al., 2008). The prevalence of Fe^{2+}-bearing minerals, including carbonates, in some pristine iron formation indicates the $pO_{2(water)}$ varied in

nearshore environments. This could possibly be a result of restricted circulation within intertidal environments, where photosynthetic oxygen was not available—away from oxygen oases.

7.2.2 Stage 2–Authigenic cementation of pristine iron formation and terrigenous clastics

Authigenic cementation of shallow-water pristine iron formation occurred contemporaneously with seafloor cementation of terrigenous clastics in deeper water environments. Pristine iron formation is cemented with microcrystalline chert. Clastic laminae are lined with 20-100 μm thick Fe-chlorite, siderite and possibly stilpnomelane (Fig. 7.8). A major distinguishing difference between the mineralogy of subtidal-middle shelf lithofacies and the supratidal-intertidal facies is the absence of hematite. F5, F6 and F7 contain abundant hematite, whereas cross-stratified sandstone in interpreted deeper water environments contains only magnetite.

Stage 2 Interpretation: Detrital quartz is interpreted as being transported to the subtidal-middle shelf environment through wind, storm events, and from the washing of clastic sediments by waves and currents in nearshore environments. The alternating laminae of magnetite and Fe-rich chlorite are interpreted to be authigenic precipitates generated in reducing pore waters. Magnetite crystals are confined to magnetite -Fe-chlorite-siderite laminae, all of which would have contained Fe^{2+}. Remobilization and precipitation of magnetite within a system occurs on a millimeter scale, therefore magnetite-rich laminae are interpreted to exist only in laminae where the precursor to magnetite was available (Klein and Fink, 1976). Stilpnomelane and greenalite are often found in Paleoproterozoic

CMTIF as the dominant Fe-silicate phases; however it is assumed contamination from terrigenous clastic sediment introduced an Al-source into the system, producing Fe- and Al-rich chlorite instead. All Fe^{2+}-bearing minerals and terrigenous clastic sediments are cemented with microcrystalline chert. The lack of hematite found associated with detrital grains, and the prevalence of Fe^{2+}-bearing minerals provides support these deposits were precipitated under anoxic conditions (Klein, 2005).

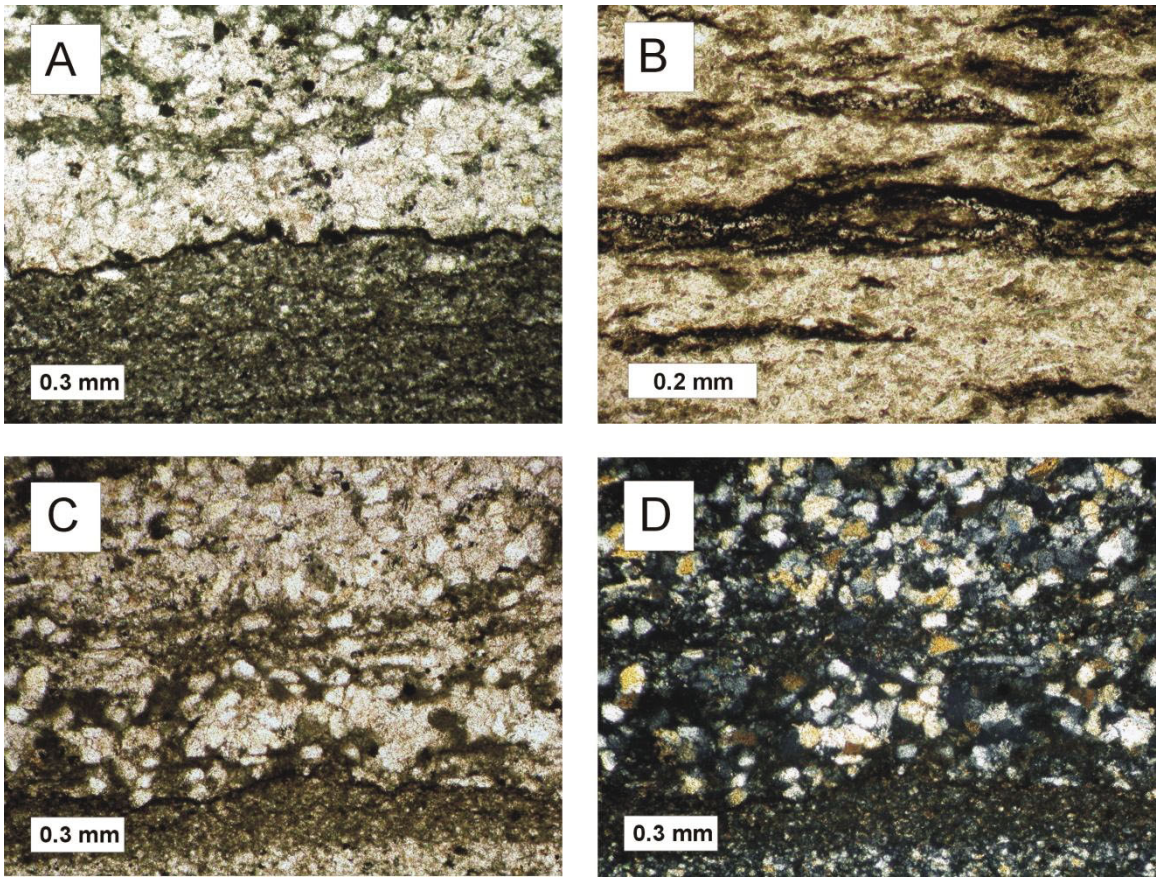

Figure 7.8. Hummocky cross-stratified siltstone from subtidal and middle shelf environments in drill core TDH-26. A) 195.2 m; bottom of photomicrograph shows silt-sized Fe-chlorite below a stylolite lined with magnetite. Stylolite is overlain by detrital quartz. B) 307 m; discontinuous magnetite laminae surrounded by siderite (brown) and possibly stilpnomelane. Laminae are organic rich, which is a common relationship with magnetite in middle shelf sandstones. C) 195.2 m, PPL; detrital quartz laminae alternating with authigenic Fe-chlorite laminae. D) 195.2 m, in XPL.

7.2.3 Stage 3— Late diagenetic processes

In quartz-rich laminae, microcrystalline chert cement is present and is rarely replaced by dolomite-ankerite. The Fe-oxide, Fe-silicate and Fe-carbonate laminae appear to contain both quartz and dolomite-ankerite cement. A few wavy, continuous stylolites occur at ~10% of the boundaries between quartz-rich and Fe-rich laminae and are commonly lined with fine-grained magnetite (Fig. 7.8 A).

Interpretation: Cementation in this environment is interpreted to have resulted from similar diagenetic processes that occurred in the grainstone lithofacies. Carbonate replacement and deep burial indicators do not appear to be widespread in any paragenetic sequences, although subtidal and middle-shelf lithofacies do contain more stylolites. This may be a result of the common occurrence of carbonate and clay minerals within this lithofacies that acted as catalysts to produce pressure-solution seams (Buxton and Sibley, 1981).

7.3 Summary

The textural relationships examined in these lithofacies are interpreted to represent primary seawater precipitates, authigenic cementation and diagenetic processes in both suboxic and anoxic environments (Fig. 7.1). Although the hydrous, amorphous precursor to minerals in crystal form cannot be preserved, material contained within intraclasts is thought to represent a well-preserved record of the paleoceanographic conditions present at the time of deposition. Shrinkage cracks within intraclasts, syn-sedimentary cementation, and a lack of minerals common in low-grade metamorphic

mineral assemblages within iron formation provide evidence the Frere Formation was not metamorphosed. The presence of both 'primary' and 'secondary' characteristics suggests that these samples were altered by diagenesis, and not metamorphism (French, 1973). Multiple relict textures remain intact, and replacement of original material is not widespread throughout all lithofacies.

The major difference identified in the two paragenetic pathways is the distinct segregation of Fe-oxide minerals in supratidal-intertidal lithofacies compared to subtidal-middle shelf lithofacies. Grainstone lithofacies contain abundant hematite, interpreted to have precipitated contemporaneously with intraclasts. Laminated cherty iron formation (pristine iron formation) contains minerals with both Fe^{3+} and Fe^{2+}, indicative of both suboxic and anoxic conditions. The alternating redox conditions needed to explain both primary hematite and magnetite in the same environment are explained through the availability of photosynthetic oxygen. Hematite was precipitated in oxygen oases, whereas magnetite was precipitated in restricted tidal pools.

Subtidal and middle shelf lithofacies contain less chemical precipitates, and Fe-bearing minerals all contain ferrous iron. These observations suggest that the redox state of the water column in which they precipitated was variable. The differences between the two paragenetic sequences will allow for correlation of redox conditions within each paleoenvironment. These data, paired with the sequence stratigraphic correlation produced in this study, will allow for development of an overall paleoceanographic model that represents the conditions during deposition of the Frere Formation.

CHAPTER 8: DEPOSITIONAL MODEL AND DISCUSSION

Deposition of the Frere Formation (~1.8 Ga) may have occurred after the proposed transition to a sulfidic ocean at ~1.84 Ga (Poulton et al., 2004). A Mesoproterozoic sulfidic ocean has major implications for biological evolution, as trace metals required for nitrogen fixation would be scavenged with the precipitation of sulfide minerals (e.g. Slack et al., 2007). The Frere Formation provides an opportunity to examine Paleoproterozoic ocean chemistry during this transition, as the mineral assemblages have only experienced diagenetic alteration (this study). Deformation of Earaheedy Group sedimentary rocks was confined to the northern limb of a large-scale syncline in the Stanley Fold Belt, therefore drill core and outcrop samples and analyses were taken from the southern limb. The lack of deformation and metamorphism in the southern limb of the Earaheedy Basin provided an opportunity to assess the paragenetic sequence in redox-sensitive minerals, and thus interpret the pore water and sea water chemistry during deposition.

The paragenetic sequences developed in this study identified both authigenic and diagenetic phases as a means to determine oceanic conditions during deposition of the Frere Formation (Chapter 7). These observations were paired with the regional sequence stratigraphic correlation (Chapter 6) to determine what factors controlled deposition of the Frere Formation. This multi-faceted approach allows for an extrapolation of genetic relationships within the chemical sediments, and the recognition of changing ocean chemistry in the Paleoproterozoic.

8.1 Depositional Model

The Earaheedy Group was deposited on a passive margin, which developed following a rifting event (Pirajno et al., 2009). This northern margin of the Yilgarn may have rifted from the supercontinent Columbia. The Frere Formation marks the transition from shallow-water, terrigenous clastic and carbonate sedimentation of the Yelma Formation, to a tidally influenced, storm-dominated shelf, that is characterized by Fe-rich chemical sedimentation. The disconformity between the Yelma and the Frere formations marks the onset of a marine transgression, punctuated by higher frequency relative sea level fluctuations and the delivery of Fe^{2+}-rich water from coastal upwelling. Just as carbonate systems are sensitive to subaerial exposure, iron formation also requires submergence in order to precipitate iron-rich deposits (Schlager, 2004). The sequence stratigraphic framework developed in this study is based on interpreted rise and fall of relative sea level, but also the position of a boundary between lithofacies deposited in suboxic and anoxic conditions—a chemocline (Fig. 8.1).

Ferrous iron and silica is interpreted to have been transported as Fe^{2+} and H_4SiO_4 by coastal upwelling onto the shelf (Pufahl, 2010). REE studies of Precambrian iron formation have shown distinct positive Eu anomalies that indicate Fe^{2+} was derived from high-temperature alteration of basalt, associated with mid-ocean ridges (Ohmoto et al., 2006). Similar REE analyses of iron-rich lithofacies of the Frere Formation also show a positive Eu anomaly suggesting that hydrothermal alteration of ocean crust was the ultimate source of Fe^{2+} upwelled onto the shelf (Price, 2003).

The Frere Formation is divided into lithofacies that represent a suboxic water column (F3, F5, F6, F7, F8), and lithofacies that represent an anoxic water column (F1, F2, F3, F4, +/- F6), which are dictated by the oxygen chemocline. The location of the

oxygen chemocline was influenced by relative sea level fluctuation and the availability of photosynthetic oxygen. This chemocline controlled vertical and lateral lithofacies stacking patterns and produced distinct mineral assemblages that indicate deposition in both suboxic and anoxic paleoenvironments. The Frere Formation is interpreted to have been deposited during an overall marine transgression in which higher-order relative sea level fluctuations occurred, causing shifting redox conditions. Lithofacies that accumulated in a suboxic water column include all chert- and hematite-rich lithofacies interpreted as components of a supratidal, intertidal and upper subtidal environment. Because of the close association between hematite-rich lithofacies and stromatolites of the peritidal environment, it is interpreted that oxidation of Fe^{2+} occurred from photosynthetically produced oxygen.

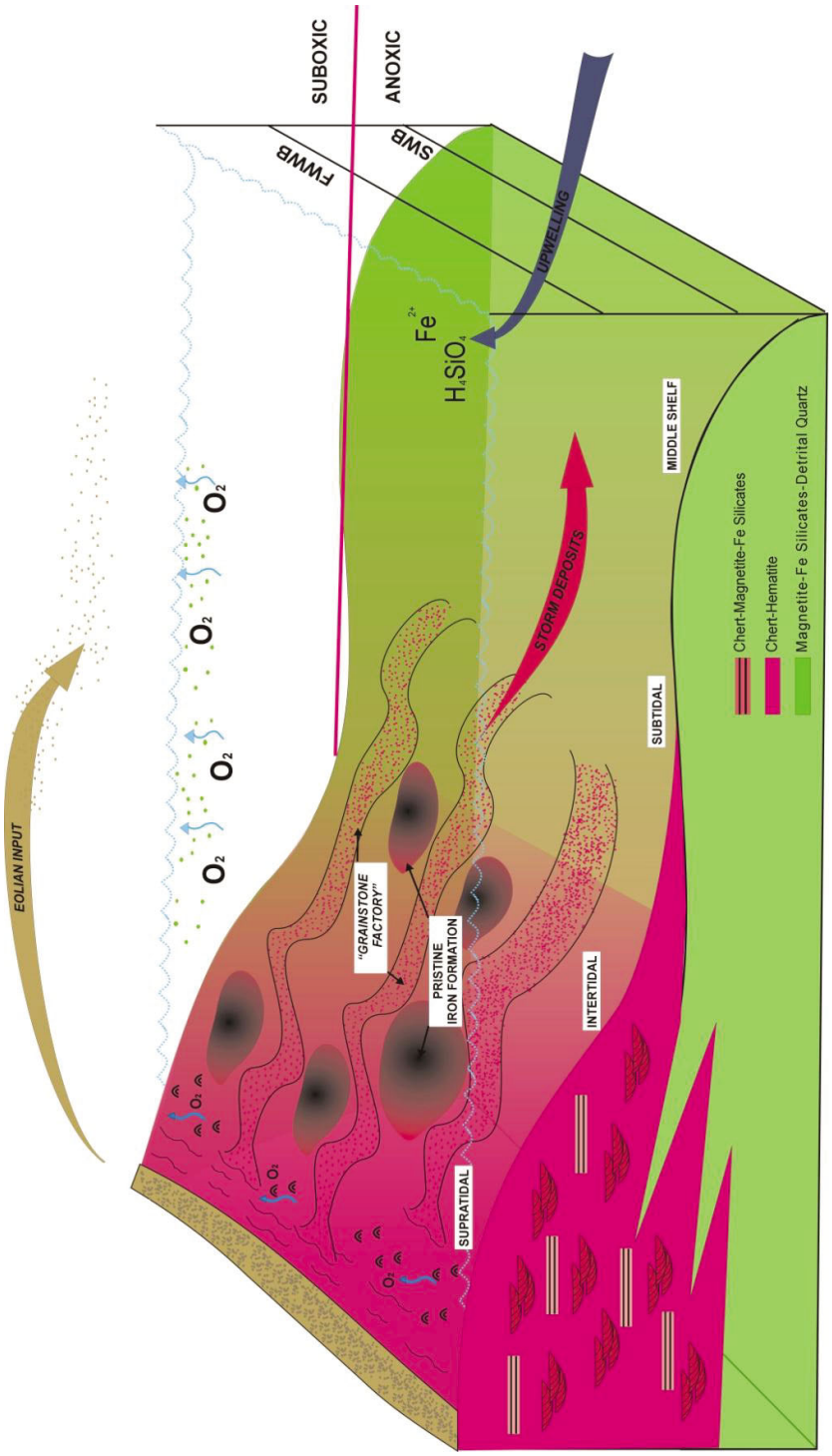

Figure 8.1. Depositional model for accumulation of the Frere Formation. Pink nearshore environments are chert- and hematite-rich, whereas green, middle shelf environments are storm- and clastic-dominated, magnetite-rich deposits. Accumulation occurs above and below a prominent chemocline.

Lithofacies indicative of an anoxic water column include those interpreted to have accumulated in the lower subtidal and middle shelf environment, and contain abundant detrital quartz and magnetite. These lithofacies contain abundant very fine- to fine-grained, sub-angular to sub-rounded, pitted quartz grains. The consistent grain size and distribution of quartz throughout mid-depth environments, as well as shared characteristics with quartz arenite in the supratidal environment suggest an eolian source of siliciclastic sediment. The lack of detrital quartz in F7, F6 and F6 indicates terrigenous clastic sediment bypassed supratidal and intertidal areas. The fine-grained sediment was most likely transported to middle shelf environments through wind, wave activity, coastal currents and storms, which depressed the clastic content of nearshore environments. Another distinct feature of anoxic lithofacies is the presence of hummocky cross-stratification and coarse-grained, graded beds. These attributes are common between fair weather wave base and storm wave base (Quin, 2011), where storm-induced combined flow produce tempestites.

The distribution of redox-sensitive minerals in pristine iron formation indicates that the oceanic oxygen content varied in nearshore environments, as pristine iron formation contains both hematite- and magnetite-rich laminae. Based on the presence of hematite-rich ripple-laminated sandstone in upper subtidal environments, it is likely the oxygen chemocline extended into deeper water. In intertidal pools where pristine iron formation precipitated, wave and current energy may not have been able to distribute photosynthetic oxygen. This would cause restricted circulation and localized anoxia, producing magnetite-rich laminae.

The Frere Formation is interpreted to have been deposited after a major rifting episode that began ~1.84 Ga as evident by the Mooloogool Group flood basalts and low-energy conditions recorded in the Minningarra Subgroup (Pirajno et al., 2009). There is no evidence of a barrier that would have restricted circulation to the open ocean in sediment of the Frere Formation. The hydrothermal source of Fe^{2+} recorded in REEs of the Frere Formation also point toward a lack of a barrier, as upwelling of Fe^{2+} onto the continental shelf would require connection to the open ocean. These observations point toward a Paleoproterozoic ocean that was stratified with respect to oxygen, with suboxic nearshore precipitation of Fe-bearing minerals, and deposition of storm-reworked, windblown sediment in anoxic environments of the middle shelf.

8.2 Iron formation depositional processes

The Frere Formation contains lithofacies that show a clear distinction between hematite-rich lithofacies in peritidal environments and magnetite-rich lithofacies in middle-shelf environments. This is in contrast to other Paleoproterozoic CMTIFs that contain abundant grainstone occurrences within mudstone, and do not display a partition between Fe^{2+}- and Fe^{3+}-bearing minerals in mid-depth environments. Physical oceanographic processes that controlled deposition were described in Chapters 5 and 6, and chemical processes in Chapter 7. By recognizing the genetic relationship between lithofacies, it was determined that hematite-dominated lithofacies were precipitated in environments where oxygen was available to oxidize Fe^{2+}. The close association of stromatolites and microbial-laminated siltstone with other hematite-bearing lithofacies suggests oxygen was supplied through photosynthesis of these microbial communities.

Because pristine iron formation is closely associated with stromatolites and microbial laminated siltstone, it is suggested Fe^{2+} was oxidized in this environment, and later reworked in tidal channels of the "grainstone factory".

8.2.1 Pristine iron formation

Pristine iron formation (F6) precipitated in intertidal flats between grainstone tidal channels. This environment had restricted circulation compared to the high-energy adjacent tidal channels (Fig. 8.1). Hydrous, amorphous precursors, Opal A and Fe-oxyhydr(oxides), precipitated and later crystallized to form chert and iron oxides (Klein, 2005; Pufahl, 2010). Chert can precipitate over a large range of Eh values and is ubiquitous throughout F6; however, hematite and magnetite-rich laminae alternate, suggesting oxygen was occasionally introduced to these paleoenvironments.

Hematite-rich laminae are often associated with microbially laminated siltstone and stromatolites (F7), which suggests there is a relationship between these facies and photosynthetically-produced oxygen. Laboratory experiments using iron-oxidizing bacteria as a means to produce the vast quantity of iron in Precambrian iron formation have proven to generate a sufficient amount of oxidized iron (Widdel et al., 1993; Konhauser et al., 2002; Konhauser et al., 2005); however, it remains unclear as to what their relationship was with Precambrian iron formations. Gunflint-type micro-assemblages have been documented by Walter et al. (1976) within the Frere Formation, however this study did not identify bacteria within Fe-rich lithofacies. It appears that the model introduced by Cloud, 1973, is supported by the lithological and mineralogical

relationships observed in this study. The biological relationship between iron formation and microbial processes still remains enigmatic.

Precipitation of magnetite in nearshore environments reflects that oxygen was not transported to intertidal pools, allowing anoxic conditions to prevail. Pristine iron formation of the Frere Formation appears similar to the micro- and meso-banded deep-water deposits of exhalative-type iron formation. The stratigraphic location and association with shallow-water deposits, however, provides evidence they did not form by the same precipitation processes.

8.2.2 Grainstone Factory

One of the distinguishing features of the Frere Formation is the prevalence of the grainstone facies (F5) and its close association with pristine iron formation (F6). Grainstone deposits of the Lake Superior and Labrador Trough regions are a distinctive characteristic of Paleoproterozoic continental-margin type iron formation (Klein, 2005). Grainstone deposits in North America are expressed as thin lenses within mudstone in deeper water environments, whereas in the Frere Formation, middle shelf environments rarely contain grainstone intervals. The clastic-dominated nature of middle-shelf environments is a distinctive characteristic that sets the Frere Formation CMTIF apart from the well-studied North American deposits.

Mineralogical components within grainstones are similar to those found in pristine iron formation, and are interpreted as grains that were reworked by tidal and storm events in intertidal flats and pools that were subsequently redistributed into high-energy tidal channels. Intraclasts composed of chert, Fe-chlorite and hematite appear to

have originated as an amorphous gel, evident by the variety in roundness of grains and in some occurrences, their stretched, elongate nature. Coated grains generally contain a quartz nucleus with a cortex that consists of multiple discontinuous laminae and are interpreted as being derived from the rolling of grains through chemical muds at the seafloor (Pufahl, 2010). Intraclasts and coated grains are dispersed together in F5, which suggests they are reworked allochthonous grains.

8.2.3 Summary of iron formation depositional processes

Pristine iron formation and hematitic grainstone both formed in peritidal environments, but are interpreted to represent very different sub-environments. Intertidal flats where pristine iron formation precipitated, served as the environment in which original precipitates formed. Precipitation of the primary precipitates occurred during intervals when photosynthetic oxygen was introduced into these areas forming oxygen oases. Fe^{2+}-bearing minerals precipitated when circulation was restricted, and oxygen was not available. These deposits were reworked in the "grainstone factory" through tidal and storm-events and were transported into agitated and oxygenated tidal channels, which are represented by cross-stratified hematite grainstone.

8.3 Paleoproterozoic ocean chemistry

The geologic record of the Paleoproterozoic contains extensive information pertaining to major changes in tectonic processes, atmosphere and ocean chemistry (Catling and Claire, 2005; Bekker et al., 2010). The development of extensive continental shelves at the Archean-Proterozoic boundary at 2.5 Ga is thought to have

produced the repositories for continental-type iron formation (Pufahl, 2010). Two major pulses of increased pO_2 occurred at the beginning and end of the Proterozoic (Catling and Claire, 2005), although ambient pO_2 levels spanning back to the Archean are disputed (Ohmoto et al., 2006). The Great Oxidation Event (GOE) in the Paleoproterozoic (ca. 2.3-2.4 Ga) is thought to have major implications for ocean chemistry (Canfield, 2005; Lyons and Gill, 2010; Pufahl, 2010; Pufahl and Hiatt, 2012), that eventually led to the demise of iron formation. The events that occurred after iron formation deposition remain ambiguous, as the preservation of Mesoproterozoic deposits is poor. The term Mesoproterozoic "Boring Billion", between ~1.84 and 0.8 Ga, is used as evolution is thought to have stagnated. This is inferred from the sulfidic ocean model (Poulton et al., 2004), where H_2S reduced trace metals needed for enzymes required for N_2 fixation (Lyons and Gill, 2010). Thus, the transition to conditions that caused this stagnation is important not only for geologic studies, but also for evolutionary biology.

The disappearance of Precambrian iron formation in the Paleoproterozoic has been attributed to a change in deep ocean chemistry at ~1.84 Ga, from either oxygenation or euxinia (Poulton et al., 2004; Scott et al., 2008; Poulton et al., 2010; Pufahl and Hiatt, 2012). The age of the Frere Formation is constrained to ca.1.80 Ga, thus placing it after the proposed transition to a sulfidic ocean (Canfield, 1998; Poulton et al., 2004). Therefore, the Frere Formation provides a window into the paleoceanography of this proposed transition.

8.3.1 Sulfidic ocean transition

The transition to a sulfidic ocean is often cited as the mechanism responsible for the demise of iron formation deposition, and the initiation of the "Boring Billion" (Shen et al., 2002; Canfield, 1998; Poulton et al., 2004; Scott et al., 2008; Pufahl and Hiatt, 2012). This transition is purportedly a response to the oxidative weathering of continental crust, increasing the amount of oceanic sulfate from fluvial sources. Through bacterial sulfate reduction, sulfide levels would increase and combine with Fe^{2+} to precipitate pyrite, thus removing the Fe^{2+} source for iron formation (Pufahl and Hiatt, 2012).

Evidence for a major transition in Paleoproterozoic ocean chemistry has thus far relied on iron formations from North America (Gunflint and Rove formations) that are slightly older (1.83 to 1.88 Ga) than the Frere Formation. Iron speciation data from North American deposits use the ratio of pyrite (Fe_P) to highly reactive iron (Fe_{HR}). Values >0.8 are considered to reflect euxinia (precipitation of pyrite), whereas values <0.8 reflect precipitation in oxic to anoxic conditions (Poulton et al., 2010). These values were placed in a paleoenvironmental context to produce an oceanographic model that incorporates oxic, euxinic and anoxic/ferruginous conditions.

A new paleoceanographic model from Poulton et al., 2010 was produced that explains the lack of pyrite in other basins by stating euxinia was persistent in mid-depth waters, producing two chemoclines. One chemocline is between oxygenated surface water and sulfidic conditions, and a deeper chemocline is between middle-shelf sulfidic conditions and deep water anoxia (Poulton et al., 2010). The euxinic water column in

middle shelf settings is interpreted to have extended at least 100 km from the paleoshoreline (Poulton et al., 2010).

Iron speciation and $\delta^{34}S$ isotope data are used to support the sulfidic ocean model in multiple basins that range in age from 1.84 Ga (Rove Formation, Lake Superior region) to 1.43 Ga (McArthur Basin, N. Australia; Slack et al., 2007). This interval spans the transition into the "Boring Billion", but it is unclear as to whether these intracratonic basins reflect global ocean chemistry, as they have recently been interpreted as having restricted circulation (Slack et al., 2007; Pufahl et al., 2010).

REE studies using Ce anomalies in the ca. 1.738 Ga VMS-related iron deposits of the Jerome district in Arizona have been used as a proxy to determine the redox state of seawater. It appears that this, paired with sedimentological evidence, may provide insight into the evolving Paleoproterozoic ocean (Kato et al., 2006; Slack et al., 2007). In the presence of dissolved oxygen Ce^{3+} is removed as Ce-hydr(oxides) or with Mn-oxides, thus producing a negative Ce anomaly (Slack et al., 2007). Oxic conditions generally produce large negative anomalies and suboxic and anoxic conditions have small negative, or no apparent anomalies (Kato et al., 2006). A minor negative Ce anomaly in jasper samples from the Jerome District iron formation implies a suboxic-anoxic deep ocean (Slack et al., 2007). This proxy does not differentiate between suboxic-anoxic and sulfidic conditions, but can help to resolve if oxygenation of the deep oceans was responsible for the demise of iron formation.

Mineral assemblages in the Frere Formation indicate deposition in a shallow-water environment both above and below an oxygen-chemocline. This interpretation is further supported by the absence of primary authigenic pyrite. Minerals in peritidal

environments indicate deposition in an Fe-rich, suboxic environment as evident by the abundance of hematite-rich lithofacies. Although clastic sedimentation appears to have out-paced chemical precipitation in subtidal and middle-shelf environments, the presence of Fe-chlorite and magnetite in these lithofacies indicates mid-depth seawater and/or pore waters were Fe-rich and anoxic.

The Frere Formation was deposited on a passive margin connected to the open ocean ~400 Ma after the proposed transition to a sulfidic ocean. Therefore, it should reflect global euxinic conditions if they persisted. This leads to the interpretation that the global ocean was more heterogeneous than previously suggested by the sulfidic ocean model (Lyons and Gill, 2010). It is apparent that a transition to a sulfidic ocean either 1) did not occur until after deposition of the Frere Formation at 1.80 Ga; or 2) occurred in basins with restricted circulation to the open ocean.

Although REEs and sulfur speciation can be used to understand the conditions that dictate chemical precipitation, they are only useful if the sedimentological and diagenetic framework is understood. The depositional model proposed for the Frere Formation indicates that the global ocean continued to actively precipitate iron formation until at least 1.8 Ga. This illustrates that ocean chemistry in the Paleoproterozoic was still evolving, 400 million years after the "Boring Billion" began. It is possible that this relatively unknown interval of geologic history may have been more dynamic than first thought.

8.4 Summary

The Frere Formation provides information on depositional processes that influenced the accumulation of continental margin-type iron formation in the Paleoproterozoic. Sedimentological evidence from this study suggests that deposition was controlled by relative sea-level fluctuations and the availability of oxygen in shallow-water environments. A clear relationship between pristine iron formation and a 'grainstone factory' was demonstrated through sequence stratigraphic and paragenetic relationships.

The lack of sulfide minerals in the Frere Formation indicates deposition was affected by oxygen availability. This is in contrast to the sulfidic Paleoproterozoic ocean that was modeled using basins that potentially do not reflect global ocean conditions. The emerging image of the "Boring Billion" is that it was significantly more textured than previously surmised.

CHAPTER 9: CONCLUSIONS

1) New sedimentologic and stratigraphic data indicate that the 1.8 Ga Frere Formation represents a single, unconformity-bound stratigraphic sequence. The basal contact with the Yelma Formation is characterized by superimposed diastem surfaces marked by pebbles from the underlying Yelma Formation. The upper contact with the Minningarra Subgroup is also inferred to be an unconformity, as stromatolites of the Windidda Member indicate further shallowing of environments. The Windidda Member is overlain by the clastic-dominated Chiall Formation.

2) The Frere Formation represents deposition within a transgressive systems tract (TST) composed of three parasequences, and a highstand systems tract (HST) composed of two parasequences. Parasequences are decameter-scale, shallowing-upward successions that transition from clastic- and storm-dominated middle shelf deposits, to Fe-rich intertidal and supratidal deposits. The TST displays an aggradational stacking pattern of nearshore sediments and is terminated with a magnetite- and organic-rich interval interpreted to represent the maximum flooding surface (MFS). The HST exhibits a progradational stacking pattern, which initiates with the thickest succession of clastic-dominated sedimentation. Intertidal and supratidal lithofacies become thicker and more prominent toward the top of the HST, indicating a major shallowing of environments, and the beginning of a poorly preserved falling stage systems tract.

3) Iron formation and associated sedimentary rocks in the Frere Formation are interpreted to have accumulated in peritidal to middle-shelf environments. Parasequences begin with a basal Fe-rich mudstone overlain by middle-shelf, Fe^{2+}-rich

hummocky cross-stratified sandstone. This sandstone transitions to intertidal, ripple-laminated hematite-rich sandstone that has a scoured contact with trough cross-stratified, hematite-rich grainstone, interbedded with pristine iron formation. Parasequences are capped with hematite-rich stromatolitic and microbial-laminated siltstone and mud-cracked surfaces indicating a supratidal environment.

4) Two paragenetic pathways within parasequences were identified by using redox-sensitive minerals. The suboxic paragenetic sequence includes lithofacies from supratidal and intertidal environments, which includes pristine iron formation and trough cross-stratified grainstone. These lithofacies contain abundant hematite and are cemented with authigenic chert and quartz. An anoxic paragenetic sequence was identified in siltstone and HCS-sandstone that represent deposition in subtidal and middle shelf environments. These lithofacies are magnetite- and Fe-chlorite-rich, and rarely contain hematite. Stacking patterns of redox-sensitive facies suggest the presence of a prominent oxygen chemocline between suboxic and anoxic lithofacies.

5) Evidence for deposition on a passive margin with connection to the open ocean is supported by the lack of barrier and lagoonal deposits. The absence of coarse clastic sediments from the north suggests the Earaheedy Basin was not a foreland basin during deposition of the Frere, and had unrestricted circulation with the open ocean. A positive Eu anomaly documented in iron-rich lithofacies (Price, 2003) indicates Fe^{2+} was transported into shallow water environments from a hydrothermal source, which would require an open shelf. Upwelled Fe^{2+} and H_4SiO_4 were concentrated in shallow water

environments above an oxygen chemocline, where photosynthetic oxygen was available in “oxygen oases”. Pristine iron formation precipitated in these intertidal flat environments and was reworked by storms and currents into tidal channels of the “grainstone factory”. Below the oxygen chemocline, wind-blown terrigenous clastics were storm-reworked and deposited with authigenically precipitated Fe-chlorite, magnetite and siderite.

6) The results of this study provide insight into the evolving Paleoproterozoic ocean. The proposed sulfidic ocean transition that led to the Mesoproterozoic “Boring Billion” purportedly occurred 400 million years prior to deposition of the Frere Formation. Accumulation of nearshore lithofacies indicates accumulation under ferruginous and suboxic conditions above an oxygen chemocline. Middle-depth deposits display evidence of deposition under ferruginous and anoxic conditions as supported by Fe^{2+}-bearing silicate, oxide and carbonate phases within clastic-dominated lithofacies. Because of the lack of pyrite in all lithofacies preserved in unweathered drill core the bottom waters across the Frere shelf were apparently not sulfidic, but anoxic and iron-rich. Results from this thesis add to a growing body of data that indicates the “Boring Billion” was appreciably more textured than previously surmised.

REFERENCES

Anbar, A.D., Knoll, A.H. 2002. Proterozoic ocean chemistry and evolution: a bioinorganic bridge? Science, **297** (5584): 1137-1142.

Anderson, S. 2009. The sedimentology of phosphatic iron formation from the Labrador Trough: implications for the accumulation of Precambrian phosphorite. M.Sc. Thesis, Acadia University.

Bekker, A., Slack, J.F., Planavsky, N., Krapez, B., Hofmann, A., Konhauser, K.O., Rouxel, O.J. 2010. Iron formation: The sedimentary product of a complex interplay among mantle, tectonic, oceanic, and biospheric processes. Economic Geology, **105**: 467-508.

Betts, P.G., Giles, D., Schaefer, B.F. 2008. Comparing 1800-1600 accretionary and basin processes in Australia and Laurentia: possible geographic connections in Columbia. Precambrian Research, **166**: 81-92.

Beukes, N.J., Gutzmer, J. 2008. Origin and paleoenvironmental significance of major iron formations at the Archean-Paleoproterozoic boundary. Society of Economic Geologists, SEG Reviews, **15**: 5-47.

Boggs, S. 2006. Principles of Sedimentology and Stratigraphy. Fourth Edition. Pearson Prentice Hall.

Braterman, P. and Cairns-Smith, A. 1987. Photoprecipitation and the banded iron formations-some quantitative aspects. Origins of Life, **17** (3-4): 221-228.

Bunting, J.A. 1986. Geology of the eastern part of the Nabberu Basin Western Australia. Geological Survey of Western Australia Bulletin 131.

Buxton, T.M. and Sibley, D.F. 1981. Pressure solution features in a shallow buried

limestone. Journal of Sedimentary Research, **51** (1): 19-26.

Canfield, D.E. 1998. A new model for Proterozoic ocean chemistry. Nature, **396**: 450-453.

Canfield, D.E. 2005. The early history of atmospheric oxygen: Homage to Rober M. Garrels. Annual Review of Earth and Planetary Science, **33**: 1-36.

Catling, D.C. and Claire, M.W. 2005. How Earth's atmosphere evolved to an oxic state: A status report. Earth and Planetary Science Letters, **237**: 1-20.

Catuneanu, O., Abreu, V., Bhattacharya, J.P., Blum, M.D., Dalrymple, R.W., Eriksson, P.G., Fielding, C.R., Fisher, W.L., Galloway, W.E., Gibling, M.R., Giles, K.A., Holbrook, J.M., Jordan, R., Kendall, C.G.St.C., Macurda, B., Martinsen, O.J., Miall, A.D., Neal, J.E., Nummedal, D., Pomar, L., Posamentier, H.W., Pratt, B.R., Sarg, J.F., Shanley, K.W., Steel, R.J., Strasser, A., Tucker, M.E., Winker, C. 2009. Towards the standardization of sequence stratigraphy. Earth Science Reviews, **92**: 1-33.

Cawood, P.A. and Tyler, I.M. 2004. Assembling and reactivating the Proterozoic Capricorn Orogen: lithotectonic elements, orogenies, and significance. Precambrian Research, **128**: 201-218.

Cloud, P., 1973. Paleoecological significance of the banded iron formation. Economic Geology, **68**: 1135-1143.

Clout, J.M.F. and Simonson, B.M. 2005. Precambrian Iron Formations and Iron Formation-Hosted Ore Deposits. Society of Economic Geologists, 100th Anniversary Volume, 37 p.

Coe. A.L., Bosence, D.W.J., Church, K.D., Flint, S.S., Howell, J.A., Wilson, R.C.L.

2003. The Sedimentary Record of Sea-Level Change *edited by* A.L. Coe. Cambridge University Press. pp. 288.

Dalrymple, R.W. 1992. Tidal depositional systems, *In* Facies Models-Response to Sea Level Changes *Edited by* Walker, R.G and James, N.P. Geological Association of Canada, p.195-218.

Dalrymple, R.W. 2010. Tidal depositional systems, *In* Facies Models 4 *Edited by* James, N.P and Dalrymple, R.W. Geological Association of Canada, p. 201-232.

Dimroth, E. and Chauvel, J. 1973. Petrography of the Sokoman Iron Formation in Part of the Central Labrador Trough, Quebec, Canada. Geological Society of America Bulletin, **84**: 111-134.

Dott, R.H, Jr. and Bourgeois, J. 1982. Hummocky stratification: Significance of its variable bedding sequences. Geological Society of America Bulletin, **93**: 663-680.

Edwards, C. 2010. The paleoecology of Paleoproterozoic microbial communities in the Ferriman Group, Labrador Trough Canada. M.Sc Thesis, Acadia University.

Edwards, C.T., Pufahl, P.K., Hiatt, E.E., *in press*. Paleoenvironmental and taphonomic controls on the occurrence of Paleoproterozoic microbial communities in the 1.88 Ga Ferriman Group, Labrador Trough, Canada. Precambrian Research.

Ehrenreich, A. and Widdel, F. 1996. Anaerobic oxidation of ferrous iron by purple bacteria, a new type of phototrophic metabolism. Applied Environmental Microbiology, **60** (12): 4517-4526.

Ekdale, A.A., and Picard, M.D. 1985. Trace fossils in a Jurassic eolianite, Entrada

Sandstone, Utah, USA. In Curran, H.A., (ed.), Biogenic Structures: Their Use in Interpreting Depositional Environments. SEPM Special Publication, **35**:3-12.

Ernst, R.E., Wingate, M.T.D., Buchan, K.L., Li, Z.X. 2008. Global record of 1600-700 Ma Large Igneous Provinces (LIPs): Implications for the reconstruction of the proposed Nuna (Columbia) and Rodinia supercontinents. Precambrian Research, **160**: 159-178.

Evans, D.A.D., and Mitchell, R.N. 2011. Assembly and breakup of the core of Paleoproterozoic-Mesoproterozoic supercontinent Nuna. Geology, **39** (5): 443-446.

French, B.M. 1973. Mineral Assemblages in Diagenetic and Low-Grade Metamorphic Iron Formation. Economic Geology, **68**: 1063-1074.

Galloway, W.E. 1989. Process framework for distinguishing the morphologic and stratigraphic evolution of deltaic depositional systems, *In* Deltas—Models for Exploration *edited by* M.L. Broussard. The Houston Geological Society, pp. 87-98.

Gole, M.J., and Klein, C. 1981. Banded iron-formations through much of Precambrian time. The Journal of Geology, **89** (2): 169-183.

Halilovic, J., Cawood, P.A., Jones, J.A., Pirajno, F., and Nemchin, A.A. 2004. Provenance of the Earaheedy Basin: implications for assembly of the Western Australian Craton. Precambrian Research, **128**: 343-366.

Hall, W.D.M., and Goode, A.D.T. 1978. The early Proterozoic Nabberu Basin and associated iron formations of Western Australia. Precambrian Research, **7**: 129-184.

Holland, H.D. 2002. Volcanic gases, black smokers and the Great Oxidation Event. Geochimica et Cosmochimica Acta, **66** (21): 3811-3826.

Holland, H.D. 2009. Why the atmosphere became oxygenated: A proposal. Geochimica et Cosmochimica Acta, **73**: 5241-5255.

James, H.J., and Sims, P.K. 1973. Precambrian iron formations of the world, introduction *In* Precambrian iron-formations of the world, Economic Geology and the Bulletin of the Society of Economic Geologists, **68** (7): 913-914

Johnson, C.M., Beard, B.L., Klein, C., Beukes, N.J.,and Roden, E.E. 2008. Iron isotopes constrain Biologic and abiologic processes in banded iron formation genesis. Geochimica et Cosmochimica Acta, **72**: 151-169.

Johnson, J.G., and Murphy, M.A. 1984. Time-rock model for Siluro-Devonian continental shelf western United States. Geological Society of America Bulletin, **95**: 1349-1359.

Jones, J.A., Pirajno, F., Hocking, R.M., and Grey, K. 2000. Revised stratigraphy for the Earaheedy Group: implications for the tectonic evolution and mineral potential of the Earaheedy Basin. Geological Survey of Western Australia, Annual Review (1999-2000)**:** 57-63.

Kappler, A., and Newman, D.K. 2003. Formation of Fe(III)-minerals by Fe(II)-oxidizing photoautotrophic bacteria. Geochimica et Cosmochimica Acta, **68** (6): 1217-1226.

Kato, Y., Yamaguchi, K.E., and Ohmoto, H. 2006. Rare-earth elements in Precambrian banded iron formations: Secular changes of Ce and Eu anomalies and evolution of atmospheric oxygen *In* Evolution of early Earth's atmosphere, hydrosphere, and

biosphere-Constraints from ore deposits *Edited by* S.E. Kessler and H. Ohmoto. Geological Society of America Memoir **198**: 269-290.

Klein, C. 2005. Some Precambrian banded iron-formations (BIFs) from around the world: Their age, geologic setting, mineralogy, metamorphism, geochemistry, and origin. American Mineralogist, **90**: 1473-1499.

Klein, C., and Fink, R.P. 1976. Petrology of the Sokomon iron formation in the Howells River area, at the western edge of the Labrador Trough. Economic Geology, **71** (2): 453-487.

Knoll, A.H., and Simonson, B. 1981. Early Proterozoic Microfossils and Penecontemporaneous Quartz Cementation in the Sokoman Iron Formation, Canada. Science, New Series, **211** (4481): 478-480.

Konhauser, K.O., Hamade, T., Raiswell, R., Morris, R.C., Rerris, f.G., Southam, G., and Canfield, D.E. 2002. Could bacteria have formed the Precambrian banded iron formations? Geology, **30**: 1079-1082.

Konhauser, K.O., Newman, D.K., and Kappler, A. 2005. The potential significance of microbial Fe(III) reduction during deposition of Precambrian banded iron formations. Geobiology, **3**: 167-177.

LaBerge, G.L. 1968. Microfossils and Precambrian iron-formations. Geological Society of America Bulletin, **78**: 331-342.

LaBerge, G.L. 1973. Possible biological origin of Precambrian iron-formations. Economic Geology, **68**: 1098-1109.

Lyons, T.W., Anbar, A.D., Severmann, S., Scott, C., and Gill, B.C. 2009. Tracking euxinia in the Ancient Ocean: A Multiproxy Perspective and Proterozoic Case Study. Annual Review of Earth and Planetary Science, **37**: 507-534.

Lyons, T.W., and Gill, B.C. 2010. Ancient sulfur cycling and oxygenation of the early biosphere. Elements, **6**: 93-99.

Maliva, R.G., Knoll, A.H., and Simonson, B.M. 2005. Secular change in the Precambrian silica Cycle: insights from chert petrology. Geological Society of America Bulletin, **117**: 835-845.

Meert, J.G. 2012. What's in a name? The Columbia (Paleopangaea/Nuna) supercontinent. Gondwanna Research, in press.

Moore, C.H., and Druckman, Y. 1981. Burial Diagenesis and Porosity Evolution, Upper Jurassic Smackover, Arkansas and Louisiana. AAPG Bulletin **65** (4): 597-628.

Muhling, J.R., Fletcher, I.R., and Rasmussen, B. 2011. Monazite dating of base-metal mineralization, Earaheedy Basin, Western Australia. Goldschmidt Conference Abstracts.

Nelson, G.J., Pufahl, P.K., and Hiatt, E.E. 2010. Paleoceanographic constraints on Precambrian phosphorite accumulation, Baraga Group, Michigan, USA. Sedimentary Geology, **226:** 9-21.

Ohmoto, H., Watanabe, Y., Yamaguchi, K.E., Naraoka, H., Kakegawa, Hayashi, K., and Kato. 2006. Chemical constraints and biological evolution of early Earth: constraints from banded iron formations *In* Evolution of Early Earth's

Atmosphere, Hydrosphere, and Biosphere—Constraints from Ore Deposits *edited by* Kessler, E. and Ohmoto, H. Geological Society of America Memoir **198**: 291-331.

Ojakangas, R.W., Morey, G.B., and Southwick, D.L. 2001. Paleoproterozoic basin development and sedimentation in the Lake Superior region, North America. Sedimentary Geology, **141-142**: 319-341.

Papineau, D. 2010. Global biogeochemical changes at both ends of the Proterozoic: Insights from phosphorites. Astrobiology, **10** (2): 165-181.

Pirajno, F., Hawke, P., Glikson, A.Y., Haines, P.W., and Usal, T. 2003. Shoemaker impact structure, Western Australia. Australian Journal of Earth Sciences, **50**: 775-796.

Pirajno, F., Jones, J.A., Hocking, R.M., and Halilovic, J. 2004. Geology and tectonic evolution of Paleoproterozoic basins of the eastern Capricorn Orogen, Western Australia. Precambrian Research, **128**: 315-342.

Pirajno, F., Hocking, R.M., Reddy, S.M., and Jones, A.J. 2009. A review of the geology and geodynamic evolution of the Paleoproterozoic Earaheedy Basin, Western Australia. Earth-Science Reviews, **94**: 39-77.

Plint, A.G. 2010. Wave- and Storm-Dominated Shoreline and Shallow-Marine Systems. *In* Facies Models, 4th Ed. *edited by* James, N.P., Dalrymple, R.W. Geological Association of Canada, pp. 167-200.

Posamentier, H.W., and Vail, P.R. 1988. Eustatic controls on clastic deposition II—sequence and systems tract models *In* Sea Level Change—An Integrated Approach *edited by* C.K. Wilgus, B.S. Hastings, C.G.St. C, Kendall, H.W.,

Posamentier, C.A. Ross, J.C. Van Wagoner. SEPM Special Publication, **42**: 125-154.

Poulton, S.W., Fralick, P.W., and Canfield, D.E. 2004. The transition to a sulphidic ocean ~1.84 billion years ago. Nature, **431**: 173-177.

Poulton, S.W., Fralick, P.W., and Canfield, D.E. 2010. Spatial variability in ocean redox structure 1.8 billion years ago. Nature Geoscience, **3**: 486-490.

Pratt, B.R. 2010. Peritidal Carbonates *In* Facies Models 4 *Edited* by N.P. James and R.W. Dalrymple. Geological Association of Canada. pp. 401-420.

Price, J. 2003. Depositional setting of granular iron formation in the Paleoproterozoic Frere Formation, Earaheedy Basin, Western Australia. B.Sc. Honours Thesis, Unviversity of Western Australia.

Pufahl, P.K. 1996. Stratigraphic architecture of a Paleoproterozoic iron formation depositional system: the Gunflint, Mesabi and Cuyuna iron ranges. Unpubl. M.Sc. Thesis, Lakehead University, 167 pp.

Pufahl, P.K. 2010. Bioelemental Sediments *In* Facies Models 4 *Edited by* N.P. James and R.W. Dalrymple. Geological Association of Canada. pp. 477-504.

Pufahl, P.K., Hiatt, E.E., and Kyser, T.K. 2010. Does the Paleoproterozoic Animikie Basin record the sulfidic ocean transition? Geology, **38** (7): 659-662.

Pufahl, P.K., and Hiatt, E.E. 2012. Oxygenation of the earth's atmosphere-ocean system: A review of physical and chemical sedimentologic responses. Marine and Petroleum Geology, accepted manuscript.

Quin, J.G. 2011. Is most hummocky cross-stratification formed by large-scale ripples? Sedimentology, **58**: 1414-1433.

Reineck, H.E., and Singh, I.B. 1980. Depositional Sedimentary Environments, 2nd Ed. Springer-Verlag, New York. 549 p.

Schlager, W. 2004. Fractal nature of stratigraphic sequences. Geology **32** (3): 185-188.

Scott, C., Lyons, T.W., Bekker, A., Shen, Y., Poulton, S.W., Chu, X., and Anbar, A.D. 2008. Tracing the stepwise oxygenation of the Proterozoic ocean. Nature, **452**: 456-459.

Shen, Y., Canfield, D.E., and Knoll, A.H. 2002. Middle Proterozoic ocean chemistry: evidence from the McArthur Basin, Northern Australia. American Journal of Science, **302**: 81-109.

Simonson, B.M. 1985. Sedimentological constraints on the origins of Precambrian iron-formations. Geological Society of America Bulletin, **96**: 244-252.

Simonson, B.M. 1987. Early silica cementation and subsequent diagenesis in arenites from four early Proterozoic iron formations of North America. Journal of Sedimentary Petrology, **57** (3): 494-511.

Simonson, B.M., and Hassler, S.W. 1996. Was the deposition of large Precambrian iron formations linked to major marine transgressions? Journal of Geology, **104**: 665-676.

Slack, J.F., Grenne, T., Bekker, A., Rouxel, O.J., and Lindberg, P.A. 2007. Suboxic deep seawater in the late Paleoproterozoic: Evidence from hematitic chert and iron formation related to seafloor-hydrothermal sulfide deposits, central Arizona, USA. Earth and Planetary Science Letters, **255**: 243-256.

Tobin, K.J. 1990. The paleoecology and significance of the Gunflint-type microbial assemblages from the Frere Formation (Early Proterozoic), Nabberu Basin,

Western Australia. Precambrian Research, **47**: 71-81.

Trendall, A.F. 1968. Three great basins of Precambrian iron formation deposition: a systematic comparison. Geologic Society of America Bulletin, **79** (11): 1527-1544.

Trendall, A.F. 2002. The significance of iron formation in the Precambrian stratigraphic record. Special Publications International Association of Sedimentologist, **33**: 33-66.

Van Wagoner, J.C., Posamentier, H.W., Mitchum, R.M, Vail, P.R., Sarg, J.F., Loutit, T.S., and Hardenbol, J. 1988. An overview of sequence stratigraphy and key definitions *In* Sea Level Change—An Integrated Approach *edited by* C.K. Wilgus, B.S. Hastings, C.G.St. C, Kendall, H.W., Posamentier, C.A. Ross, J.C. Van Wagoner. SEPM Special Publication, **42**: 39-45.

Walker, T.R. 1960. Carbonate Replacement of Detrital Crystalline Silicate Minerals as a Source of Authigenic Silica in Sedimentary Rocks. Bulletin of the Geological Society of America, **71**: 145-152.

Walter, M.R., Goode, A.D.T., and Hall, W.D.M. 1976. Microfossils from a newly discovered Precambrian stromatolitic iron formation in Western Australia. Nature, **261**: 221-223.

Widdel, F., Schnell, S., Heising, S., Ehrenreich, A., Assmus, B., and Schink, B. 1993. Ferrous iron oxidation by anoxygenic phototrophic bacteria. Nature, **362** (6423): 834-836.

APPENDIX I: OUTCROP STRATIGRAPHIC SECTIONS

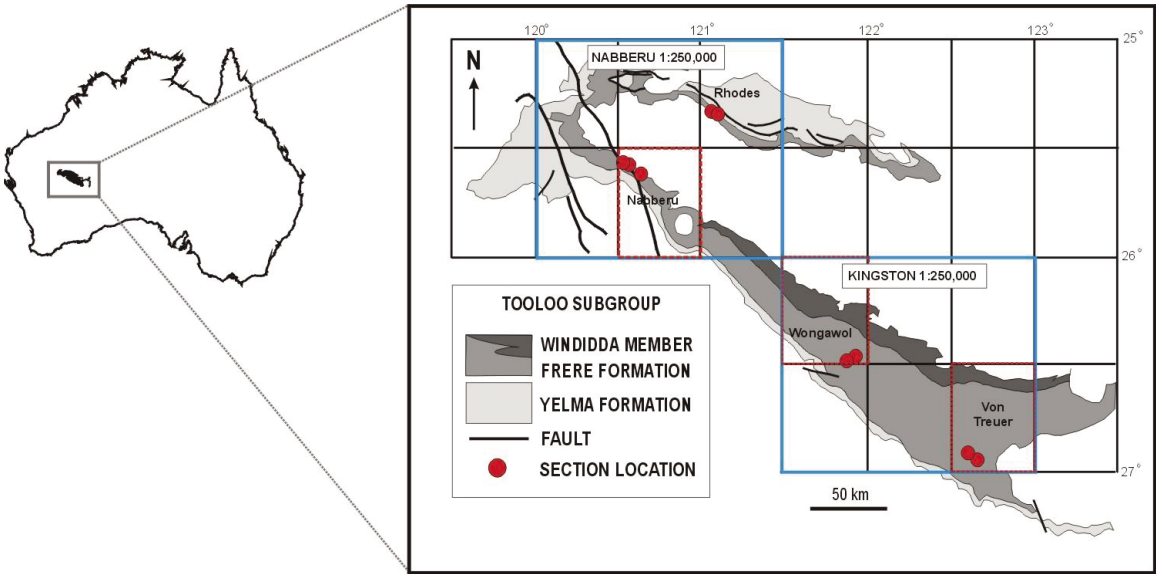

Figure A.1. Location of stratigraphic sections in outcrop and drill core. The 1:250 000 map sheets Nabberu and Kingston, and 1:100 000 map sheets Rhodes, Nabberu, Wongawol, Von Treuer were used to determine Frere Formation occurrences.

Nabberu Creek Section
Thickness=90 m

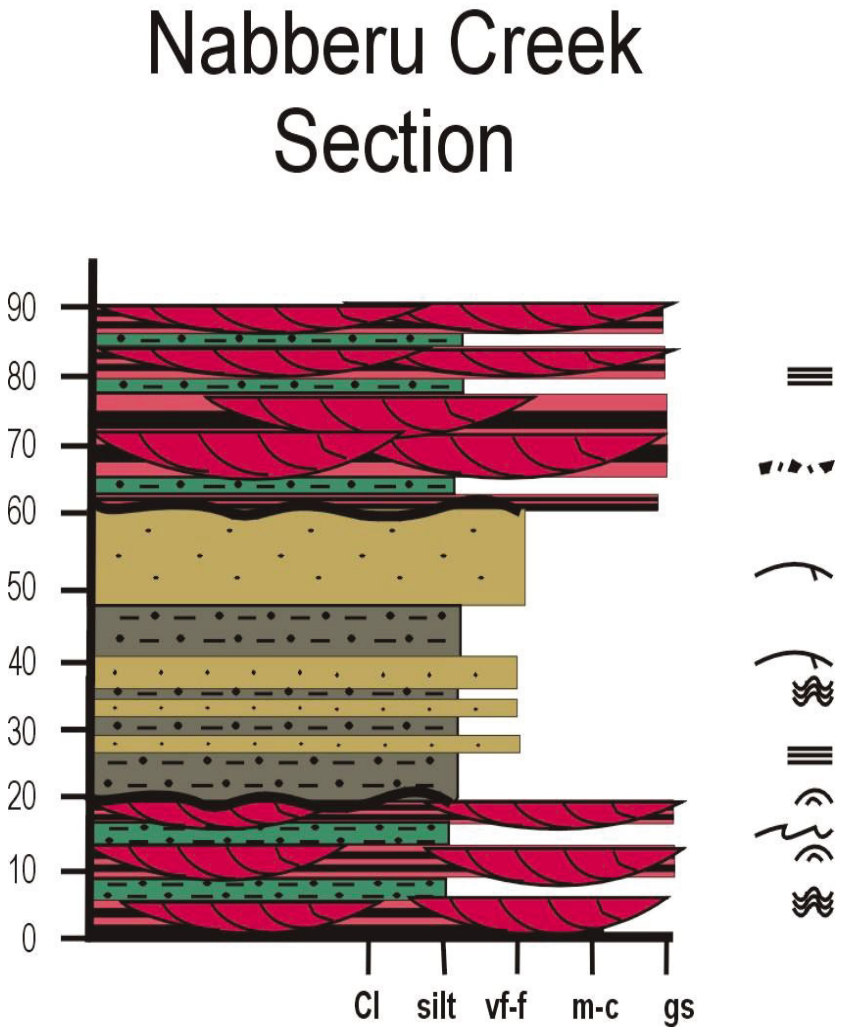

Nabberu Creek Section **(Interval)**	UTM at 0m: 51 J 0266285, 7158216 Comments: This was the best outcrop section representing parasequence 4 and 5, as it was able to be included into the stratigraphic correlation. It contains the thickest interval of clastic-dominated sediments and maximum flooding surface. The iron-rich and grainstone successions are resistant, whereas the sandstone/siltstone successions are recessive. Outcrop is easily accessible, and strata are flat lying.
80-90 m	The top of this section is very weathered; laterite samples taken from this area. Microbial laminae was identified with some asymmetrical ripples. Some peloidal grainstone intervals with low angle cross beds and discontinuous.
75-80 m	White, black and green cherty laminae 0.5-1 cm thick with lenses of cherty grainstone containing hematite, chert. Grainstone intervals have a sharp contact with chemical muds/chert and is planar to wavy. Rip up clasts are associated with the base of grainstone.
65-75m	Hematitic siltstone overlies conglomerate from below for ~5 m. Erosional scoured contact at 70 m overlain by 5 cm packages of grainstone. Scour contact is 10-15 cm thick and silicified.
63-65 m	First occurrence of thick laminae/beds of hematite rich mudstone, 0.5-4 cm thick with interval on conglomerate containing rip ups of underlying sand/siltstone. Conglomerate consistes of 30-40% clasts with a red, silty matrix, pink in color.
30-63 m	Thickest clastic-dominated succession in proximal stratigraphic sections. Very fine to fine-grained subangular to subrounded quartz, coarsens upward. HCS (very good exposure in the recessive "hole" in outcrop), showing low angle truncation and hummocks and swales. Near 55 m, HCS is overlain by ripple laminated sand/siltstone, possibly flaser bedded (dark red hematite mud drapes in troughs, some lining of ripple crests). This interval is devoid of grainstone lenses or beds, and chemical sediments are not present, with the exception of the hematite-rich muds that produced the flaser-fabric.
20-30 m	Hardground at 20 m (possible MFS). Overlain by vf-f grained silty sandstone with carbonate cement and a few occurrences of stromatolites. Recessive unit in outcrop. Ripple cross-laminae (1-2 mm foresets and bidirectional), potentially HCS. Red-pink in color. Quartz grains are vf-f with some medium to coarse grained intervals.
0-20 m	This interval is extremely silicified and was sporadically covered. Walking out gullies allowed for an overall view of the bottom part of the section, and the best exposure of the Frere Formation in outcrop lies above this interval. 0-20 m is primarily black chert and jasper laminae, 0.3-1 cm thick with some alteration to chlorite. Alternates with laminae of chert, jasper, hematite grainstone. Grainstone is composed of subangular to rounded peloids, 0.5-1 cm diameter. Jasper nodules, 2-10 cm in size were also documented. Some wavy bedding, mainly planar. Hardground surface is silicified. Domal stromatolites were found at the top (most of photos in thesis from this location).

Von Treuer Section 1
Thickness: 54 meters

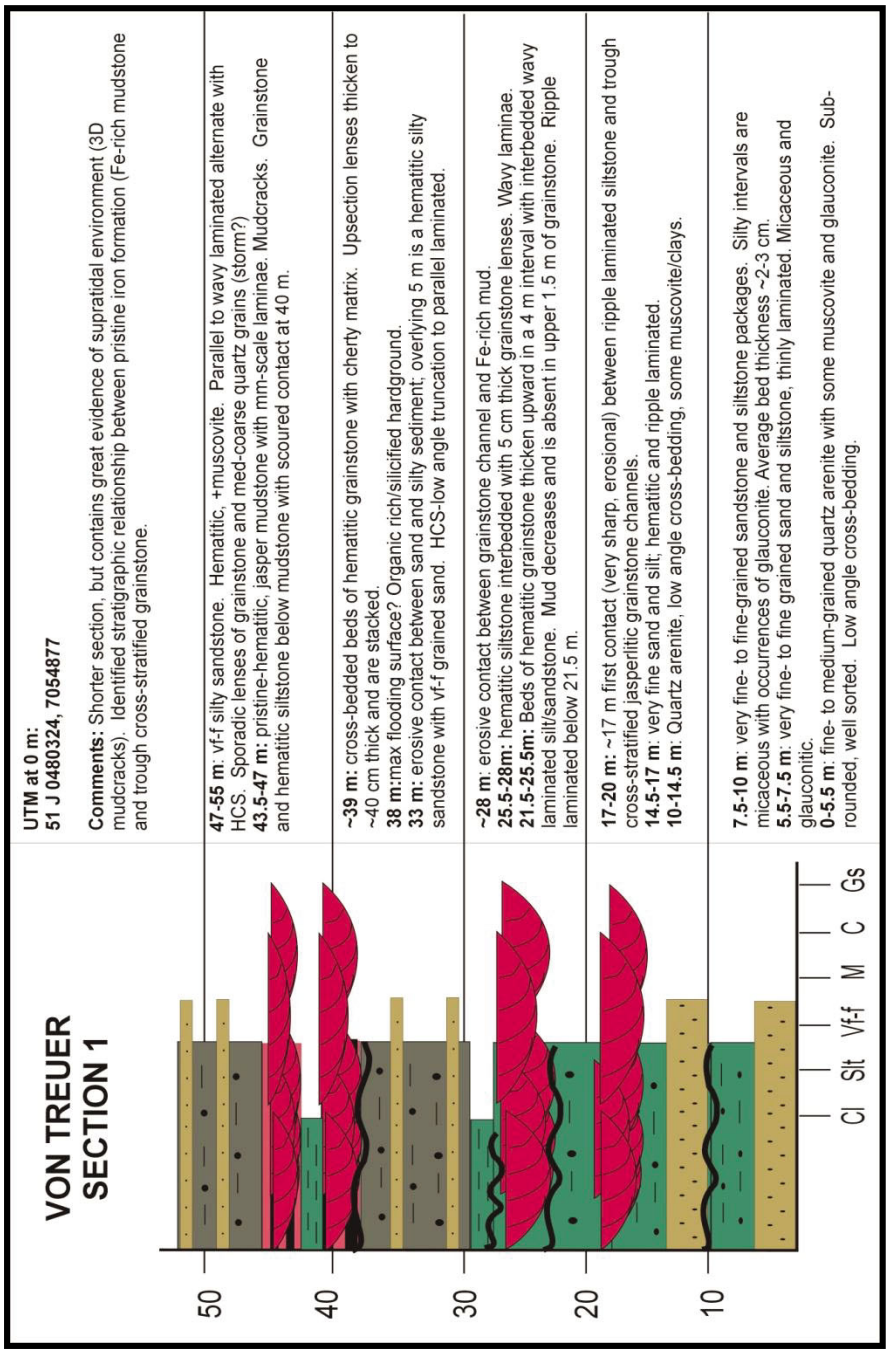

Von Treuer Section
Total thickness: 22 meters

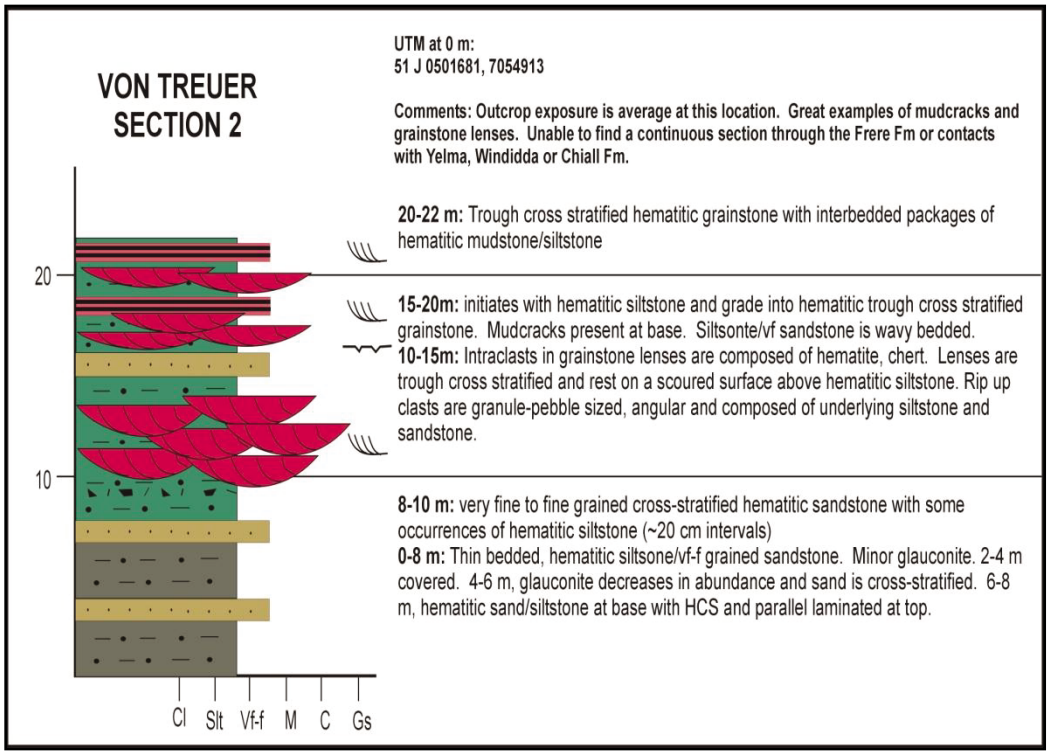

Kingston Section 1 (composite section)
Total thickness: 5 meters (Scale bar increment = 1 m)

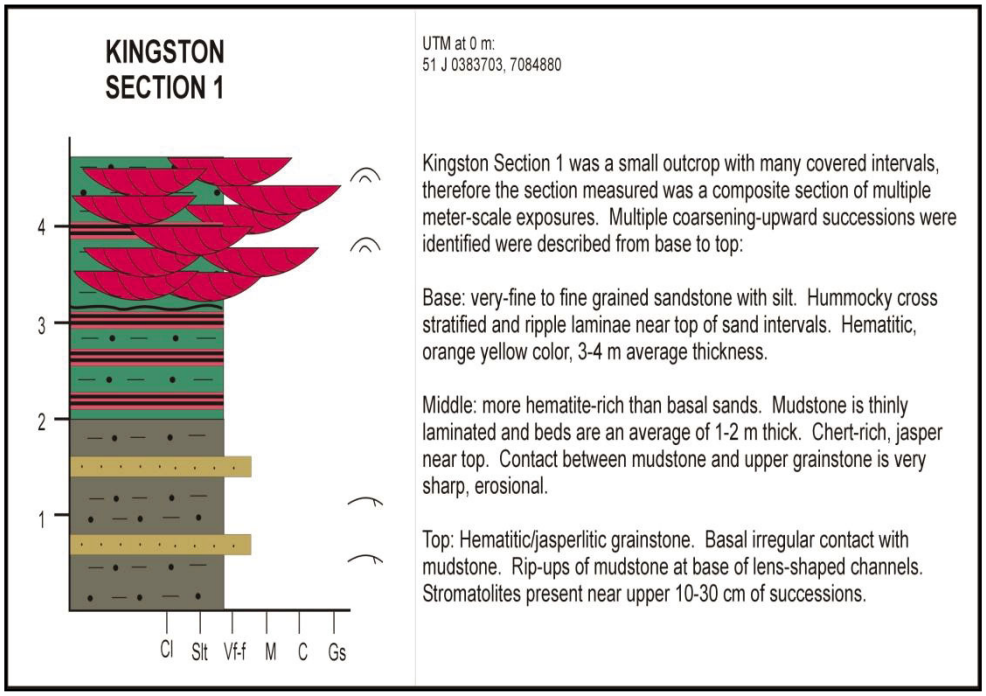

Kingston Section 2
Thickness: 11 m

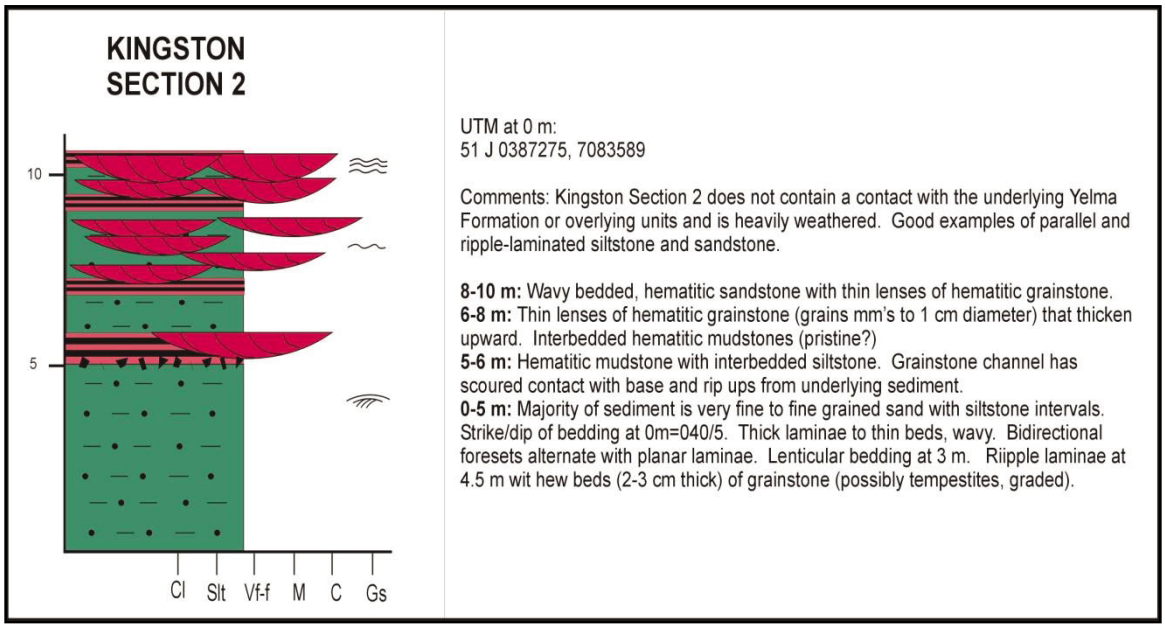

Yappi Creek Section

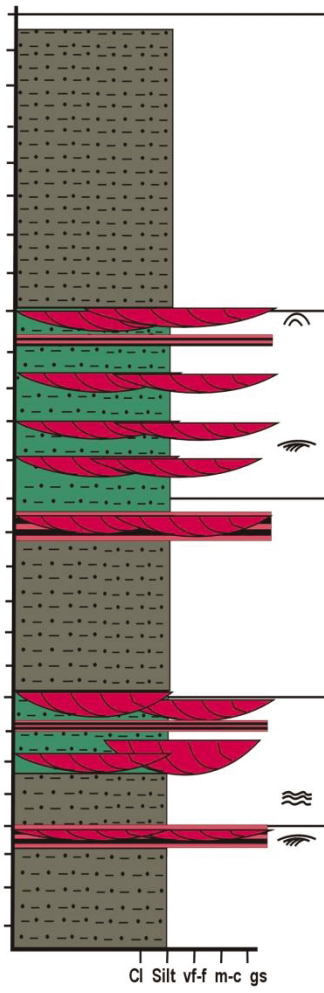

Yappi Creek Section	**UTM at 0m:** 51 J 0347334, 7177644 **Comments:** Heavily folded, clastic dominated section.
	190 to top of section: Hematitic siltstone with interbedded chert (alteration?). Muscovite-rich and coarsens upward.
	140-190 m: Grainstone lenses interbedded with hematitic siltstone, riipple cross laminated. Grainstone beds are thinner , 10-15 cm thick. Stromatolites are abundant near top of succession.
	130-138 m: Peloidal grainstone intervals thicken upward. Beds ~60 cm thick and interbedded with cherty laminae (fabric is destroyed). **80-130 m:**Hematitic siltstone, beds near vertical.
	60-80 m: Thick grainstone lenses, heavily silicified. **40-60 m:** microbial laminated hematitic siltstone. Scoured contact at 57 m with grainstone lenses. Beds are ~50 cm thick and coarsen upward.
	30-40 m: Silicified, cherty grainstone, ~20 cm thick beds alternating with ripple laminated siltstone/sandstone. **0-31m:**Hematitic siltstone Below start of section, 60 m of hematitic siltstone.

West Yappi Creek Section

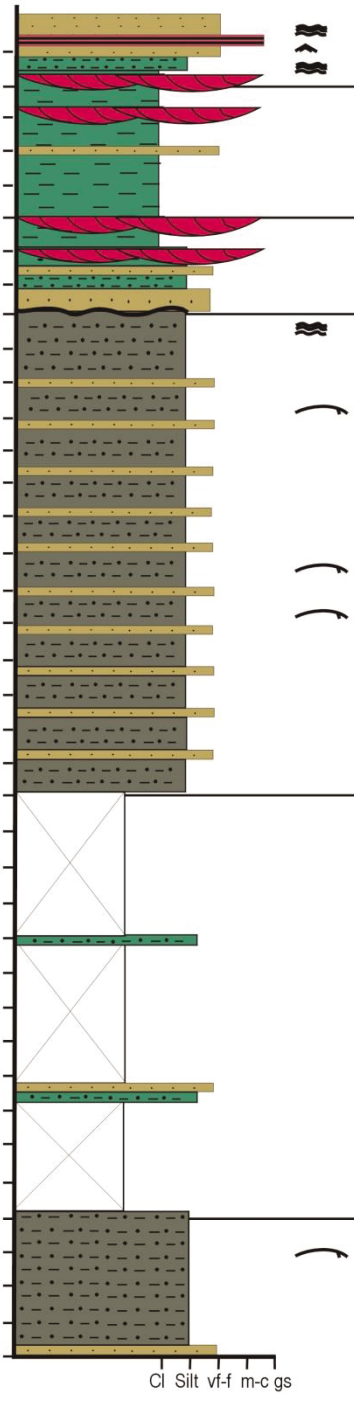

UTM at 420 m: 51 J 0343139, 7177737. End of section, possible structural repetition

375 to top of section: Cherty and sandy laminae with abundant microbial laminae and teepee structures

330-375 m: Hematitic mudstone with sandy intervals; planar laminated. Grainstone lenses ~30 cm thick. Microbial laminae in sandy intervals

300-330 m: Hardground surface (flooding?) Overlain by hematitic silt/sandstone and trough cross stratified grainstone lenses.

200-300 m: Thick succession of silty very fine to fine grained sandstone. HCS, with hummocks 20-25 cm wide, discontinuous. Possible fault at 275 m. Bed thickness ~1-3 cm. Some lateritic weathering near 250 m. UTM at 270=51J 0343126, 7177640. S/D of bedding=300/45

172-198 m:very fine to fine sandstone with hummocky cross stratification. Coarsens upward

163-172 m: hematitic siltstone, contact at 172 with overlying sandstone, erosional.

41-163 m: Covered intervals 41-73m, 77-93 m, 93.5-119m, 121-163m.
Hematitic siltstone and very fine sand stone intervals were identified sporadically throughout the covered interval. Strike/dip of bedding at 120 m=085/60S; cleavage=265/80.

4-41m: Hematitic siltstone and very fine to fine sandstone. HCS overlain by planar laminae. Carbonate cement, ~10% muscovite.

0-4m: Yelma Formation. Carbonate-rich, very fine to fine sand

APPENDIX II: PALEOCURRENT DATA

A. Nabberu Creek Section Measurements
UTM Location: 51J 0264134/7155463
n=20

Bedform	**Plunge (direction of flow)**
Ripple lamina	260
Ripple lamina	330
Ripple lamina	200
Ripple lamina	040
Ripple lamina	190
Ripple lamina	170
Ripple lamina	100
Ripple lamina	340
Ripple lamina	250
Ripple lamina	250
Ripple lamina	010
Ripple lamina	020
Ripple lamina	325
Ripple lamina	290
Ripple lamina	000
Ripple lamina	330
Ripple lamina	340
Ripple lamina	170
Ripple lamina	040
Ripple lamina	000

B. Von Treuer Section 1 Measurements

Location: 51J 0480324/7054877

n=18

Bedform	**Plunge (direction of flow)**
Trough cross-bedding	015
Trough cross-bedding	010
Trough cross-bedding	015
Trough cross-bedding	040
Trough cross-bedding	015
Trough cross-bedding	012
Trough cross-bedding	020
Trough cross-bedding	040
Trough cross-bedding	015
Trough cross-bedding	015
Trough cross-bedding	020
Trough cross-bedding	025
Trough cross-bedding	035
Trough cross-bedding	030
Trough cross-bedding	030
Trough cross-bedding	025
Trough cross-bedding	020
Trough cross-bedding	015

The Paleoproterozoic Frere Formation (ca. 1.88 Ga) of the Earaheedy Basin, Western Australia, is a ca. 600 m thick succession of iron formation and fine-grained, clastic sedimentary rocks that accumulated on an unrimmed continental margin with oceanic upwelling. Lithofacies stacking patterns suggest deposition occurred during a marine transgression punctuated by higher frequency relative sea-level fluctuations that produced five parasequences. Decimeter-scale parasequences are defined by flooding surfaces overlain by either laminated magnetite or magnetite-bearing, hummocky cross-stratified sandstone that grades upward into interbedded hematite-rich mudstone and trough cross-stratified granular iron formation. Each aggradational cycle is interpreted to record progradation of intertidal and tidal channel sediments over shallow subtidal and storm-generated deposits of the middle shelf. The presence of eolian dunes, mud cracks and absence of coarse clastics in nearshore and deeper subtidal settings indicate deposition along an arid coastline with wind-blown sediment.

Iron formation in the Frere Formation is almost exclusively peritidal, contrasting with other Paleoproterozoic iron formations. These continental margin iron formations also reflect upwelling of anoxic, iron-rich seawater, but accumulated in the full spectrum of shelf environments. Dilution by fine-grained, wind-blown terrigenous clastic sediment likely prevented Frere iron formation from forming in deeper settings. Lithofacies associations and interpreted paragenetic pathways of iron-rich lithofacies further suggest precipitation in seawater with a prominent oxygen chemocline.

Further details of geological products and maps produced by the Geological Survey of Western Australia are available from:

Information Centre
Department of Mines and Petroleum
100 Plain Street
EAST PERTH WA 6004
Phone: (08) 9222 3459 Fax: (08) 9222 3444

www.dmp.wa.gov.au/GSWApublications

AKIN

SEDIMENTOLOGY AND STRATIGRAPHY OF THE PALEOPROTEROZOIC FRERE FORMATION, WESTERN AUSTRALIA: IMPLICATIONS FOR THE EVOLUTION OF THE PRECAMBRIAN OCEAN

REPORT 130